DEVELOPMENT OF BIO-BASED WOOD ADHESIVE BY USING CELLULOSE NANOFIBER REINFORCEMENT AND CROSSLINKING AGENT FOR IMPROVED BONDING STRENGTH

A Thesis
Submitted to Graduate Faculty
of the
North Dakota State University
of Agriculture and Applied Science

By

Myungkeun Oh

In Partial Fulfillment of the Requirements
for the Degree of
MASTER OF SCIENCE

Major Program:
Materials and Nanotechnology

April 2017

Fargo, North Dakota

North Dakota State University
Graduate School

Title

Development of Bio-based Wood Adhesive by Using Cellulose Nanofiber Reinforcement and Crosslinking Agent for Improved Bonding Strength

By

Myungkeun Oh

The Supervisory Committee certifies that this ***disquisition*** complies with North Dakota State University's regulations and meets the accepted standards for the degree of

MASTER OF SCIENCE

SUPERVISORY COMMITTEE:

Dr. Long Jiang
Chair

Dr. Dilpreet Bajwa

Dr. Dennis Wiesenborn

Approved:

6/2/2017
Date

Dr. Erik K. Hobbie
Department Chair

ABSTRACT

Engineered woods, plywood, particle board, and oriented strand board, are widely used as a low-cost wood replacement in many applications. Many of the currently used wood adhesives contain chemicals that are harmful to human health and the environment. Increasing environmental and human health concerns have made the development of safe bio-based adhesives a priority. In this study, two plant proteins, zein from corn and wheat gluten, were used to develop wood adhesives. To increase their bond strength, cellulose nanofibers were added to create nanocomposite adhesives and a crosslinking agent was also used. Single-lap shear test, flexural and internal bond tests were performed on dry and water-immersed samples to measure the bond strength. Fractured bond surfaces were studied using optical observation and scanning electron microscopy (SEM) to determine bond failure mechanisms. Thermal and chemical properties of the adhesives were evaluated using thermogravimetric analysis (TGA) and Fourier transform infrared spectroscopy (FTIR), respectively.

ACKNOWLEDGEMENTS

I would like to thank to my advisor Professor Long Jiang for his guidance and support, and for providing me an opportunity to work in his research group; without his help, I would not have been able to complete this research. I would also like to thank my committee members, Professor Dilpreet Bajwa and Professor Dennis Wiesenborn for their consultancy and encouragement.

I would like to express my gratitude to Jayma Moore at the Electron Microscopy Center for SEM micrographs. I would like to thank Rob Sailer, Tanya Erickson and Kimberly Caslson in the Mechanical Engineering Department for their technical and administrative assistance. Special thanks to Professor Seung Won Hyun in the statistics department for his assistance with statistical analysis.

Moreover, I would also like to thank former and current graduate and undergraduate students Xuezhu Xu, Alex Sinclair, David Gutschmidt, Qian Ma, Yong Wang, Xiaoyi Zhou, and Siwakorn Tangpong for their help and friendship.

Last, my deepest thanks go to my family in South Korea for their love and supports. This thesis would not be possible without them.

TABLE OF CONTENTS

LIST OF TABLES

LIST OF FIGURES

CHAPTER 1. LITERATURE REVIEW

1.1. Introduction

In this chapter, the structure, production, properties, and surface modifications of cellulose nanofibers are first discussed. Applications of the nanofibers in polymer nanocomposites and biomedical materials are subsequently reviewed. Discussion on the structures, properties, and applications of zein and gluten proteins are followed. Finally, the test of wood adhesives and the use of cellulose nanofibers in wood adhesives are introduced.

1.2. Cellulose Nanofibers

1.2.1. Overview

Cellulose is one of the most abundant and ubiquitous bio-based polymers on the planet. It is widely used in many industries such as paper making, textile, construction, and packaging. Cellulose is naturally synthesized by living organisms including plants, bacteria, algae, and some sea animals. Due to its renewability, low-cost, non-toxicity, biocompatibility, and high mechanical strength, cellulose has attracted remarkable attention from researchers in different fields. Woody biomass contains three major components: cellulose, hemicellulose, and lignin, with the cellulose being the largest component (about 50 wt%). Cellulose possesses a fibrous structure and functions as a structural component in wood; hemicellulose and lignin serve as “glue” to bind the cellulose fibers together to form wood cell walls.

1.2.2. Cellulose Nanofibers

As shown in Figure 1-1, the fibrous cellulose exhibits a hierarchical structure. The micro-sized cellulosic fiber is composed of nano-sized elementary fibrils that contain both amorphous and crystalline regions. The elementary fibrils can be isolated from different lignocellulosic

biomass using mechanical fibrillation [1], mechanical fibrillation with enzymatic hydrolysis [2], and mechanical fibrillation with 2,2,6,6-tetramethylpiperidine-1-oxyl radical (TEMPO)-mediated oxidation [3].

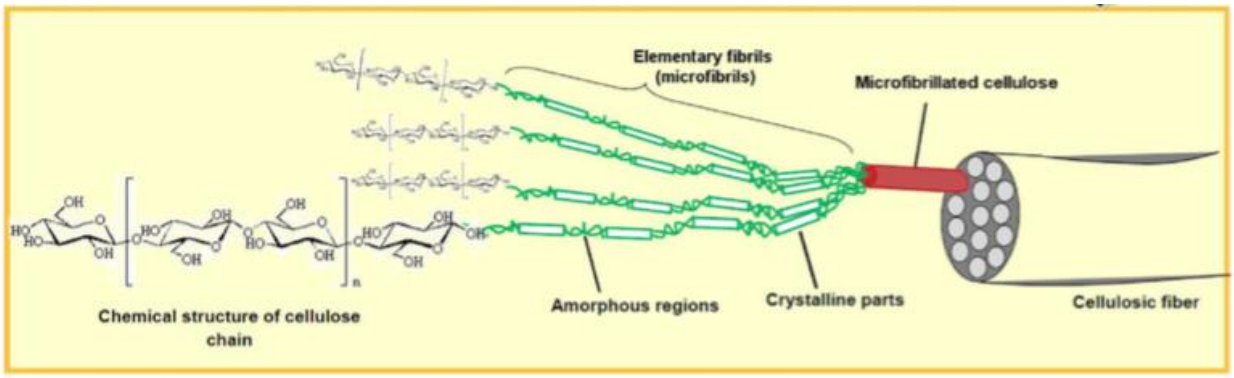

Figure 1-1. Hierarchical structure of cellulose fibers [4].

Two different terms, i.e., cellulose nanofibrilas (CNFs) and cellulose nanocrystals (CNCs), have been used to denote the nano-sized cellulose fibers. CNFs refer to the long flexible elementary fibrils that contain both crystalline and amorphous cellulose (Figure 1-2A), while CNCs refer to the pure needle-like cellulose crystals after the amorphous regions of CNFs are removed by acid hydrolysis (Figure 1-2B). Mechanically-prepared CNFs have large quantities of reactive hydroxyl groups (-OH) on their surfaces due to the molecular structure of cellulose. The CNFs produced using TEMPO oxidation also have carboxyl groups and the CNCs produced by sulfuric acid hydrolysis contain sulfate groups because of the chemical reactions. Sacui et al. reported that CNCs and CNFs had dimensions of 2-100 nm in width and tens of nanometer to micrometers in length [5].

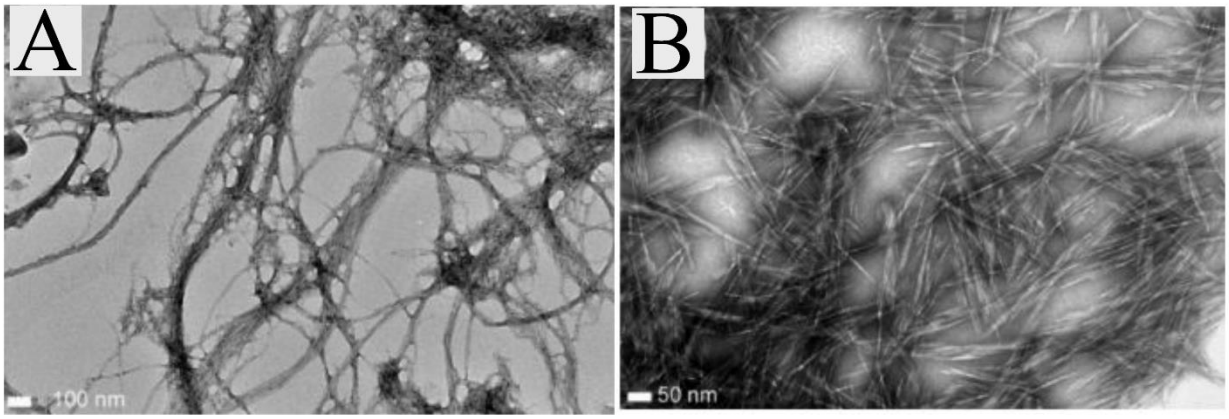

Figure 1-2. TEM micrographs of (A) CNFs and (B) CNCs derived from eucalyptus [6].

Bacterial cellulose (BC) is another classification of cellulose nanofibers, which is produced by gram-negative bacteria called *Gluconacetobacter xylinum* (or *Acetobacter xylinum*) through a fermentation process. BC pellicle is formed at the air/liquid interface of the culture medium and is essentially a BC hydrogel containing networked BC nanofibrils (Figure 1-3). Compared to plant based cellulose nanofibers, BC possesses high water uptake capacity, ultrafine nanofibril network structure, high cellulose purity and crystallinity [7]. Because of these reasons, BC tends to be more used in the biomedical engineering field and the plant based cellulose nanofibers are widely used for nanocomposites.

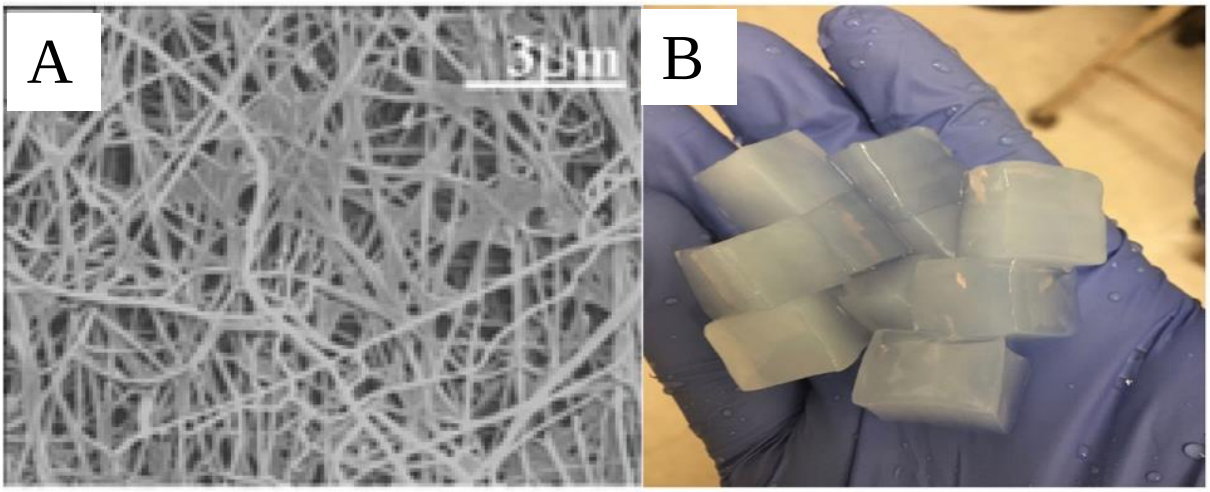

Figure 1-3. (A) SEM image of BC [8]. (B) BC pellicle cubes after purification.

1.2.3. Extraction of Cellulose Nanofibers

The biomass sources for producing CNCs and CNFs are diverse; pineapple leaves [9], wheat straw and soy hull [10], banana rachis [11], potato tuber [12], bamboo [13], [14], coconut husk fibers [15] and many other sources have been reported. CNCs are commonly produced from micro-sized cellulose fibers (e.g., cotton) through acid hydrolysis. The acid reacts with and removes amorphous cellulose and non-cellulose materials from the cellulose fibers to yield cellulose crystals, i.e., CNCs. The acid treatment also imparts negative charges on the surface of CNCs, which prevent CNC particles from aggregation in water. The reported diameter and length of CNCs vary substantially depending on the biomass origins and the hydrolysis conditions that are used in the studies. For instance, Santos et al. extracted CNCs from pineapple leaves with different conditions of sulfuric acid hydrolysis, the CNCs extracted for 30 min have a diameter of 4.45 ± 1.41 nm and a length of 249.7 ± 51.5 nm, while the CNCs extracted for 60 min have a diameter of 4.18 ± 1.44 nm and a length of 190.2 ± 36.5 nm [16]. Yu et al. produced CNCs from commercial microcrystalline cellulose using hydrochloric acid hydrolysis. The diameter and

length were reported to be 16 nm and 230 nm, respectively [17]. Espinosa et al. extracted CNCs from cotton using phosphoric acid hydrolysis and the obtained CNCs possessed a diameter of 31 ± 14 nm and a length of 316 ± 127 nm [18]. Sadeghifar et al. produced CNCs showing a rectangular cross-section (8.6 × 7.7 nm) and having a length of 100 – 400 nm through hydrobromic acid hydrolysis [19]. Carboxylated CNCs were also produced using TEMPO-mediated oxidation. Their sizes were reported to be 9 ± 3 nm (diameter) and 189 ± 40 nm (length) [20].

To produce CNFs, lignin, semicellulose and other impurities in raw lignocellulosic biomass are first removed through a pulping process using sodium chlorite ($NaClO_2$) [14] and sodium hydroxide (NaOH). A nanofibrillation process is followed to break up the obtained cellulose microfibers using mechanical grinding [1], [21], microfluidization [22] or intensive ultrasonication [14]. For example, Chen et al. derived CNFs from bamboo fibers using ultrasonication. The produced nanofibrils are over 1 mm in length and 30-80 nm in diameter and have a crystallinity of 61.25% [14]. Chemical and bio-pretreatments including TEMPO oxidation and enzymetic hydrolysis have been developed to facilitate the nanofibrillation process and reduce its energy consumption. CNFs produced by TEMPO pretreatment are highly uniform and have a high aspect ratio. The treatment also results in carboxylation of the CNF surfaces, which helps to stabilize CNF colloidal suspensions.

1.2.4. Mechanical Properties of Cellulose Nanofibers

The mechanical properties of cellulose nanofibers are crucial to their use as reinforcement materials in nanocomposites. High mechanical properties of the nanofibers, combined with their homogenous dispersion in a polymer matrix, allow a high level of reinforcement to the matrix polymer at low nanofiber concentrations. In determining the strength and Young's modulus of cellulose nanofibers, the variations in source materials (e.g., plants, bacteria, etc.), preparation

methods (mechanical process, acid hydrolysis, enzymatic hydrolysis, *etc.*), and testing methods (tension, bending, nano-indentation, or simulation) lead to a wide distribution of the properties. Lahiji et al. reported the modulus of CNCs to be between 18-50 GPa [23]; Guhados et al. showed that the modulus of BC was up to 130 GPa [24]. Table 1-1 compares the specific modulus (i.e., modulus/density) of crystalline cellulose to three other materials. Due to their high modulus and low density, cellulose nanofibers exhibit much higher specific modulus than the others. Their remarkable mechanical properties, in combination with their large surface area, high aspect ratio, and environmental friendliness, make them an ideal reinforcement material for polymer nanocomposites.

Table 1-1. Modulus comparison of engineering materials and cellulose [25].

Material	Modulus (GPa)	Density (Mg/m^3)	Specific modulus ($GPa \cdot m^3/Mg$)	Reference
Steel	200	7.8	26	Ashby et al.[26]
Aluminum	69	2.7	26	Ashby et al.[26]
Glass	69	2.5	28	Ashby et al.[26]
Crystalline cellulose	138	1.5	92	Sakurada et al.[27]

1.2.5. Interfacial Bonding between Cellulose Nanofibers and Polymer Matrix

Interfacial bonding between the nanofiber and the host polymer is a key factor that determines the mechanical properties of their composite. Both CNCs and CNFs are hydrophilic because of the abundant polar groups (e.g., hydroxyl, carboxylic or sulfate groups) on their surfaces. They form stable colloidal suspensions in water or other strong polar organic solvents, and aggregate into large, hard-to-break particles when dried. Surface chemical modifications to

the cellulose nanofibers are necessary to reduce their hydrophilicity and allow their homogeneous dispersion in mostly hydrophobic host polymers. Some modifications also graft the fiber surfaces with functional groups that can react with the host polymer and hence form strong chemical bonding between the two phases. Various chemical modifications such as esterification, etherification, polymer grafting, and oxidation have been reported [25], [28], [29]. Figure 1-4 shows the different surface modification methods that have been reported in recent years [30].

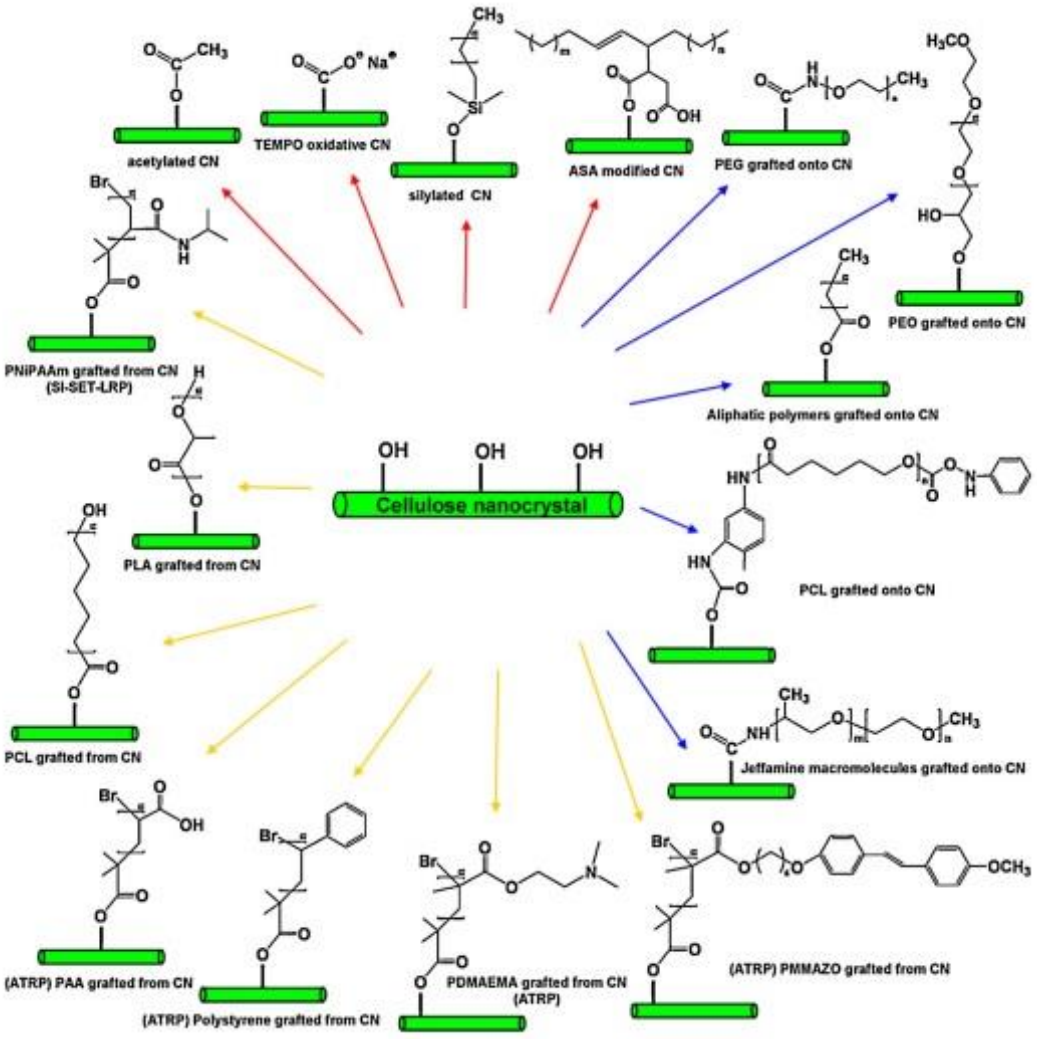

Figure 1-4. Various chemical modification methods for cellulose nanofiber surfaces [30].

Esterification is broadly used for modification of hydroxyl groups at the surface of cellulose nanofibers due to its ease and directness. Acetylation of cellulose nanofiber is the most extensively researched route among the esterification reactions. Braun et al. and Sobkowicz et al. reported that both hydrolysis and acetylation of the hydroxyl group at the surface of cellulose nanofibers occured simultaneously [31], [32]. In the early development of cellulose nanofibers, Herrick et al reported on the simultaneous acetylation of cellulose nanofibers in a mechanical process with sulfuric acid acting as a catalyst in a mixture of acetic anhydride and acetic acid [33]. A one-step procedure of defibrillation and esterification of cellulose nanofibers was reported by Huang et al. [34].

Etherification with carboxymethylation of cellulose fibers is widely used to prepare cellulose nanofibers for chemical treatments and defibrillation of fibers because it is highly efficient and cost effective. The process is simple and normally proceeds to activate the fibers with mostly sodium hydroxide and randomly converted hydroxyl groups [35]–[38]. This process holds many disadvantages related to using toxic halocarbon reactants, and the resulting cellulose nanofibers are more hydrophilic than the original ones, which limits its applications in polar media.

Polymer grafting of cellulose nanofibers is categorized into two methods: “grafting onto” and “grafting from”. In the “grafting onto” approach, pre-synthesized polymer chains that hold reactive end groups are added onto the surface of cellulose nanofibers through reacting with the surface hydroxyl groups. The polymer needs to be fully characterized before the grafting, and it offers the possibility of adjusting the properties of the cellulose nanofibers. However, an unfavorably reduced density of surface grafting is frequently shown on the “grafting onto” method because the steric hindrance would avert optimal attachment in the grafting reaction. Ljungberg et al. reported grafting maleic anhydride grafted polypropylene (MA-g-PP) onto the tunicate

extracted CNCs surface [39]. Amine-terminated polymers grafted onto TEMPO oxidized CNCs by using carbodiimide catalysis was studied by Araki et al. [40]. The "grafting from" method includes growing the polymer brushes directly on the surface of the cellulose nanofibers, with the hydroxyl group helping to initiate ring opening polymerization (ROP), or the nanocellulose surface would be modified to introduce controlled polymerization techniques such as atom transfer radical polymerization (ATRP). Habii et al. , who first applied ROP for grafting and polymerizing cyclic monomers to CNCs, grafted polycaprolactone (PCL) onto the nanocellulose surface using stannous octoate ($Sn(Oct)_2$) as a catalyst [41]. Yi et al. first studied using SI-ATRP to grow polymers on the surface of CNCs [42]–[44].

To convert the hydroxyl groups on the nanocellulose surface to the carboxylic form, TEMPO-mediated oxidation is used. This oxidation method is highly selective for primary hydroxyl groups; it is eco-friendly, and easy to use. TEMPO-mediated oxidation is commonly used as a cost-effective pre-treatment before mechanical nanofibrilation in cellulose nanofiber production. Araki et al. first proposed that TEMPO-mediated oxidation of CNCs from the HCl hydrolysis of cellulose fibers [45]. The authors demonstrated the CNCs keep their original morphological integrity and form a homogeneous suspension when dispersed in water after the TEMPO-medicated oxidation. Okita et al. proposed the integration of sodium carboxylate groups on the surface of CNCs for better dispersion in aprotic organic solvents such as DMAc, DMF, DMI, and NMP [46].

1.2.6. Applications of Cellulose Nanofibers

1.2.6.1. Reinforcement in polymer nanocomposites

Xu et al. compared the reinforcing effects of CNCs and CNFs in polyethylene oxide (PEO) nanocomposite films [6]. The films containing different contents of cellulose nanofibers were

prepared using solution casting. Both types of cellulose nanofibers could substantially increase the strength, modulus and fracture toughness of PEO. The films containing 7 wt% of CNCs or CNFs showed the best overall properties. Higher nanofiber contents resulted in decreases in the properties due to nanofiber agglomeration. At the same nanofiber content, CNFs showed higher reinforcement (strength and modulus) than CNCs because of CNFs' larger aspect ratio. Xu et al. also studied electrospun PEO nanofiber mats reinforced by CNCs and CNFs [47]. Rheological properties of the PEO-cellulose nanofiber solutions, diameter distribution of the spun nanofibers, and mechanical properties of the nanofiber mats were found to be very different due to the physical and chemical differences between CNCs and CNFs. The mechanical properties of the nanofibers mats were significantly improved in both cases. Shish-kebab like PEO crystalline structure was discovered for the first time in the CNC-reinforced electrospun nanofibers.

Svagan et al. developed starch nanocomposite foams containing CNF reinforcement [48]. CNFs and starch were mixed in water to form solutions, which was subsequently frozen and underwent lyophilization to produce foams. The foam cells transition from closed cells to open cells and eventually to no well-defined cell structures with increasing CNF concentration (Figure 1-5). Compression test results show that the modulus, yield strength and stress of the plateau region of the foams are significantly increased up to 40 wt% CNF content (Figure 1-6). However, the properties decrease at 70 wt% CNF content due to the lack of well-defined cell structure.

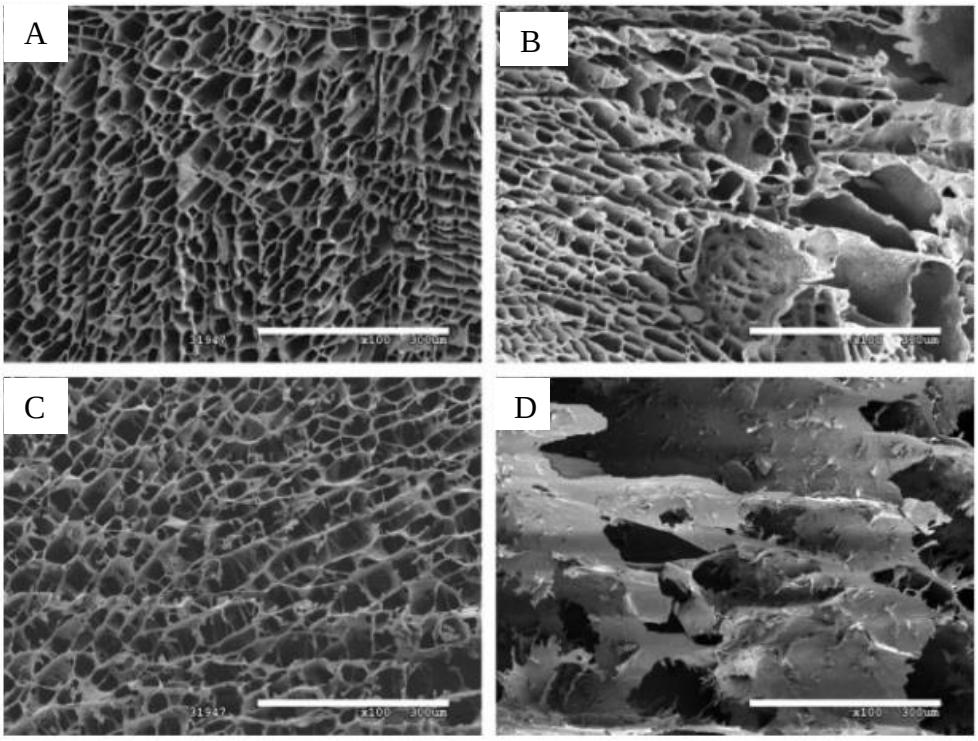

Figure 1-5. The cell structure of starch nanocomposite foams with 0% (A), 10% (B), 40% (C), and 70% CNFs (D) [48].

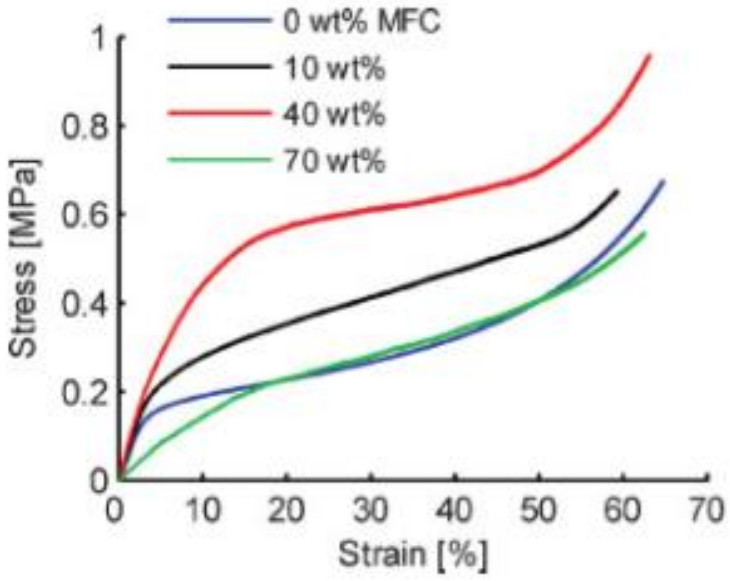

Figure 1-6. Compressive stress-strain curves of the starch nanocomposite foam reinforced by different contents of CNFs [48].

Huq et al. used CNCs to reinforced biodegradable alginate [49]. They prepared alginate films containing 1 wt% to 8 wt% CNCs using solution casting. Scanning electron microscopy (SEM) was carried out to study the dispersion of CNCs in the films (Figure 1-7). The tensile strength and tensile modulus increased up to 5 wt% CNCs but decreased at 8% NCC as shown in Figure 1-8. The authors attributed this to nanoparticle agglomeration at 8 wt% concentration.

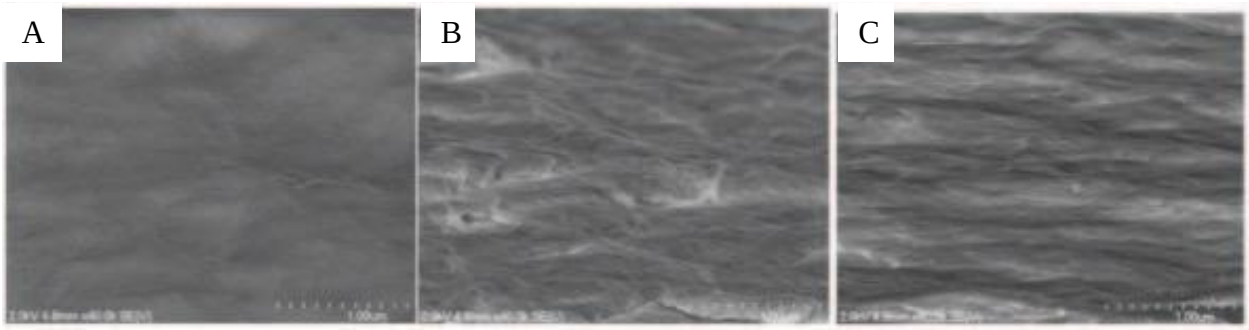

Figure 1-7. SEM images of the fracture surface of alginate films containing no CNCs (A), 5 wt% CNCs (B), and 8 wt% CNCs (C) [49].

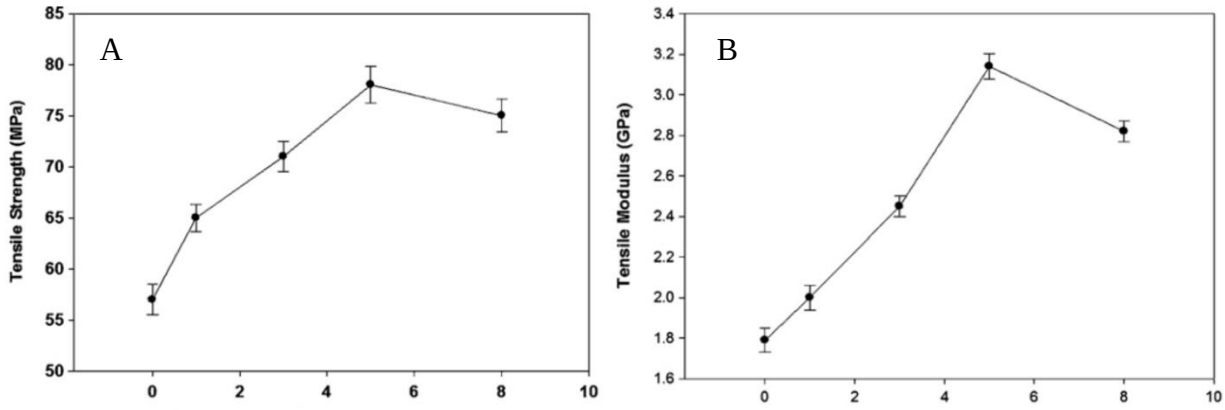

Figure 1-8. The effect of CNC concentration on the tensile strength (A) and tensile modulus (B) of the alginate films [49].

1.2.6.2 Applying cellulose in biomedical materials

Yang et al. prepared cellulose nanocrystals-poly(acrylamide) (CNC-PAM) composite hydrogels through in-situ acrylamide polymerization [50]. CNCs underwent TEMPO-mediated

oxidation first to have rich sodium C6-carboxyl groups on their surfaces. Potassium persulfate was used as the initiator to polymerize acrylamide monomer in the CNC suspension. Figure 1-9A shows that the tensile strength, elongation at break, and Young's modulus of the composite increases with CNC concentration. The Young's modulus also complies with the prediction of the Halpin-Tsai model, which is a classic model to predict composite modulus based on the modulus of the individual phases and their volume ratios (Figure 1-9B).

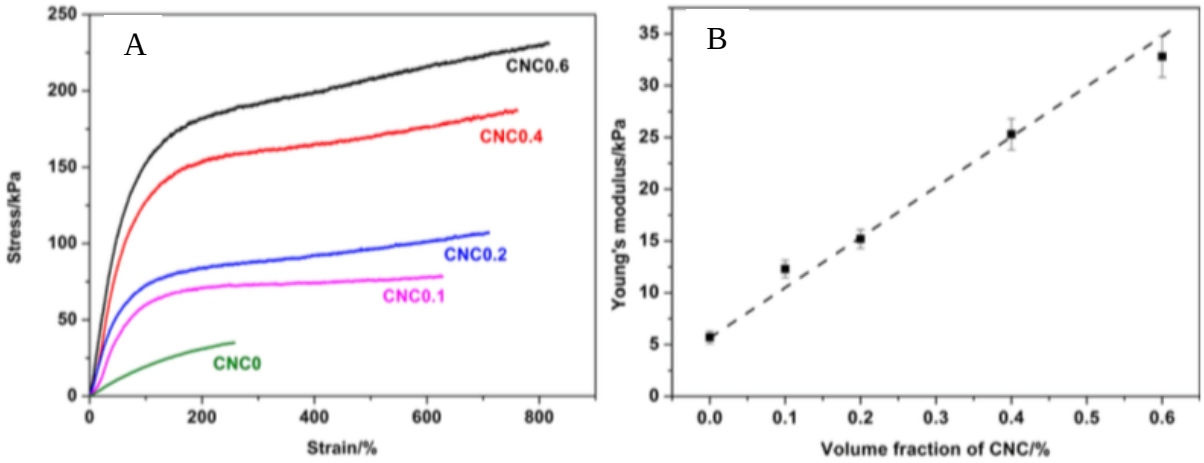

Figure 1-9. Mechanical properties of CNC-PAM hydrogels. (A) Representative stress-strain curves of the hydrogels containing different fractions of CNCs; (B) Young's modulus as a fraction of the volume fraction of CNCs. Dashed line represents Halpin-Tsai prediction [50].

Research about bacterial cellulose (BC) used in a wound care system was reported by Fu et al. [51]. The authors produced BC with *gluconacetobacter xylinus* and conducted tensile test on BC sheets/films. Table 1-2 compares the mechanical properties of dry and wet BC with other traditional biomaterials. The properties of wet BC and dry BC are higher than those of commercially used wet gauze and dry gauze due to the 3D network structure of BC nanofibers. To evaluate the biocompatibility of the BC films, the authors seeded and cultured human adipose-

derived stem cells (hASCs) on the BC films and on cell plates for comparison. The results in Figure 1-10 indicates that BC has biocompatibility comparable to the control cell plate.

Table 1-2. Comparison of tensile properties for different materials [51].

Sample	Thickness (mm)	δ (Mpa)	ε (%)	*E* (MPa)
Wet BC	2.10	1.96	23.00	17
Wet gauze	0.14	1.23	11.88	18
Pig skin	2.25	10.04	42.79	46
Mouse skin	0.88	1.13	33.29	6
Dry BC	0.55	10.32	9.00	131
Dry gauze	0.18	7.02	17.00	65

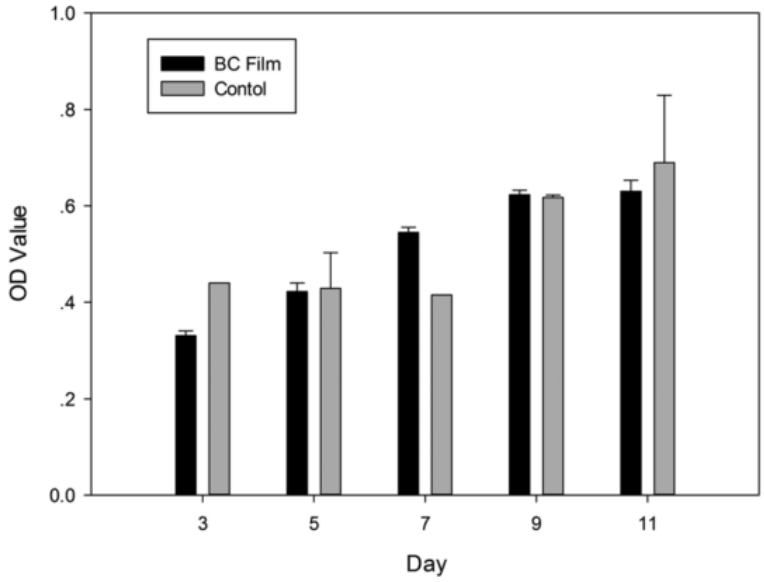

Figure 1-10. hASCs proliferation on BC film and control plate [51].

1.3. Zein

1.3.1. Overview

Zein is a prolamine (energy storage) protein present in corn or maize. Corn is consists of 60% starch and 6-12% of protein [52], of which 44-79% is zein [53]. Zein was first named by John

Gorham in 1821 after he isolated the material from corn [54]. Commercial zein production did not start until the mid-1930s. In the following twenty years, the utilization of zein continued to increase as it was made into buttons, fiber, adhesive, coating, and binder. About 15 million pounds of zein was produced in the United States each year in the late 1950s, and the production had decreased to one million pounds a year by 1978 due to cheap replacement products made of petroleum-based polymers. Zein has regained attention in recent years because of increasing environmental concerns about petroleum-based products and improved customer awareness of renewable materials.

1.3.2. Structure and Properties of Zein

Zein is composed of different polypeptides linked by disulfide bonds. Zein can be classified into four types, i.e., α-, β-, γ- and δ-zein, based on their solubility, charges, molecular size, and molecular weight [55]. The first three types represent the major fractions of zein [56], [57]. α-zein accounts for about 75-85 wt% of the whole zein and it is soluble in 60-95% aqueous ethanol without any buffers and reducing agents [55]. The solubility of α-zein is much higher than the other fractions of zein, which can only be solubilized with buffers and/or with assistance of reducing agents in an aqueous ethanol solution. α-zein again consists of two types of polypeptides Z19 and Z22, which have a molecular weight of 19kDa and 22kDa, respectively [58]. β-zein makes up about 10-15 wt% of the total zein present in corn while γ-zein represents about 5-10 wt%; δ-zein only presents in a small fraction. Zein is a hydrophobic protein (average 1.365 J/mol hydrophobicity [59], [60]) because of the presence of a high proportion of non-polar amino acid residues. α-zein is more hydrophobic than the other fractions of zein. α-zein has a helix secondary structure and assumes an asymmetric globular form. The high-level structure of zein varies when

it is dissolved in different solvents; the structure also depends on the temperature and pH of the solvent.

A molecular structure model of α-zein is shown in Figure 1-11 [61]. This model demonstrates the amphiphilic characteristic of zein, which features a hydrophilic top and bottom connected by glutamine bridges and a hydrophobic helices outer surface. Zein provides an exceptional water barrier characteristic because of the hydrophobic internal core, so that it is used as a coating material. Some important physicochemical properties of zein are shown in Table 1-3 [52].

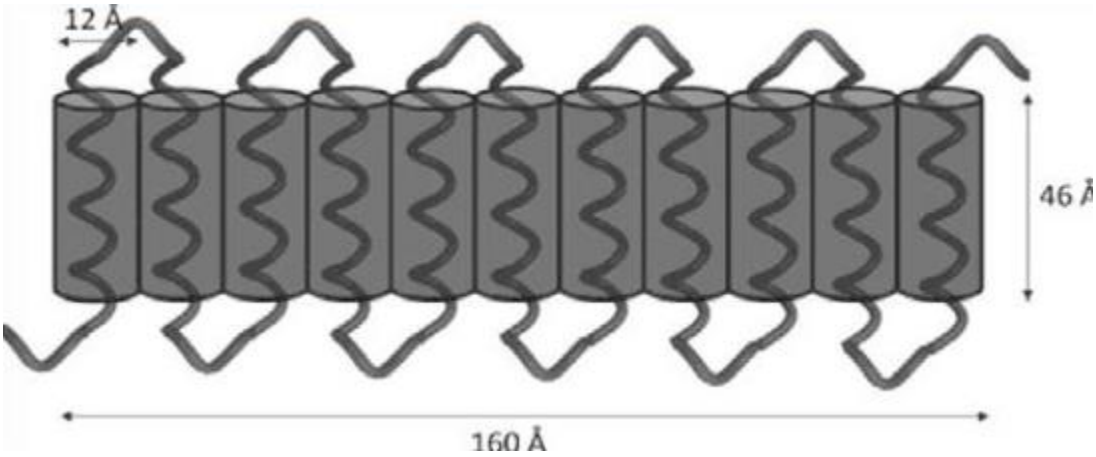

Figure 1-11. Structural model of zein protein. [61].

Table 1-3. Properties of zein protein [52].

Property	Characteristics
Bulking value, 1/kg	0.805
Color	Light cream
Dielectric constant (500 V, 60 cycles, 25-90 °C)	4.9-5.0
Diffusion coefficient	3.7×10^{-14} m^2/s
Einstein viscosity cofeeicient	25
Glass transition temperature	165 °C
Isoelectric point, pH	6.2 (varies 5 to 9)
Molecular weight	35 kDa (varies 9.6 to 44 kDa)
Partial specific volume	0.771
Physical form	Amorphous powder
Sedimentation coefficient	1.5s
Specific Gravity, at 25 °C	1.25
thermal degradation point	320 °C

FTIR spectrum of the α-zein shows four characteristic bands (Figure 1-12). The band at 1650 cm^{-1} is called amide I, which is attributed to the stretching vibration of the carbonyl (C=O) bond; the one at 1540 cm^{-1} is amide II, which is due to the bending vibration of N-H. Amide A band occurs at 3280 cm^{-1} and it is caused by stretching of N-H. The band at 1239 cm^{-1} is Amide III, which is mainly due to the stretching vibration of C-N.

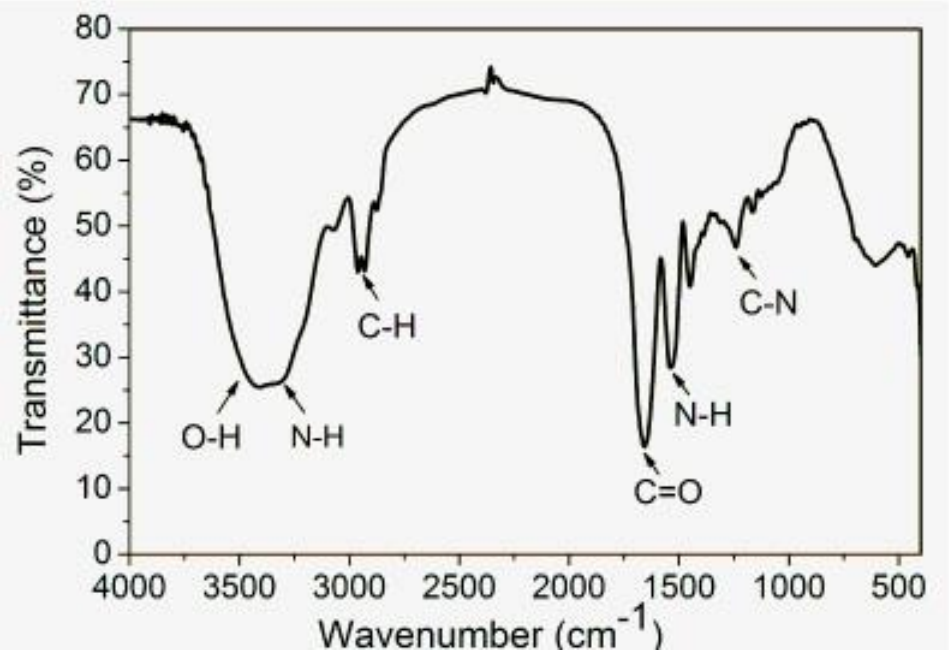

Figure 1-12. FTIR spectrum of zein powder in 1 w/w% of KBr [62].

1.3.3. Solubility of Zein

Zein's defining characteristic is its alcohol solubility, which is due to its strongly hydrophobic amino acid residues, including various sulfur-containing amino acids. Because zein behaves as an amphiphilic and, more precisely, as a hydrophobic protein, ethanol at high concentration (60-95%) is widely used to dissolve and maintain its molecular structure. The molecular structure and amino acid composition are the main factors in determining the properties of zein. Beside the aqueous ethanol, isopropanol, N,N-Dimethylformamide (DMF) solution, acetic acid, and methanol are also commonly used to dissolve zein with the assistance of sodium dodecyl sulfate (SDS) surfactant. The solvents for zein often contain functional groups such as -OH, $-NH_2$, $-CONH_2$, or -COOH [52].

Nonthanum et al. [63] studied the rheology of zein solution (20% w/w) containing γ-zein in different concentrations of ethanol (60-95%) and under different pH conditions (2, 6, and 12). Steady shear tests and oscillatory time sweeps were used to determine the flow behavior and

gelation time of the solution. They found that pure α-zein solutions demonstrated near Newtonian behavior, but inclusion of γ-zein led to shear thinning of the solutions. γ-zein also shortened gelation time while increasing the consistency index (K) at high pH. The rheology of zein in N,N-dimethylformamide (DMF) solution was studied by Selling et al. under different concentrations, aging times, and temperatures [64]. The solutions showed shear thinning behavior. Their viscosity increased exponentially with increasing zein concentration, and decreased exponentially with increasing temperature.

Aggregate formation of zein and its analysis were conducted by Kim and Xu (2008) [65]. The authors used a dynamic light scattering instrument to monitor the hydrodynamic radii of zein molecules in ethanol. It was found that the composition of the aqueous ethanol solvent strongly affected zein aggregation. When the ethanol concentration increases from 70% to 92%, zein molecular aggregation number decreases dramatically and reaches the minimum at about 90% before it surges again **(**Figure 1-13**)**.

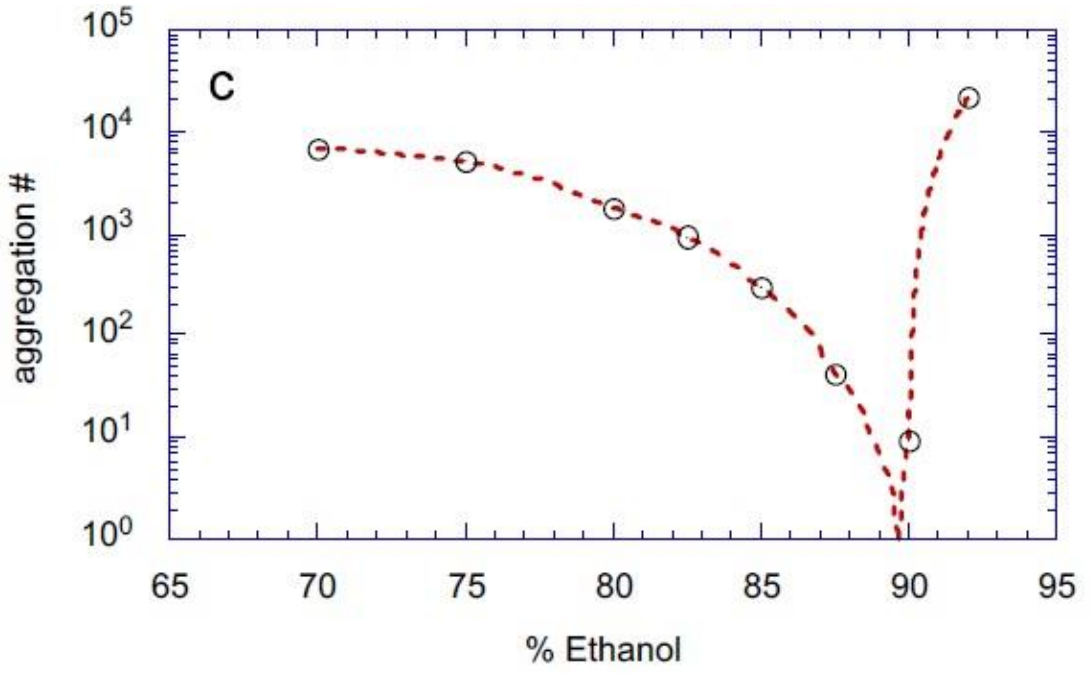

Figure 1-13. Number of aggregation with various ethanol concentration [65].

Chen et al. investigated physicochemical properties of zein nanoparticles [66]. The authors dissolved zein in ethanol/isopropanol mixtures (with different ratios) at 60ºC for 10 min. They found that zein particle size in the solution increased with ethanol ratio from 13.4 nm (at 70%) to 29 nm (at 85%). Guo et al. [67] investigated the characterization of zein particles in 70% aqueous ethanol solution using Atomic Force Microscopy (AFM). Based on their AFM image **(**Figure 1-14**),** zein globules show a diameter between 150 and 550 nm and a height between 50 and 150 nm, which are consistent with the results from Yamada et al. [68], [69].

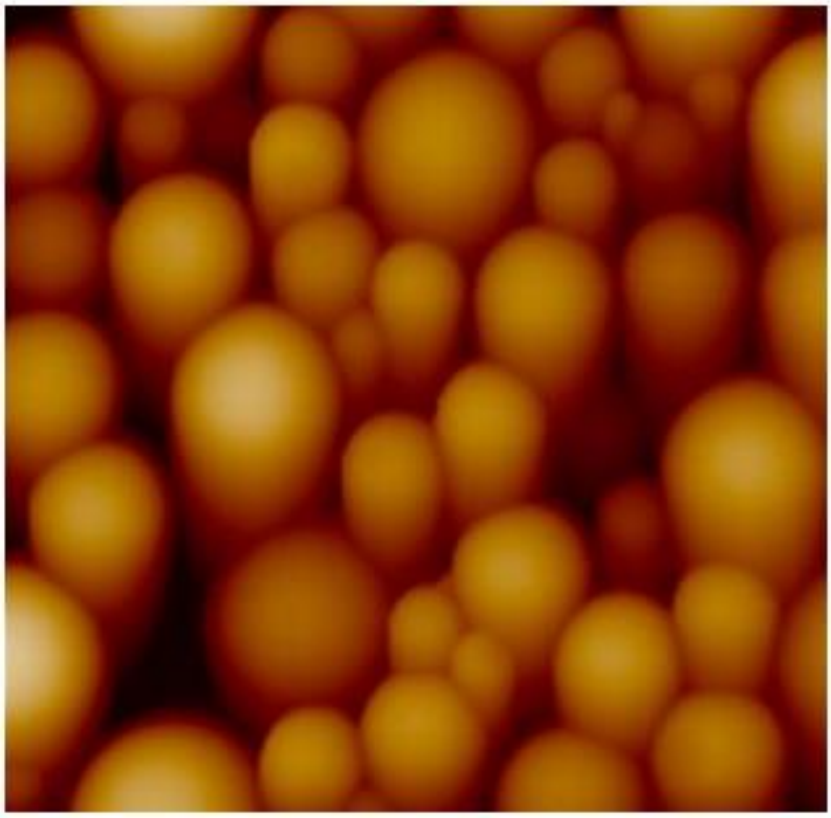

Figure 1-14. AFM image of zein protein globules [67].

Li et al. [70] investigated the structure and rheological properties of α-zein in acetic acid by using scaling relationships of size of protein and viscosity of protein solution. The authors found that the radii of gyration of zein particle was decreased by increasing zein concentration, and α-zein was more swollen in acetic acid than in aqueous methanol and ethanol solutions. Moreover, they found that the viscosity of zein in acetic acid increased with increasing zein concentration. Shi et al. prepared zein film using acetic acid solution of zein [71]. The authors used tapping mode atomic force microscopy (TP-AFM) and x-ray photoelectron spectroscopy (XPS) to study film surface morphology and hydrophilicity. The authors found that surface smoothness and hydrophilicity were much higher for the zein films prepared using acetic acid than using aqueous ethanol.

Zein modification was conducted by Wheelwright et al. [72] through the formation of methyl ester via reacting zein with methanol containing *para*-toluenesulphonic acid. A new signal at 3.67 ppm from proton nuclear magnetic resonance (NMR) and a strong C=O stretching vibration in the Frourier transform infrared spectroscopy (FTIR) spectrum confirmed the reaction. Zein solubilization by using different surfactants was studied by Moore et al. [73]. The authors used anionic surfactants, sodium dodecyl sulfate (SDS), and a mixture of SDS and dodecyl n(ethylene oxide) ($C_{12}E_n$) (*n*=4,6, and 8) to disperse zein in water. They studied zein-SDS interactions under different surfacant conidtions and their findings can be used to tailor the ability of a surfactant to denature proteins through the appropriate mixing with other surfactants.

1.3.4. Applications of Zein

Zein had been extensively used in adhesives, binders, films, and coatings in the 1960s. Later, petroleum-based products received the spotlight due to its low cost, lightness, and flexibility in thermal and mechanical properties, etc. One major drawback of petroleum-based polymers is their non-renewability. In recent years, increasing environmental concern and consumer awareness have made biobased polymers attractive materials in academic research and industrial developments. Many biobased polymers including cellulose, lignin, zein, soy protein, gluten, starch, etc., have been extensively studied for different applications with an aim of replacing petroleum-based polymers. Biobased polymers have shown great potential in the health industry, e.g., tissue engineering, cell culture application, and controlled drug delivery systems. Zein has been accepted as GRAS (generally recognized as safe) by the FDA and is suitable for use as oxygen or moisture barriers in the food packing industry.

1.3.4.1. Film application

Zein protein film has attracted attention from many researchers in the field of edible films and coating materials. Ozcalik and Tihminlioglu studied zein nanocomposite coatings to improve barrier properties of polypropylene (PP) films [74]. Organo-modified montmorillonite (OMMT) was added to zein to increase its hydrophobicity and barrier performance. It was found that the nanocomposite coating containing 5 wt% OMMT reduced oxygen permeability of the coated PP film nearly four times and reduced water vapor permeability by 30%. Zein was also used to encapsulate alpha-tocopherol, an antioxidant, through an electro-hydrodynamic process [75]. The encapsulated antioxidant was then electrosprayed onto a gluten film as a coating layer, thus producing an active/bioactive bilayer packaging structure. The water vapor barrier efficiency of the film was found to be improved with the coating layer. The stability of alpha-tocopherol was also improved when subjecting the bilayer structure to a typical industrial sterilization process. The release of alpha-tocopherol was delayed after zein encapsulation. This work provides a new method for developing active/bioactive packaging systems in food applications.

Gaona-Sánchez et al. [76] prepared zein films by electrospraying zein solutions. The spraying conditions and zein concentration that allowed film formation were determined; the structural characteristics and mechanical/thermal properties of the resulting films were studies; the properties were compared to those prepared using a traditional casting method. Cheng et al. reported preparation of edible zein/chitosan composite films filled with phenolic compounds and dicarboxylic acids [77]. The composite films showed improved mechanical and water vapor barrier properties. By containing phenolic compounds and chitosan, the composite films also showed antioxidant and antimicrobial functional activities. Oymaci and Altinkaya incorporated zein nanoparticles in whey protein isolate (WPI) films by solution casing [78]. The nanoparticles were

coated with caseinate to achieve uniform dispersion. The water vapor barrier and mechanical properties of the WPI film were improved after the addition of the nanoparticles.

1.3.4.2. Application for biomaterials

Zein shows many advantages when used as a drug delivery vehicle due to its outstanding biocompatibility, biodegradability, and high surface area [79], [80]. Additionally, zein can interact efficiently with hydrophobic and hydrophilic drugs; it is not soluble in a physiological condition and is able to protect encapsulated drug compounds because it comprises high percentages of hydrophobic amino acids [81], [82]. Liu et al. reported on a microsphere drug delivery system containing ivermectin (IVM), an anti-parasite and zein [83]. The system was made using a phase separation method and it showed a zero-order release behavior of IVM. Müller et al. prepared zein and zein/chitosan based microspheres and studied their chemical, thermal and morphological properties [84]. Zein microspheres were shown to have smooth surfaces while the surfaces of zein/chitosan microspheres were rough (Figure 1-15). The average diameters for the two microspheres were 1.23 ± 0.47 μm and 4.30 ± 1.93 μm, respectively.

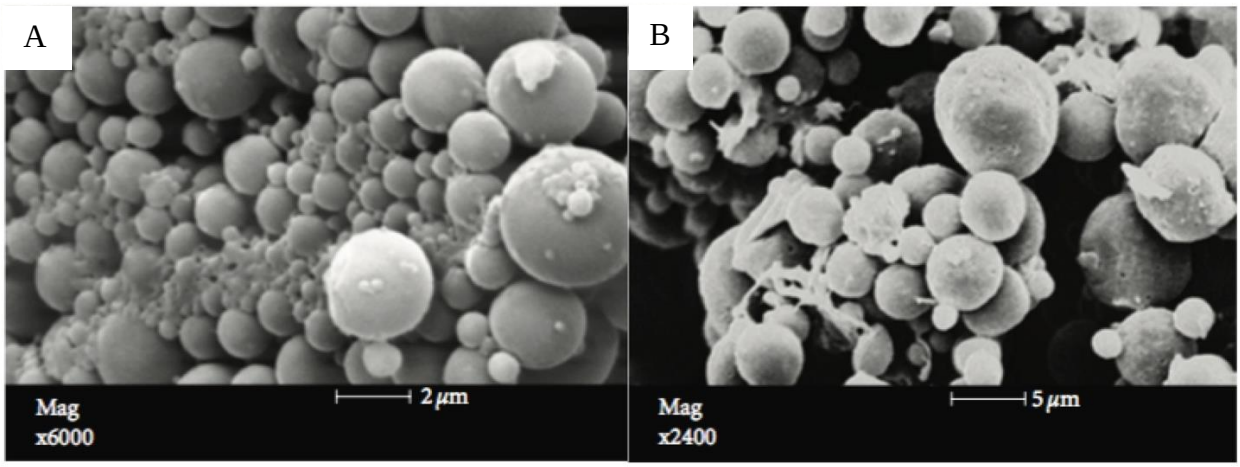

Figure 1-15. SEM images of zein (A) and zein/chitosan (B) microspheres [84].

Luo et al. used zein/chitosan complex to encapsulate α-tocopherol (TOC), a hydrophobic nutrient, for enhanced bioactivities (Figure 1-16) [85]. Coating the TOC/zein nanoparticles with chitosan led to significant decrease in the nanoparticle size. The coating also greatly improved controlled release properties of TOC.

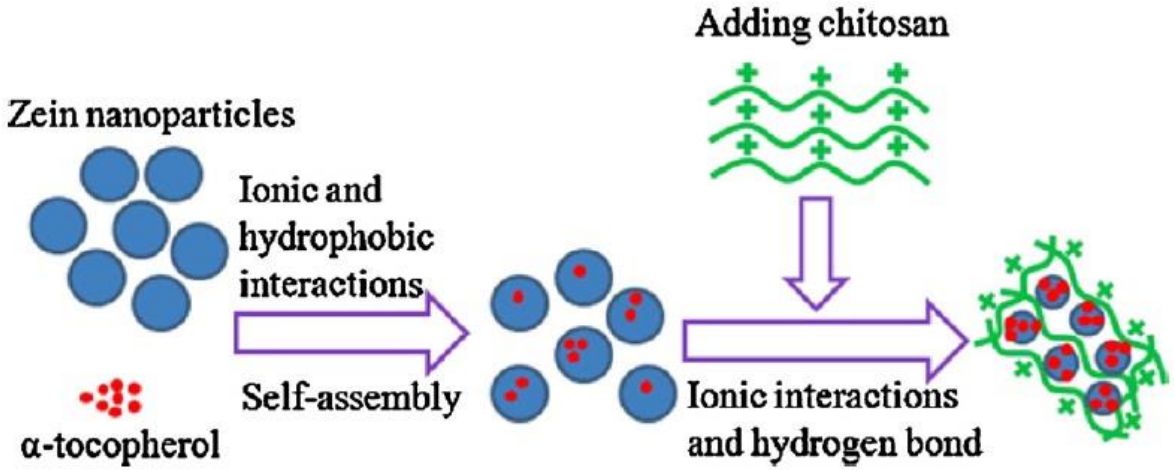

Figure 1-16. Schematic illustration of encapsulated α-tocopherol in zein/chitosan composite [85].

Chen et al. developed a laccase biosensor made of gold nanoparticle-crosslinked zein ultrafine fibers by using electrospinning and a one-step reduction method [86]. Poly(ethyleneimine) (PEI) was used as the reducing and crosslinking agent. The biosensor possessed high sensitivity, good reproducibility, stability and selectivity. Dhandayuthapani et al. fabricated fluorescent zein nanofibers containing quantum dot (QD) using an electrospinning process [87]. The authors claimed that the composite nanofibers showed robust fluorescent properties without photo bleaching for several months and proposed to use them as optical/biological sensors and for biological labelling and tissue engineering applications.

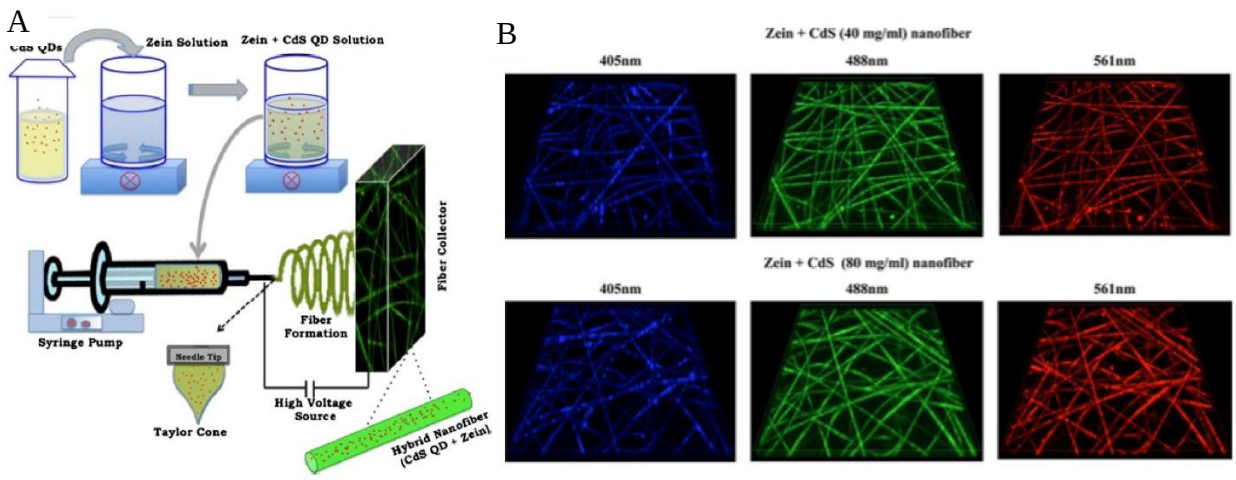

Figure 1-17. (A) Schematic preparation procedure of composite QDs/zein nanofibers. (B) Microscope images of the fluorescent nanofibers [87].

1.4. Gluten

1.4.1. Overview

Gluten is the storage protein of wheat and is a byproduct of the starch isolation process from wheat flour. Gluten is a low-cost natural material exhibiting good viscoelastic properties, excellent gas barrier properties, and strong tensile strength. Wheat gluten is mostly composed of two protein types: gliadin and glutenin. Gliadin is consisted of single chain polypeptides with relatively low molecular weight (average molecular weight is 25 – 100 kDa). The molecules contain intramolecular disulfide bonds and are ethanol soluble. By contrast, glutenin molecules have relatively high molecular weight (average molecular weight is over 105 kDa), are linked through intermolecular disulfide bonds, and are ethanol insoluble [88]. Gluten is not soluble in water but it can absorb approximately twice its dry weight in water to become a viscoelastic material [89]. Many modifications have been conducted on gluten, including chemical modifications such as deamidation [90], acid and alkali treatments [91]–[93], and enzyme

treatment [94], and physical modifications such as heat treatment, high pressure processing, and UV irradiation.

1.4.2. Application of Gluten

1.4.2.1. Wood adhesive

Khosravi et al. [95] developed wood adhesive for use in particle boards using gluten and soy protein isolate. The authors prepared laboratory size particle boards and performed internal bond, thickness swelling, and water absorption tests. Gluten was dispersed in water to make the adhesive. The authors found that the temperature used to disperse gluten had a more significant impact to adhesive bonding that the time of dispersion. Nordqvist et al. separated gluten into glutenin and gliadin fractions and examined their bonding performance (using gluten as control) [96]. They found that the bonding strength of gliadin were lower than that of both glutenin and gluten. The strength, however, could be increased by reducing over-penetration of gliadin into the wood material.

Lei et al. used hydroxymethylated and glyoxalated hydrolysed gluten as adhesives to prepare wood particleboards [97]. They found that the produced boards possessed satisfactory properties for interior wood boards. Adding a small portion of pMDI to the adhesives improved the properties further. Nordqvist et al. modified gluten by enzymatic hydrolysis and heat treatment. They discovered that the gluten treated at 90 °C and with a low level of hydrolysis showed optimal bond strength and improved water resistance [98]. The bond strength and cold water resistance of alkali-modified soy protein isolate and gluten were compared [99]. Both proteins were denatured by 0.1 M NaOH and the samples for bond strength tests were produced under different press time and temperature conditions. They found the soy protein had higher bond strength than gluten and the protein particle size in the adhesive had a negligible effect on the strength.

El-Wakil et al. used reed fibers and gluten/urea-formaldehyde as binder to prepare particleboards [100]. The mechanical properties, including modulus of elasticity (MOE), modulus of rupture (MOR), and internal bond of the boards were measured. The results showed that the mechanical properties increased with increasing UF content, pressing time, or pressing temperature. Figure 1-18 shows the SEM picture of reed fibers inside the particleboard.

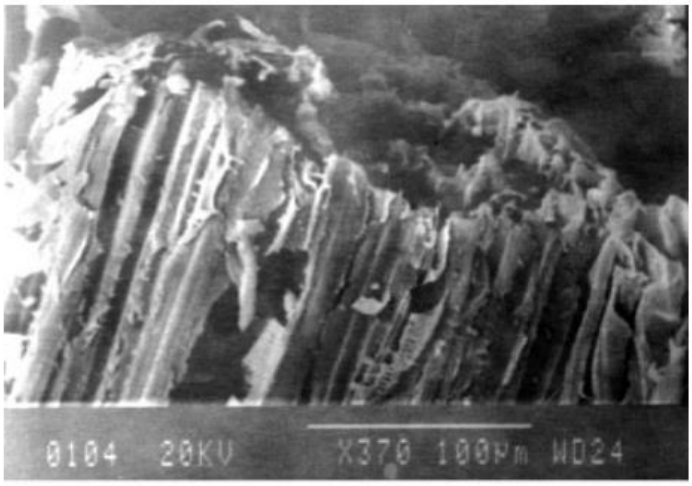

Figure 1-18. SEM picture of reed fibers in the particleboard [100].

Reddy et al. (2008) [101] have researched how glutaraldehyde as a crosslinker affects the strength and water stability of gluten fibers. The authors dissolved gluten powder in 8M aqueous urea solution with 1 wt% of sodium sulfite. The gluten fibers were dipped in the glutaraldehyde solution, dried and annealed. The authors reported improved strength and excellent water stability of the fibers by using a 0.05% glutaraldehyde solution. Chiou et al. modified gluten using citric acid [102]. The carboxylic acid groups on the acid react with the hydroxyl groups on protein to form ester bonds. With this modification, the authors produced a superabsorbent fiber material that could absorb about 78 times its weight in DI water.

1.5. Wood Bonding Adhesive Test

Adhesive bonding of solid wood, wood particles of various size and shapes and wood fibre plays a significant role in producing modern wood products. They are used in construction, furniture, and other applications. In the past, bio-based materials such as starch, protein, and pectin were mainly used to produce adhesive [103]. However, the bio-based adhesive has been replaced by petroleum-based adhesive due to its relatively low bonding strength and poor water resistances [104]. Application of the petroleum-based adhesive that contains phenol and formaldehyde has caused environmental and health concerns [105]–[108]. Besides the environmental and health issues, the depleting supply and fluctuating price of petroleum have led to renewed interests in developing renewable bio-based adhesives in recent years.

The adhesion strength of wood is critical in numerous wood products. Among the factors including adherent materials, loading conditions, and geometric design of the bond line, adhesive properties play a significant role in the strength of an adhesive bond [109]. The adhesives based on urea-formaldehyde (UF) and melamine-urea-formaldehyde (MUF) are widely used in wood panel industries. Polyvinyl acetate (PVAc) is a good alternative to the two adhesives without causing health and environmental concerns. Using nano-sized cellulose fibers to reinforce the adhesive materials and hence to increase their bond strength have been explored.

Cellulose nanofibers have been used as a reinforcement in formaldehyde-based [110]–[113] and polyvinyl acetate (PVA) adhesives [106], [114], [115]. All of these studies show increased bond properties after adding different percentages of cellulose nanofibers to the adhesives. The authors added a maximum 5% nanocellulose and studied the shear strength [106], [112]–[115] and fracture energy [110], [111] (Figure 1-19) of the adhesives. They further prepare different wood products such as wood panels [106], [110], [112], [114], [115] and particle or oriented strand

boards [111], [113] for adhesive tests. Table 1-4 summarizes the adhesives and their properties from the abovementioned studies.

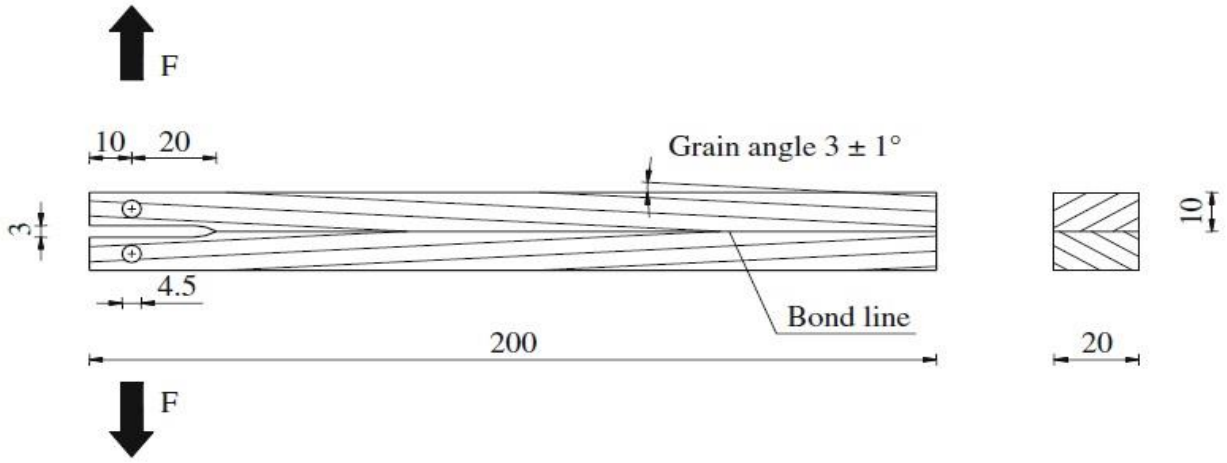

Figure 1-19. Geometry of flat double cantilever beam (DCB) specimens for fracture energy tests. [110]

Table 1-4. Cellulose reinforcement in adhesive

Adhesive resin	Filler	Filler Concentration	Evaluation methods	Mechanical Performance	Reference	Year
Polyvinyl acetate (PVA)	Cellulose nanofibrils (CNFs)	≤3 wt%	Lap joint shear strength test	Optizied at 3% of filler with WATT 91 test	López-Suevos et al.[114]	2010
Urea-formaldehyde (UF)	Cellulose nanofibrils (CNFs) Bacterial cellulose (BC)	≤2 wt%	Double cantilever beam fracture test	Maximum value at 2% of CNFs	Veigel et al.[110]	2011
Urea-formaldehyde (UF) Melmine-urea-formaldehyde (MUF)	Cellulose nanofibrils (CNFs)	≤3 wt%	Oriented strand boards (OSBs) mechanical fracture tests	Optimized at 1 wt% of CNF	Veigel et al.[111]	2012
Polyvinyl acetate (PVA)	Nanocrystalline cellulose (NCC)	≤3 wt%	Shear strength of wood joint test	Maximum value at 3% of NCC	Kaboorani et al.[106]	2012
Polyvinyl acetate (PVA)	Cellulose fibers (CFs)	≤4 wt%	Lab joint shear strength test with two different woods	Optimized at 2%CF for Poplar wood Optimized at 4%CF for Scots Pine wood	Aydemir[115]	2014
Urea-formaldehyde (UF)	Microfibrillated Cellulose (MFC)	≤5 wt%	Beech lamellas tensile shear strength test	Optimized at 3 wt% and decreased at 5 wt % of MFC	Kwon et al.[112]	2015
Urea-formaldehyde (UF)	Microfibrillated cellulose (MFC)	5% of total mass	Internal board strength	30% higher average value than UF board	Mahrdt et al.[113]	2015

1.6. Research Gap and Needs

Engineered wood, including oriented strand board (OSB), plywood, particle board, and medium-density fiberboard (MDF), represents a huge global market, which is projected to grow to $41 billion by 2022 [116] . The most commonly used adhesives to produce engineered wood are urea-formaldehyde (UF), phenol-formaldehyde (PF), and melamine-formaldehyde (MF) resins. Unfortunately, all of them contains formaldehyde - a carcinogen that posts serious human health and environmental problems [117]–[119]. Besides the formaldehyde, VOCs such as toluene or trichloroethane from synthetic adhesives can also cause human health [120] and environmental problems [121], [122]. To eliminate its health and environmental risks, there is an urgent need to develop safe and environmental-friendly adhesives that can be used to manufacture formaldehyde-free engineered wood.

Many biobased wood adhesives have been developed using soy protein [95], [108], [123], [124], starch [125]–[128], bio-based polyurethane [107] and natural gum [129]. Zein and gluten have also been studied for the uses as wood adhesives [95]–[99], [130]. However, the developed adhesives have shown drawbacks such as low bond strength and low water resistance. Cellulose nanofibers, a highly effective natural nanofiber reinforcement, have not been used in zein and gluten adhesives to increase their bond strength. Zein and gluten, together with their nanocomposites, have not been comparatively studied for their strength and weakness as adhesives. The overall goal of this research is to develop zein- and gluten-based nanocomposite adhesives that have the potential to replace traditional petroleum-based wood adhesives.

1.7. Hypothesis and Objectives

1.7.1. Hypothesis

The hypothesis of this research is that cellulose nanofibers and crosslinking agents can be used to increase the bond strength of zein- and gluten-based adhesives to a level that allows them to replace traditional petroleum-based wood adhesives.

1.7.2. Objectives

We intend to achieve the following research objectives through this master project:

Objective 1: Preparation of zein- and gluten-based adhesives containing cellulose nanofibers and crosslinking agents.

Objective 2: Investigation of the thermal and chemical properties of the adhesives

Objective 3: Study of the bond strength of the adhesives using single-lap shear samples and plywood samples.

Objective 4: Study of the bond fracture mechanism of the adhesives.

CHAPTER 2. EXPERIMENTAL DETAILS

2.1. Introduction

This chapter discusses material information, preparation of nanocomposite adhesives, preparation of single-lap shear specimens and three-layer plywood samples. Mechanical testing methods for single-lap shear test, flexural test, and internal bond test are provided. Material characterization procedures for surface morphology, chemical property, and thermal property are also discussed.

2.2. Materials

Zein (88 – 96 % of protein concentration) and sodium sulfite were purchased from Sigma-Aldrich (St. Louis, MO). Gluten was supplied by Bob's Red Mill (Milwaukie, OR) and it contained 8 wt% moisture and 1.5 wt% ash. 98% of the gluten particles were less than 212 μm. The CNCs and CNFs were manufactured by USDA Forest Products Laboratory (Madison, WI) using bleached dry eucalyptus pulp. The CNCs were prepared by sulfuric acid hydrolysis and the CNFs were produced through a multi-pass, high-pressure grinding process. The produced CNCs and CNFs were aqueous suspensions with a nanofiber concentration of 5.7 wt% and 1.8 wt%, respectively. The width and length of the CNCs are 19 ± 5 nm and 151 ± 39 nm; the dimensions for the CNFs are 20 ± 14 nm and 1030 ± 334 nm, respectively [6]. Glutaraldehyde (GTA) (49%) was purchased from EM Science. Birch plywood (1.5 mm thickness, 3 plies) was purchased from Aircraft Spruce in Corona, CA.

2.3. Preparation of Nanocomposite Adhesives Reinforced with Nanocellulose

Zein was dissolved in ethanol (85 wt%) to make a 15 wt% solution by stirring at 300 rpm at 60 ^{o}C for 30 min. A predetermined amount of the CNC or CNF suspension was added into the solution and the mixture was homogenized using an IKA T25 digital ultra-turrax homogenizer (6,000 rpm) for 5 min at room temperature. The amount of the nanofiber suspension was adjusted so that a nanofiber concentration of 1 wt%, 3 wt%, or 5 wt% in zein was achieved (based on the dry weight of both nanofiber and zein) (Figure 2-1). Gluten-based nanocomposite adhesives were prepared using the same method. A 15 wt% of gluten solution was first prepared by dissolving gluten in 8M aqueous urea containing 1 wt% of sodium sulfate reducing agent (stirring at 400 rpm at 60 ^{o}C for 30 min) (Figure 2-2). CNF was then added and the mixture was homogenized. Glutaraldehyde (2%, 4%, 6%, or 8 wt% based on gluten weight) was added to the homogenized mixture and manually stirred.

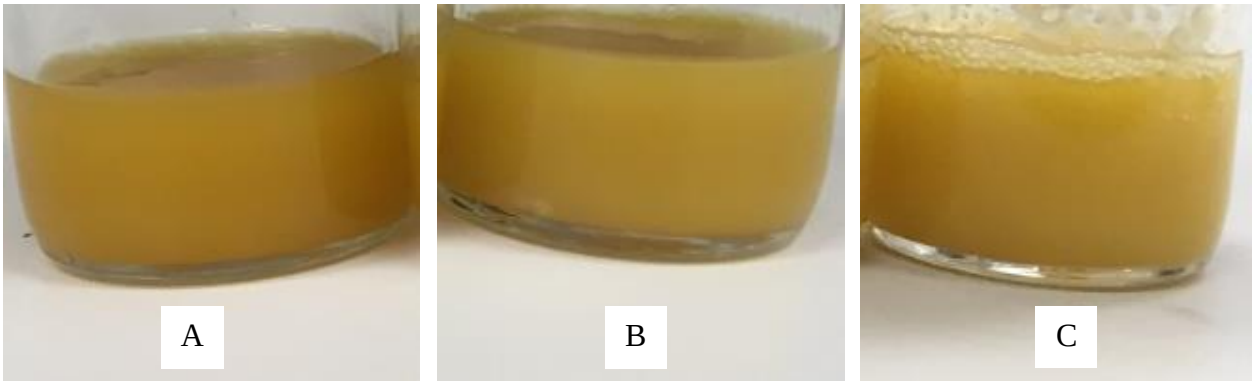

Figure 2-1. Photos of zein adhesives: (A) pure zein, (B) zein with 5% CNC, (C) zein with 5% CNF.

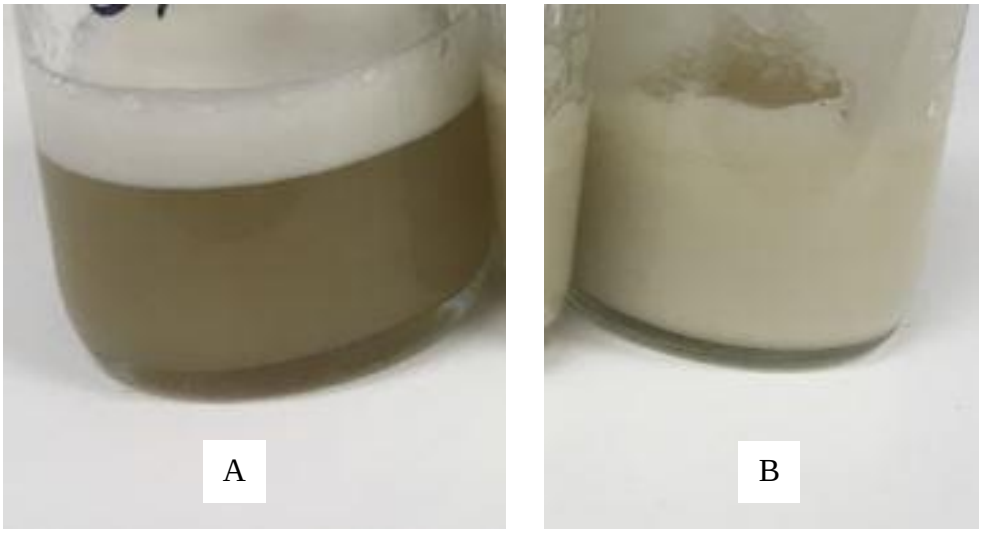

Figure 2-2. Photos of gluten adhesives: (A) pure gluten, (B) gluten with 8% CNF.

2.4. Single-Lap Shear Test

Single-lap shear test was used to study the bonding strength of the adhesives following slightly modified ASTM D5868. Wood samples (2.54 cm × 10.16 cm) were cut from the birch plywood sheets. Two samples were bonded together (same wood grain orientation) with an overlap length of 2.54 cm using one of the prepared adhesives (Figure 2-3). The adhesive was evenly applied on one sample surface (155 g/m^2) before the two were pressed and clamped together (~ 50 KPa). The adhesive was cured in an oven under different curing temperatures for 10 min. After curing, the samples were stored in a sealed plastic bag under ambient condition for 16 hours before being tested on an Instron 5567 (Norwood, MA) that was equipped with a 2 KN load cell. The samples were tested in tension mode with a crosshead speed of 2 mm/min (Figure 2-4). Seven to ten replicates were tested for each sample. The single lap shear strength was calculated using the following equation:

$$\tau_s(MPa) = \frac{F_{max}\ (N)}{A\ (mm^2)} = \frac{F_{max}\ (N)}{a \times b\ (mm^2)}$$

where τ_s is the tensile shear strength (MPa), F_{max} is the maximum load (N), A is the adherend surface area (mm^2), a is the width (mm) and b is the length (mm) of the adherend surface.

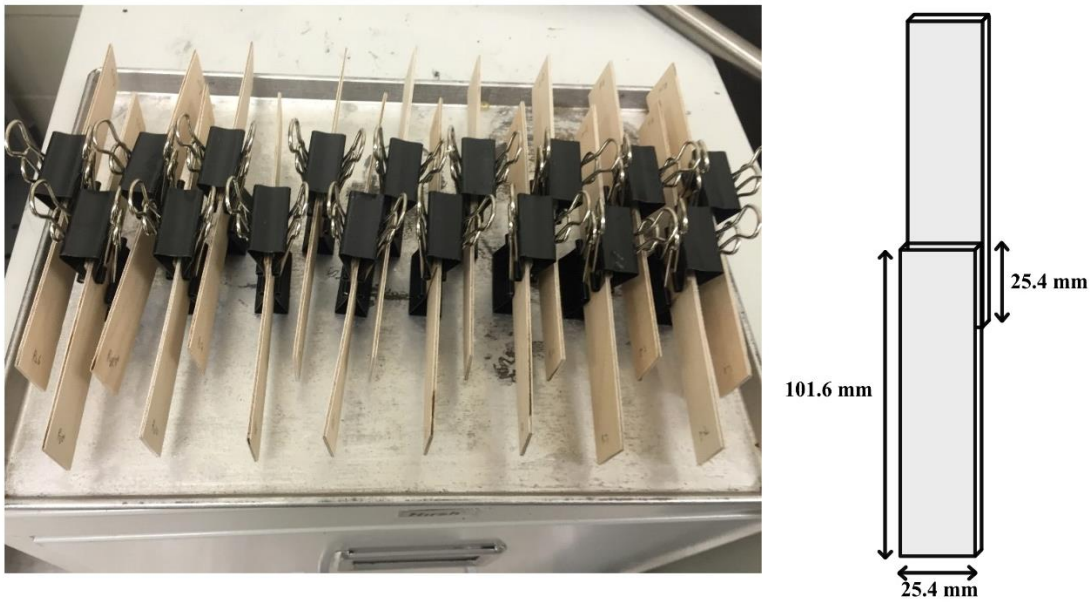

Figure 2-3. Preparation of the single-lap shear test samples and the dimensions of the samples.

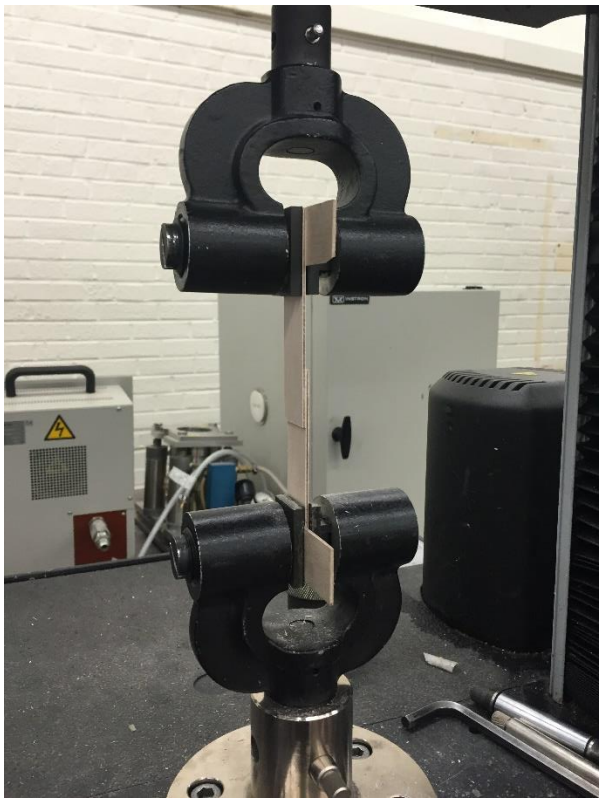

Figure 2-4. Single-lap shear test on Instron 5567.

2.5. Manufacturing of Three-layer Plywood and Sample Preparation

The birch plywood sheets were cut into 30 cm × 30 cm squares. Adhesive was evenly applied on one side of each square (about 166 g/m^2). Three squares were stacked (cross-laminated) in a 30.5 cm × 30.5 cm aluminum mold that is covered with wax paper for easy demolding (Figure 2-5). The mold was pressed using a preheated (140 ºC) hot press (Carver Model 4122, Wabash, IN) under a pressure of 1.08 MPa (10 metric tons) for 3 min and then 2 MPa (18 metric tons) for 10 min. Two laminate boards were produced using each adhesive. One board was cut into four 50 mm × 171 mm specimens for flexural testing while the other one was cut to provide one more 50 mm × 171 mm specimen and ten 50 mm × 50 mm pieces for interanal bond testing (Figure 2-6). Five of the ten 50 mm × 50 mm pieces were immersed in water for 24 hours and then dried in

ambient condition for 72 hours before they undergo the internal bond test. The other 5 specimens were tested directly without water immersion.

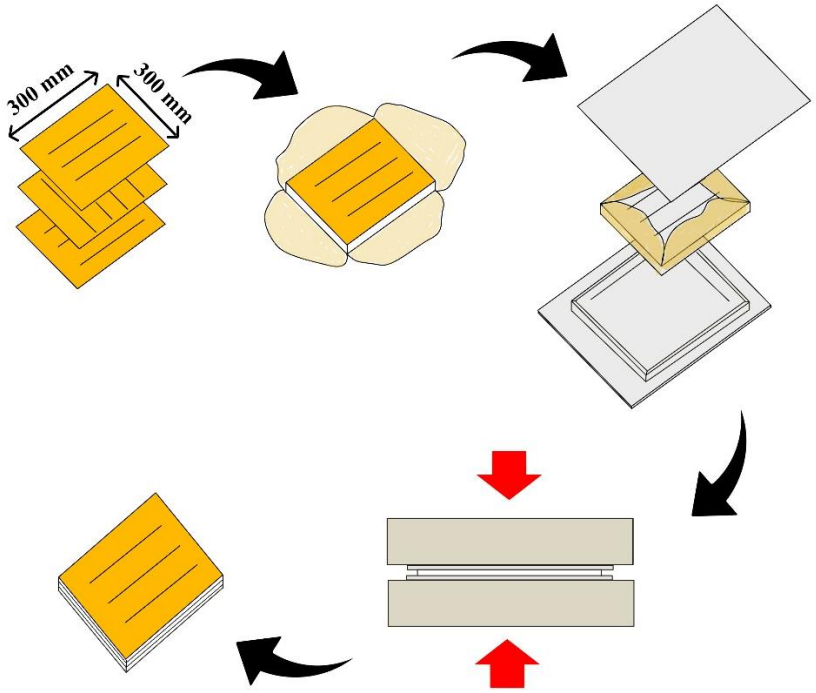

Figure 2-5. Plywood manufacturing procedure.

Figure 2-6. Photo showing three layers of birch sheets stacked in an aluminum mold before pressing.

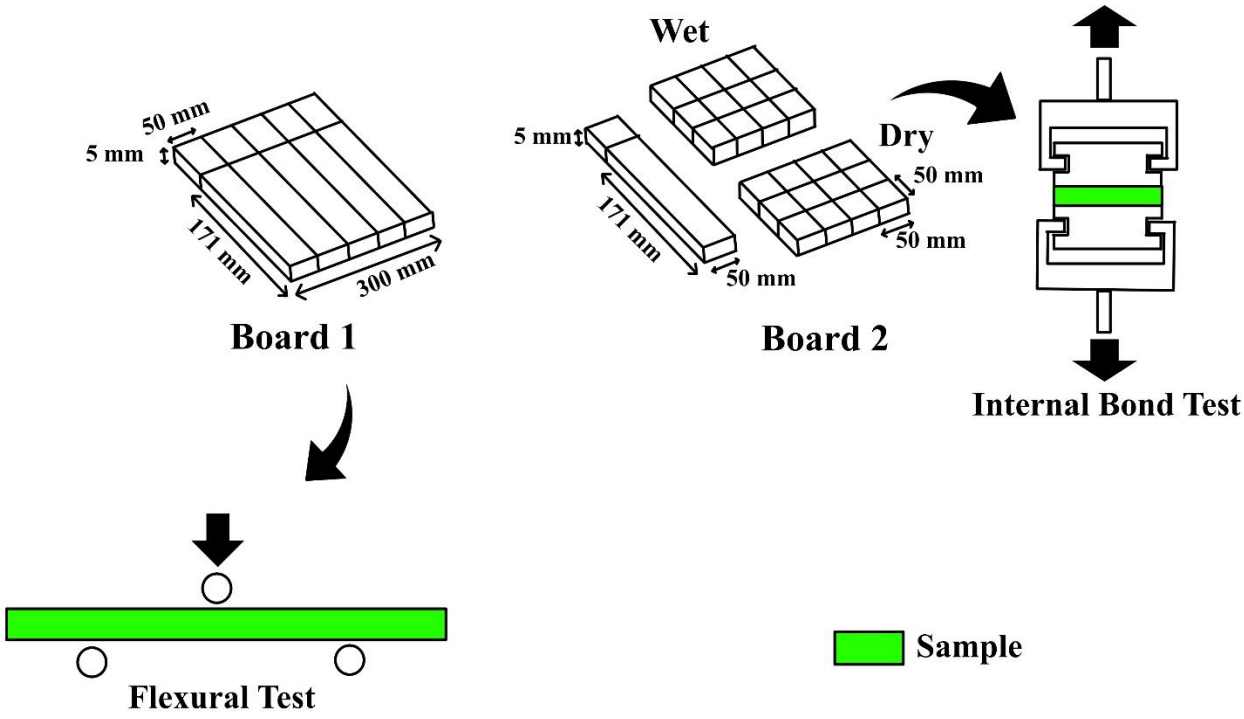

Figure 2-7. Schematic of plywood sample preparation and testing.

2.5.1. Flexural Test

Three-point bending test was used to obtain the modulus of rupture (MOR) and the modulus of elasticity (MOE) of the plywood following ASTM 1037. The specimen was placed on two support noses and the load was applied to the center of the specimen though the loading nose (Figure 2-7). The support span was 120 mm, 24 times the specimen thickness as required by ASTM 1037. The radius of each nose was 25.4 mm. The moving rate of the loading nose was 2.5 mm/min, which was calculated using the equation below:

$$\mathrm{N} = \frac{zL^2}{6d}$$

where N is the speed of the central loading nose, z is the outer fiber strain rate (z = 0.005 min^{-1}, ASTM 1037), and L and d are the support span and thickness of the specimen, respectively. The MOR was calculated by the following equation:

$$\text{MOR} = \frac{3P_{max}L}{2bd^2}$$

where P_{max} is the maximum load and b is the width of the sample. The MOE was calculated using the following equation:

$$\text{MOE} = \frac{L^3}{4bd^3}\left(\frac{\Delta P}{\Delta y}\right)$$

where $\frac{\Delta P}{\Delta y}$ is the slope of the linear portion of the load-deflection curve between 10% and 40% of the maximum load. Five replicates were tested for each formulation for the static bending test.

Figure 2-8. Three-point bending test of plywood specimen.

2.5.2. Internal Bond Test

The three-layer plywood was cut into ten pieces of 50 mm × 50 mm squares in accordance with ASTM D1037. Five pieces were tested after a water immersion process and the other five were tested as-prepared. Each sample was sandwiched betweem two aluminum loading blocks using a thermoplastic glue provided by Primeboard Masonite in Wahpeton, North Dakota (Figure 2-8). The loading blocks were preheated to melt the thermoplastic glue before making the sandwich structure. The finished samples were kept under room temperature for at least six hours without applying any pressure before they were tested. To examine water effect on the bonding strength, five squares were immersed in tap water for 24 hours and then dried under ambient condition for 72 hours before they were made into the sandwich structure. The test was performed under tension using an Instron 5567 equipped with a 30 KN load cell. The loading rate was 1 mm/min. The internal bond strength was calculated by the following equation:

$$\mathrm{I} = \frac{P_{max}}{ab}$$

where *I* is the internal bond strength, *a* and *b* are width and length of samples, respectively. Five replicates were tested for dry and water-soaked samples.

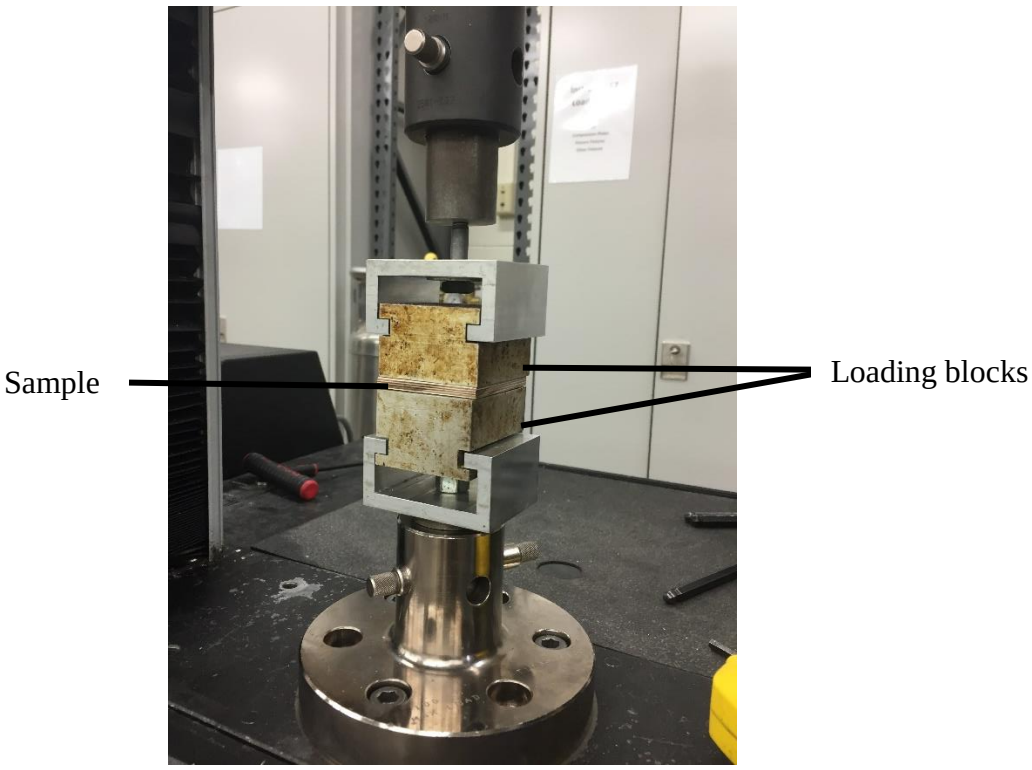

Figure 2-9. Setup of the internal bond test on Instron 5567.

2.6. Scanning Electron Microscopy

Wood samples were attached to cylindrical aluminum mounts with silver paint (SPI Products, West Chester, Pennsylvania, USA) or double-stick carbon tape (Ted Pella, Redding, California, USA), and then sputter coated (Cressington 108auto, Ted Pella, Redding, California, USA) with a conductive layer of gold. Images were obtained with a JEOL JSM-6490LV scanning electron microscope (JEOL USA, Inc., Peabody MA, USA).

2.7. Thermal Stability Analysis

Thermal properties of zein and gluten adhesives were analyzed using thermogravimetric analysis (TGA). A TA Instrument Q500 TGA (New Castle, DE) was used in this test. Several drops of each adhesive solution were placed on an aluminum pan and then put in an oven (100 ºC)

to dry/cure for 10 min. The dried adhesive was loaded into the TGA sample pan. Each sample was heated from room temperature to 600 ºC at a rate of 10 ºC/min under a continuous nitrogen flow (60 ml/min). Sample weight as a function of temperature and its first derivative was plotted for thermal stability analysis.

2.8. Fourier Transform Infrared Spectroscopy

A Thermo Scienttific Nicolet iS10 – Smart iTR (Waltham, MA) was used to evaluate the chemical composition of the zein and gluten adhesives. The dried adhesive from the last section was examined using an attenuated total reflection (ATR) accessory. Each sample was scanned 32 times over a wavelength range of 500 – 4000 cm^{-1} with a resolution of 4 cm^{-1}.

2.9. Wood Moisture Content Test

The moisture content of the birch plywood sheets would affect its mechanical properties. Before use, all the purchased wood sheets were stored in a laboratory room whose temperature and humidity are very stable. The moisture content of the sheets after 72 hours of storage was measured. The mass of a sheet (30 cm × 30 cm) was measured before and after being dried in an oven for 24 hours at 105^0C [131], [132]. The moisture content was calcualted using the equation below:

$$\text{MC}\ (\%) = \frac{(M_I - M_D)}{M_I} \times 100\%$$

where MC is moisture content, M_I is the initial mass of the sample and M_D is the sample mass after drying. Three replicates were tested. The average moisture content of the sheets was found to be 4.5 %.

2.10. Statistical Analysis

Statistical analysis was performed in this research to ensure that we interpreted the data correctly, determined accurate relationships/trends and made right conclusions. The result data were analyzed with analysis of variance (ANOVA) using statistical software Minitab. The analysis was carried out to investigate how the mechanical and physical properties of the adhesives were affected by the curing temperature and the nanocellulose and GTA crosslinking contents in the adhesives.

CHAPTER 3. PROPERTY STUDIES OF ZEIN- AND GLUTEN-ADHESIVES

3.1. Introduction

The results from single-lap shear, three-point bending, and internal bond tests for different adhesive formulations are discussed in this chapter. Statistical analysis of the results is performed and optimal formulations and processing conditions are derived. Fracture bond surfaces are studied using microscopy to determine failure mechanisms. Thermal and chemical properties of the adhesives are investigated and discussed.

3.2. Single-Lap Shear Test

3.2.1 Zein-based Nanocomposite Adhesives

The effects of CNC content and adhesive curing condition on the lap shear strength and modulus of the zein/CNC adhesives are shown in Figure 3-1. For the samples that are cured at 60 ^{o}C under vacuum, the lap shear strength shows a clear increasing trend with the CNC content. The sample containing 5% CNCs shows the highest strength. The samples cured at the same temperature but under atmospheric pressure exhibit the same increasing trend. However, the samples cured under atmospheric pressure possess higher strength than the samples cured under vacuum (except for the sample containing 5% CNCs). The reason is postulated to be that under vacuum more adhesive is absorbed into the porous structure of the wood sample and therefore less is left on the interface for bonding. The viscosity of the adhesive increases with increasing CNC content. At 5% CNC content, the viscosity of the adhesive is high enough to hinder the absorption process, which causes sufficient amount of adhesive to be left on the interface to form a strong bond. Because vacuum causes lower bonding strength and also leads to higher production cost, it was not used in the following adhesive curing process.

Curing the adhesive at 100 ^{o}C led to higher strength than at 60 ^{o}C under that same CNC contents. High temperature promotes denaturing and crosslinking of protein molecules, which increases the bonding strength. Under this new curing temperature, the strength also increases with increasing CNC content, although to a smaller degree compared with the first two series of samples discussed above. When the curing temperature is too high, i.e., 180 ^{o}C, both wood and zein can undergo some forms of thermal degradation, which can be observed from the browning of the samples. Therefore, the strength of the adhesives cured at 180 ^{o}C is lower than that of the samples cured at 100 ^{o}C. It also appears that at 180 ^{o}C the bonding strength is negatively impacted by the low thermal stability of CNCs, which is indicated by the sample's decreasing strength with increasing CNC content (at 3% and 5% of CNCs). In terms of modulus (Figure 3-1B), although it is also affected by the CNC content and the curing conditions, their influences are much smaller. This can be at least partially attributed to the nature of modulus, i.e., it is a value that is calculated using only the strains and stresses within the initial sample deformation range. The representative stress-strain curves of the zein/CNC adhesives are shown in Figure 3-2. The strengths of all the samples increase constantly with strain without showing any sign of yielding or strain hardening.

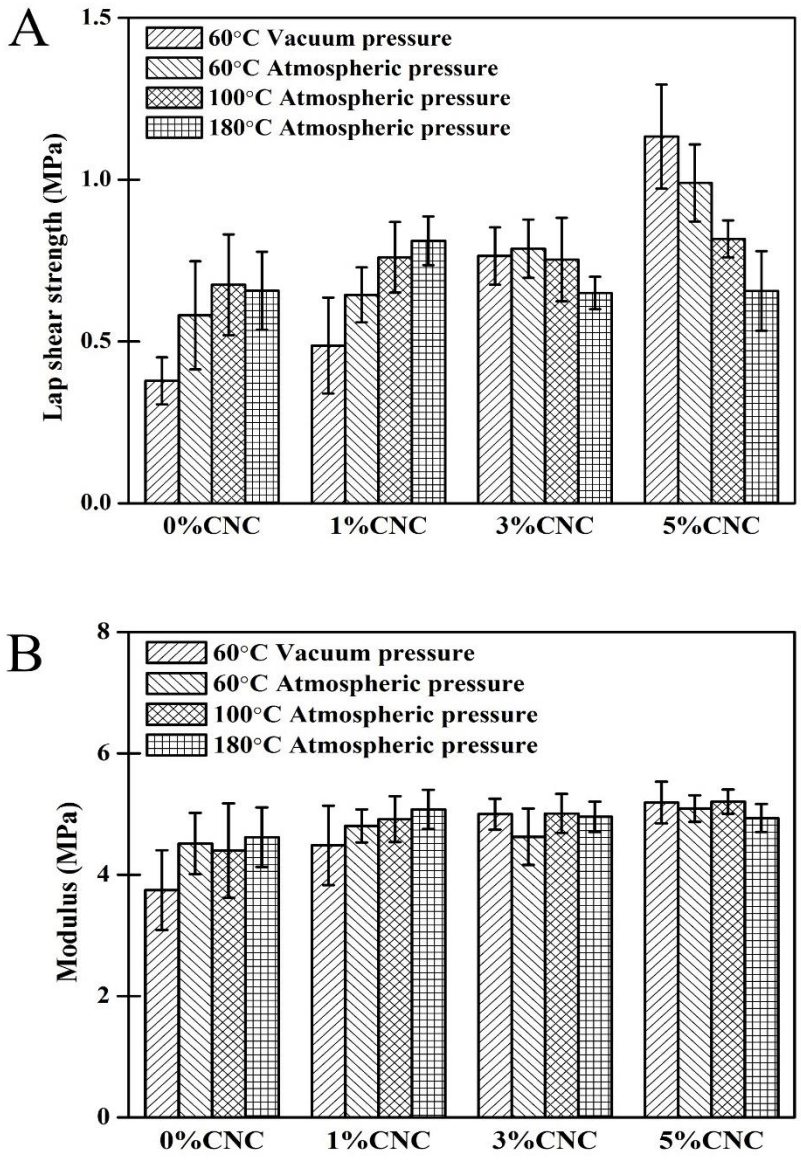

Figure 3-1. Single-lap shear test results of the zein/CNC adhesives prepared under different curing conditions. (A) lap shear strength, (B) modulus.

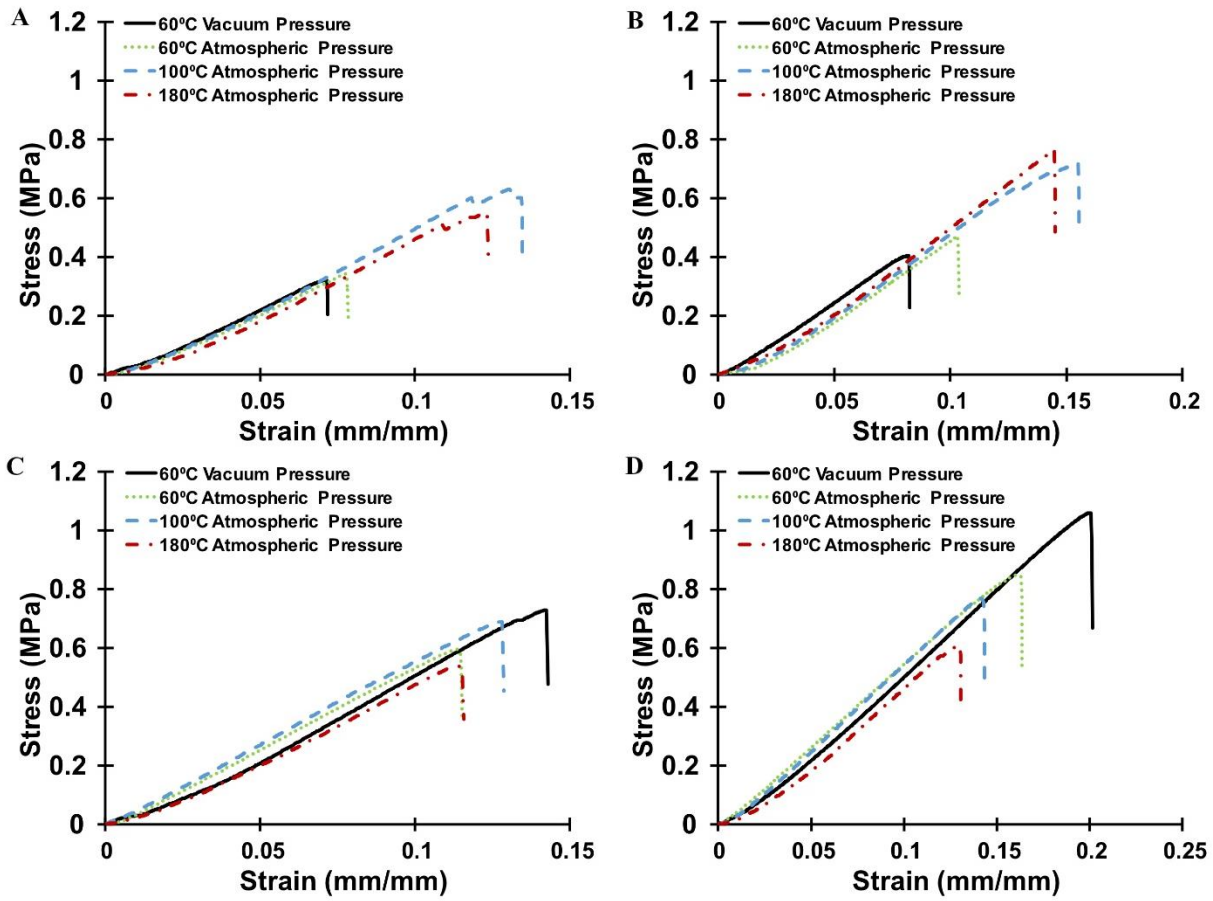

Figure 3-2. Representative stress-strain curves of the zein/CNC nanocomposite adhesives with (A) 0%, (B) 1%, (C) 3%, and (D) 5% CNCs cured under different conditions.

Figure 3-3 shows the effects of CNF content and adhesive cure conditions on the bonding strength of the zein/CNF adhesives. The many relationships found in the zein/CNC adhesives still apply to the new nanocomposite adhesives. For instance, the lap shear strength increases with increasing CNF content for the adhesives cured at 60°C (vacuum or atmospheric pressure) and 100°C, and higher temperature and pressure in general causes higher strength and modulus. 180°C is still too high a temperature for adhesive curing, which leads to decreased bond strength. Figure 3-4 shows the representative stress-strain curves of the zein/CNF adhesives, which are similar to those of the zein/CNC adhesives.

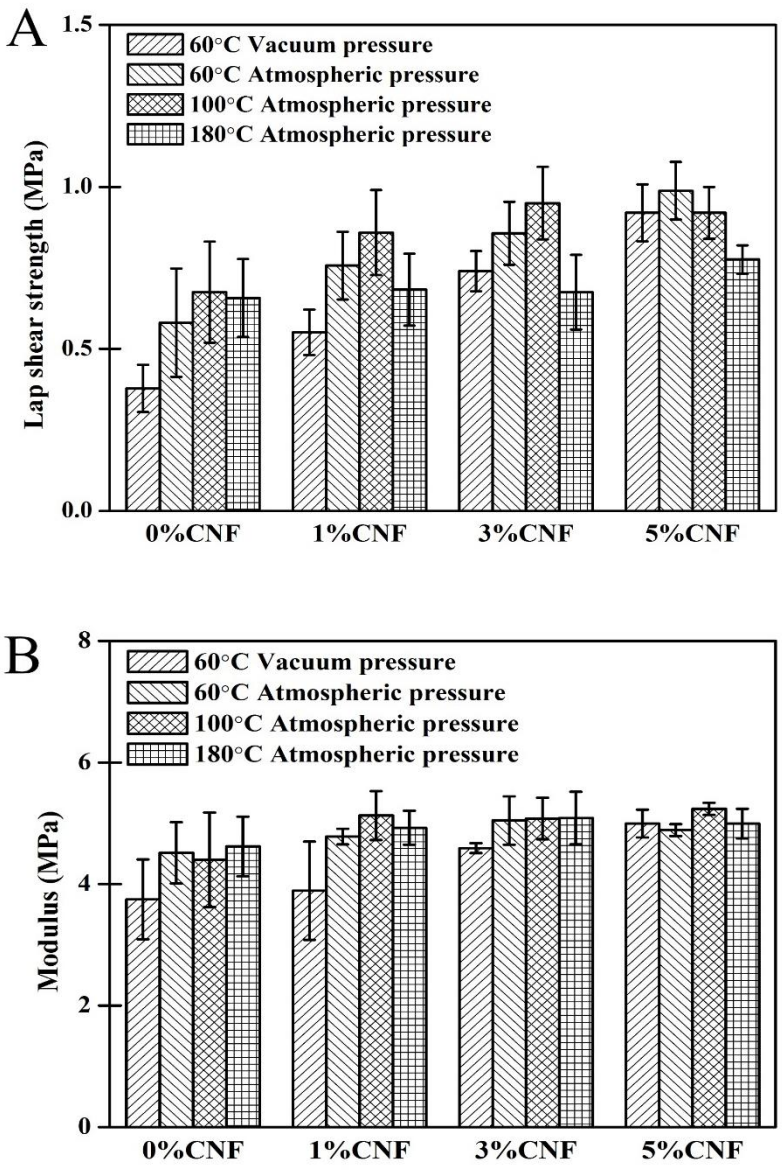

Figure 3-3. Single-lap shear test results of the zein/CNF adhesives prepared under different curing conditions. (A) lap shear strength, (B) modulus.

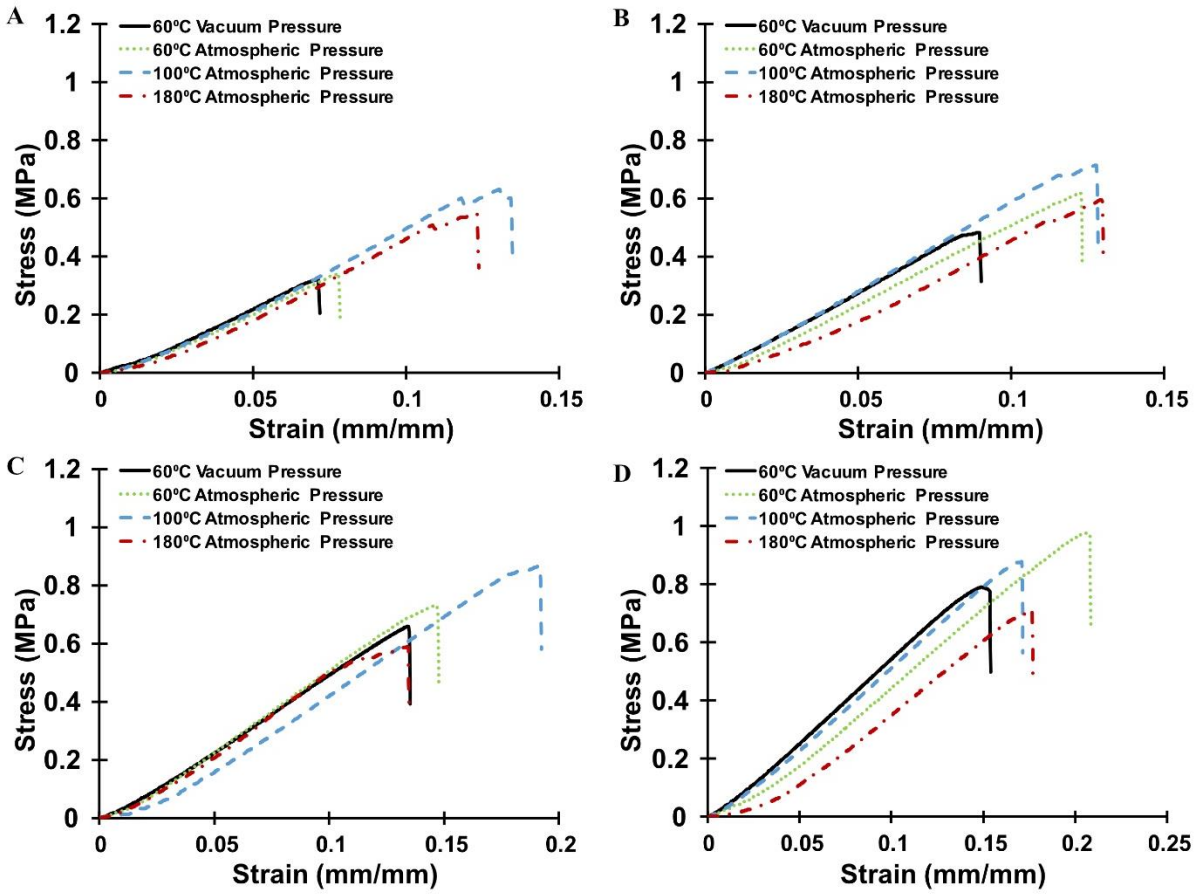

Figure 3-4. Representative stress-strain curves of the zein-CNF nanocomposite adhesives containing (A) 0%, (B) 1%, (C) 3%, and (D) 5% CNFs and cured under different conditions.

Tables 3-1 and 3-2 summarize the single-lap shear strength and modulus for all the zein/CNC and zein/CNF formulations. In many cases, under the same nanofiber content and curing conditions, the zein/CNF adhesives appear to show slightly higher properties than the zein/CNC adhesives. This can be attributed to CNF's larger aspect ratio, which facilitates higher load sharing on the nanofibers and results in stronger reinforcement effect.

Table 3-1. Single-lap shear strength and modulus of zein/CNC adhesives.

			Neat zein	1% CNC	3% CNC	5% CNC
60 ºC VP	Shear strength(MPa)	Avg	0.378	0.487	0.764	1.133
		SD	0.073	0.148	0.089	0.161
	Modulus (MPa)	Avg	3.748	4.485	5.000	5.192
		SD	0.657	0.653	0.255	0.344
60 ºC AP	Shear strength (MPa)	Avg	0.581	0.644	0.787	0.990
		SD	0.167	0.085	0.090	0.119
	Modulus (MPa)	Avg	4.515	4.806	4.626	5.091
		SD	0.503	0.272	0.464	0.219
100 ºC AP	Shear strength (MPa)	Avg	0.675	0.760	0.753	0.817
		SD	0.156	0.109	0.129	0.057
	Modulus (MPa)	Avg	4.399	4.917	5.012	5.206
		SD	0.778	0.380	0.322	0.199
180 ºC AP	Shear strength (MPa)	Avg	0.657	0.811	0.650	0.656
		SD	0.120	0.075	0.050	0.123
	Modulus (MPa)	Avg	4.621	5.078	4.956	4.936
		SD	0.492	0.323	0.252	0.230

VP: vacuum pressure, SD: standard deviation, AP: atmospheric pressure.

Table 3-2. Single-lap shear strength and modulus of zein/CNF adhesives.

			Neat zein	1% CNF	3% CNF	5% CNF
60 ºC VP	Shear strength (MPa)	Avg	0.378	0.551	0.740	0.920
		SD	0.073	0.070	0.062	0.088
	Modulus (MPa)	Avg	3.748	3.890	4.591	4.996
		SD	0.657	0.809	0.082	0.228
60 ºC AP	Shear strength (MPa)	Avg	0.581	0.757	0.857	0.988
		SD	0.167	0.104	0.097	0.089
	Modulus (MPa)	Avg	4.515	4.782	5.048	4.890
		SD	0.503	0.128	0.398	0.098
100 ºC AP	Shear strength (MPa)	Avg	0.675	0.859	0.950	0.920
		SD	0.156	0.131	0.112	0.080
	Modulus (MPa)	Avg	4.399	5.128	5.079	5.240
		SD	0.778	0.401	0.342	0.099
180 ºC AP	Shear strength (MPa)	Avg	0.657	0.683	0.675	0.776
		SD	0.120	0.111	0.115	0.044
	Modulus (MPa)	Avg	4.621	4.927	5.087	4.996
		SD	0.492	0.277	0.435	0.243

VP: vacuum pressure, SD: standard deviation, AP: atmospheric pressure.

To examine the effects of crosslinkers on the adhesive strength, different concentrations of glutaraldehyde (GTA) was added to neat zein and the zein adhesive containing 3% CNF. Figure 3-5 compares the lap shear strength and modulus of the samples as a function of GTA content. For the neat zein adhesive, the variations in the shear strength are small regardless of the content of GTA. The modulus of the adhesive was decreased by 22% after the addition of GTA. For the zein adhesive containing 3% CNF, the strength was reduced by ~ 13% with the addition of 3% GTA and remained almost constant at higher GTA concentrations. The modulus was reduced by 18% at 1% GTA content and remained almost constant afterwards. GTA is a known protein crosslinker and the reason that it cannot improve the adhesive strength in this study has not been fully understood yet [133]. It may be due to the ethanol solvent in the zein adhesives that hinders the crosslinking reactions between the functional groups of zein and GTA. Due to the ineffectiveness of GTA crosslinking, GTA is therefore not used any further in the zein adhesives in this study.

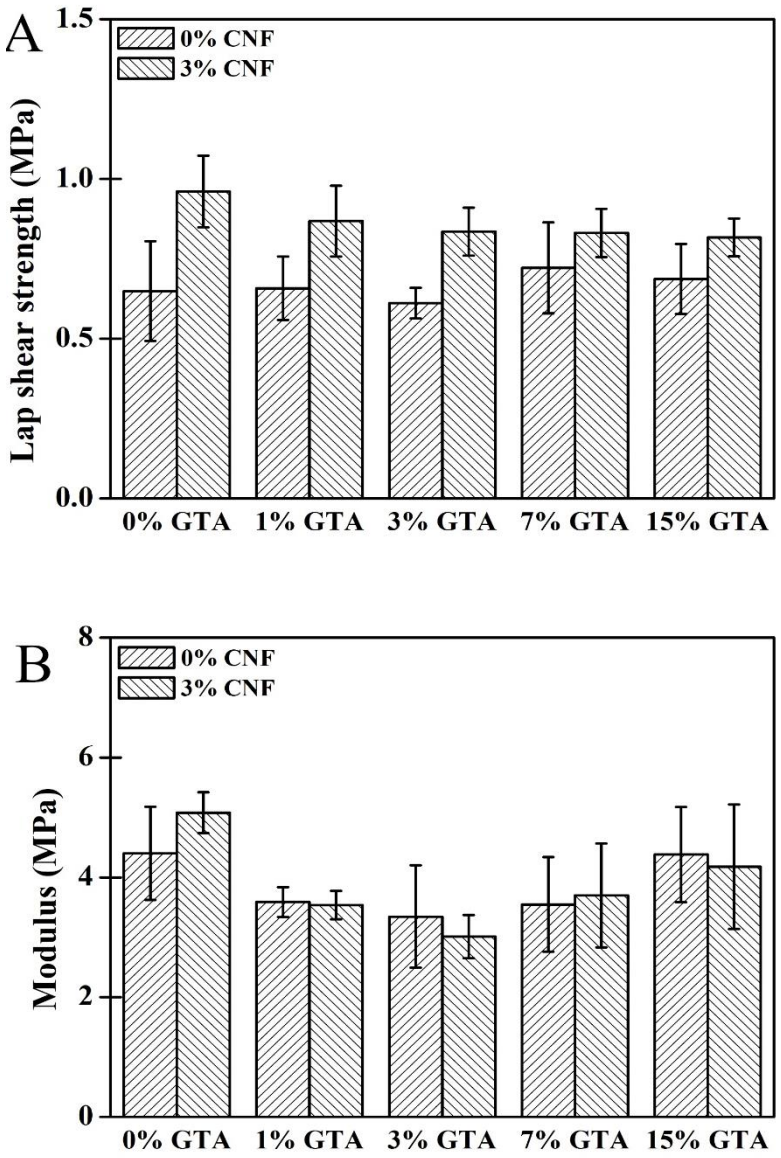

Figure 3-5. Single-lap shear test results of the zein adhesives containing different concentrations of GTA. The samples were cured at 100^{o}C under atmospheric pressure. (A) lap shear strength, (B) modulus.

3.2.2. Gluten-based Nanocomposite Adhesives

The effects of curing conditions on the single-lap shear strength and modulus of the gluten adhesives are shown in Figure 3-6. For each adhesive formulation, temperature appears to show negligible effect on the shear strength and modulus, even though the color of the wood turned

brown for the sample cured at 180ºC. In contrast, for the zein adhesives, the shear strength of the sample cured at 180ºC is lower than that cured at 100ºC. The different results for the zein and gluten adhesives are probably due to the different protein structures between gluten and zein.

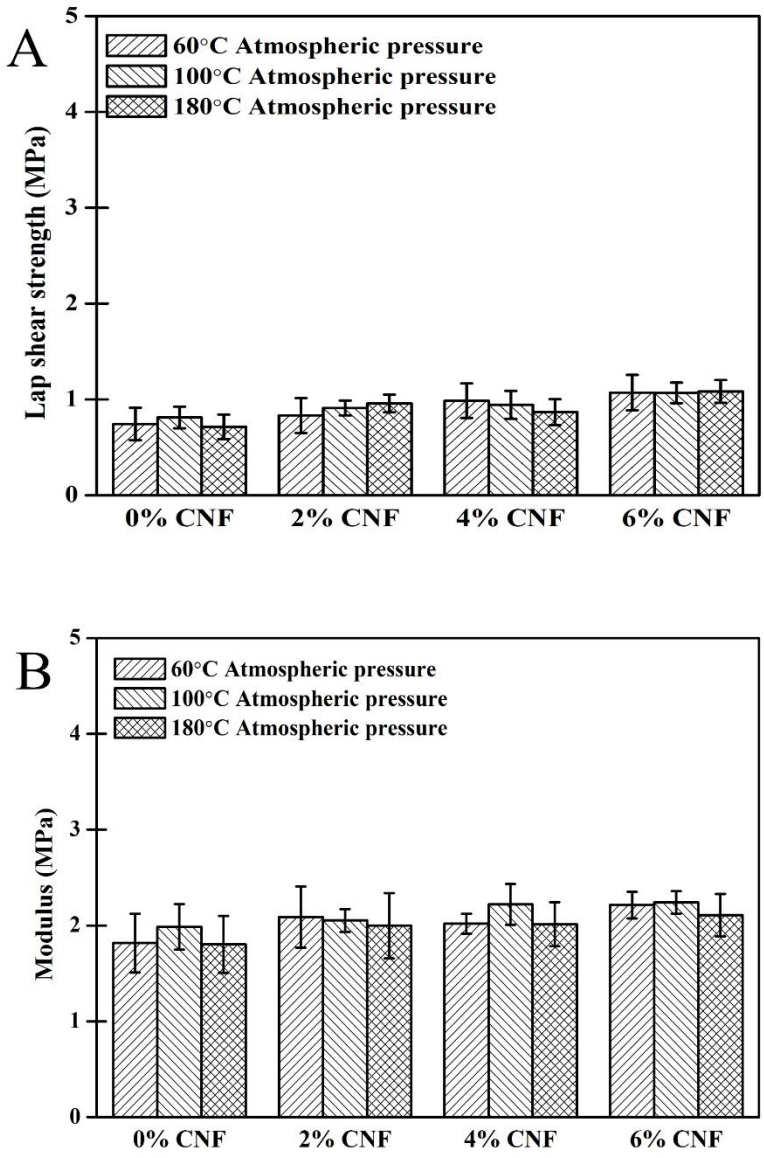

Figure 3-6. Single lap-shear test results of the gluten/CNF adhesives prepared under different curing conditions. (A) lap shear strength, (B) modulus.

Figure 3-7 shows the lap shear strength and modulus of gluten/CNF adhesives that was crosslinked with different contents of GTA and cured at 100ºC under atmospheric pressure. For the adhesives that contain no GTA, their strength and modulus increase only mildly with increasing CNF content. The strength of the adhesive containing 8% CNFs is 44% higher than that of the adhesive containing no CNFs. GTA, on the other hand, shows a much stronger effect on the strength and modulus of the adhesives. For the samples containing no CNFs, the addition of 2% GTA more than double the lap shear strength; at 4% (and higher) GTA concentration, the strength is increased further by 56%; the strength levels off at high GTA contents, i.e., 4%, 6% and 8%. For the adhesives containing CNFs, the concentration of GTA does not appear to have a strong influence on the strength. All four concentrations, i.e., 2%, 4%, 6% and 8%, cause a similar, large increase in the strength.

The reason for the less pronounced effect of CNFs on gluten than on zein is not clear yet. We hypothesize that it can be due to the weaker interaction between CNFs and gluten than between CNFs and zein. In this study gluten adhesive was prepared using urea as the solvent. Urea is a known hydrogen bond breaking agent that can prevent hydrogen bonding between CNFs and gluten and therefore reduces the interactions between the two phases. Moreover, this weakened interaction also causes less homogeneous dispersion of CNFs in the gluten matrix. Both would lead to reduced reinforcement to the gluten adhesives. Because of the weak effect of the CNFs on the bonding strength of gluten, it would make more economic sense to just use the GTA to improve its properties. The addition of 4% GTA alone leads to one of the highest lap shear strengths (Figure 3-7A). Overall, 2% CNFs in combination with 2-8% GTA produces the best results. Due to the small strength differences between the samples containing different concentrations of GTA, a lower GTA concentration would be preferred industrially.

Figure 3-7B shows that without using GTA, the modulus of gluten increases slightly with increasing CNF content. The modulus of the gluten containing 8% CNFs is 13% higher than that of the neat gluten. The effect of GTA on the modulus is more pronounced: a 25% increase is achieved at 2% GTA concentration for the gluten containing no CNFs. Higher contrations seems to have negligible further effect. For the gluten containing CNFs, the increase in modulus after adding GTA is smaller. For instance, a 14% increase is observed at 2% GTA concentration for the gluten containing 2% CNFs. Overall, varing GTA and CNF concentrations shows only small effects on the modulus. Figure 3-8 shows the representative stress-strain curves for the gluten/CNFs adhesives. All the samples demonstrate an elastic deformation behavior and the effects of GTA at different concentrations can be clearly identified.

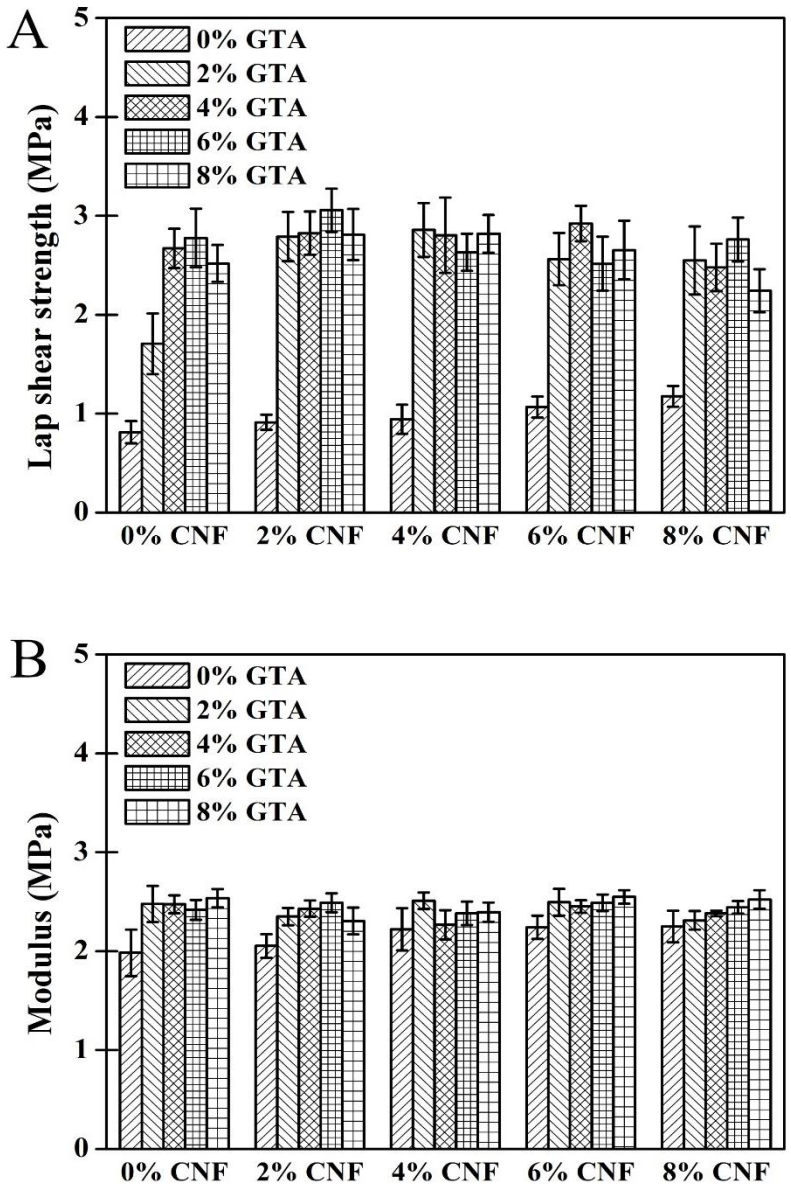

Figure 3-7. Single-lap shear test results of the gluten/CNF adhesives prepared under different crosslinker concentrations. (A) lap shear strength, (B) modulus.

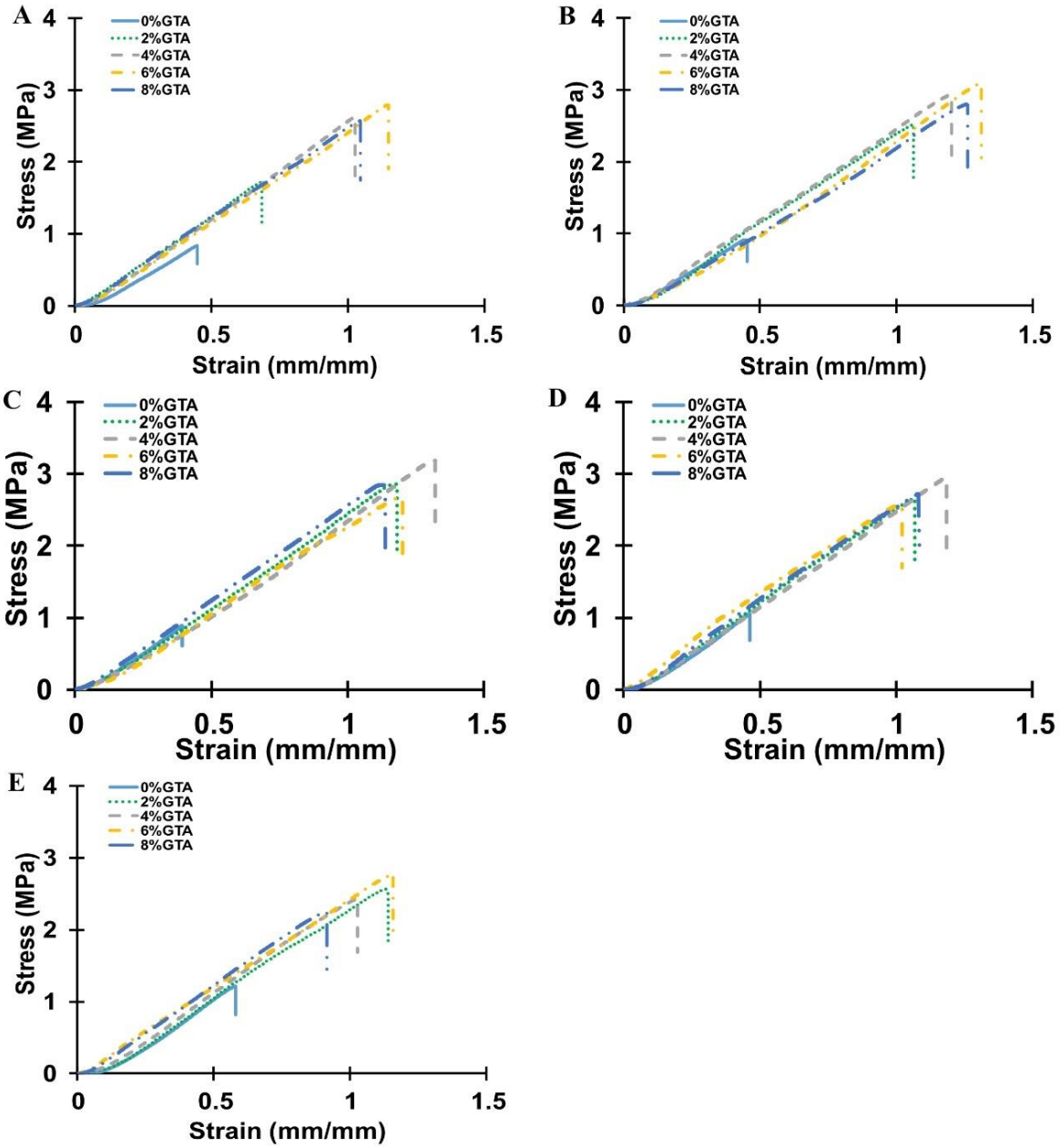

Figure 3-8. Representative stress-strain curves of the gluten/CNF nanocomposite adhesives containing (A) 0%, (B) 2%, (C) 4%, (D) 6%, and (E) 8% CNFs and crosslinked using different concentrations of GTA.

Table 3-3. Single-lap shear strength and modulus of gluten/CNF adhesives.

			0% CNF	2% CNF	4% CNF	6% CNF	8% CNF
0% GTA	Shear strength (MPa)	Avg	0.813	0.912	0.943	1.068	1.176
		SD	0.113	0.077	0.146	0.107	0.106
	Modulus (MPa)	Avg	1.984	2.053	2.221	2.241	2.250
		SD	0.236	0.120	0.214	0.119	0.160
2% GTA	Shear strength (MPa)	Avg	1.707	2.791	2.858	2.563	2.550
		SD	0.307	0.250	0.273	0.265	0.345
	Modulus (MPa)	Avg	2.477	2.350	2.509	2.495	2.312
		SD	0.183	0.087	0.084	0.135	0.093
4% GTA	Shear strength (MPa)	Avg	2.672	2.825	2.804	2.923	2.479
		SD	0.200	0.218	0.381	0.179	0.240
	Modulus (MPa)	Avg	2.475	2.430	2.267	2.453	2.382
		SD	0.091	0.082	0.147	0.063	0.027
6% GTA	Shear strength (MPa)	Avg	2.777	3.057	2.631	2.517	2.761
		SD	0.297	0.219	0.188	0.273	0.221
	Modulus (MPa)	Avg	2.418	2.490	2.384	2.490	2.443
		SD	0.100	0.094	0.118	0.085	0.064
8% GTA	Shear strength (MPa)	Avg	2.519	2.811	2.819	2.655	2.244
		SD	0.186	0.259	0.190	0.296	0.218
	Modulus (MPa)	Avg	2.535	2.305	2.395	2.550	2.522
		SD	0.092	0.136	0.098	0.068	0.094

GTA: glutaraldehyde, SD: standard deviation.

3.3. Statistical Analysis of Single-Lap Shear Test

3.3.1. Zein-based Nanocomposite Adhesives

Figure 3-9 shows the statistical analysis results of lap shear strength for the samples containing different contents of CNCs and cured under different conditions. As shown in the main effects plot, both curing temperature and CNC content influence the shear strength. The shear strength increases with increasing CNC content. The property also increases with increasing temperature before it decreases at 180°C. The points on the normal probability plot form a nearly linear pattern, indication that the distribution of the strength data set is normal. The interaction plot shows an interaction between CNC content and the curing conditions because the lines are not

parallel. The shear strength of the specimen cured under 60ºC/vacuum is lower compared to the specimens prepared under atmospheric pressure (60ºC, 100ºC and 180ºC) at low CNC concentrations, i.e., 0% and 1%. However, at 5% CNC concentration, the shear strength is higher for the specimen prepared under vacuum than under atmospheric pressure.

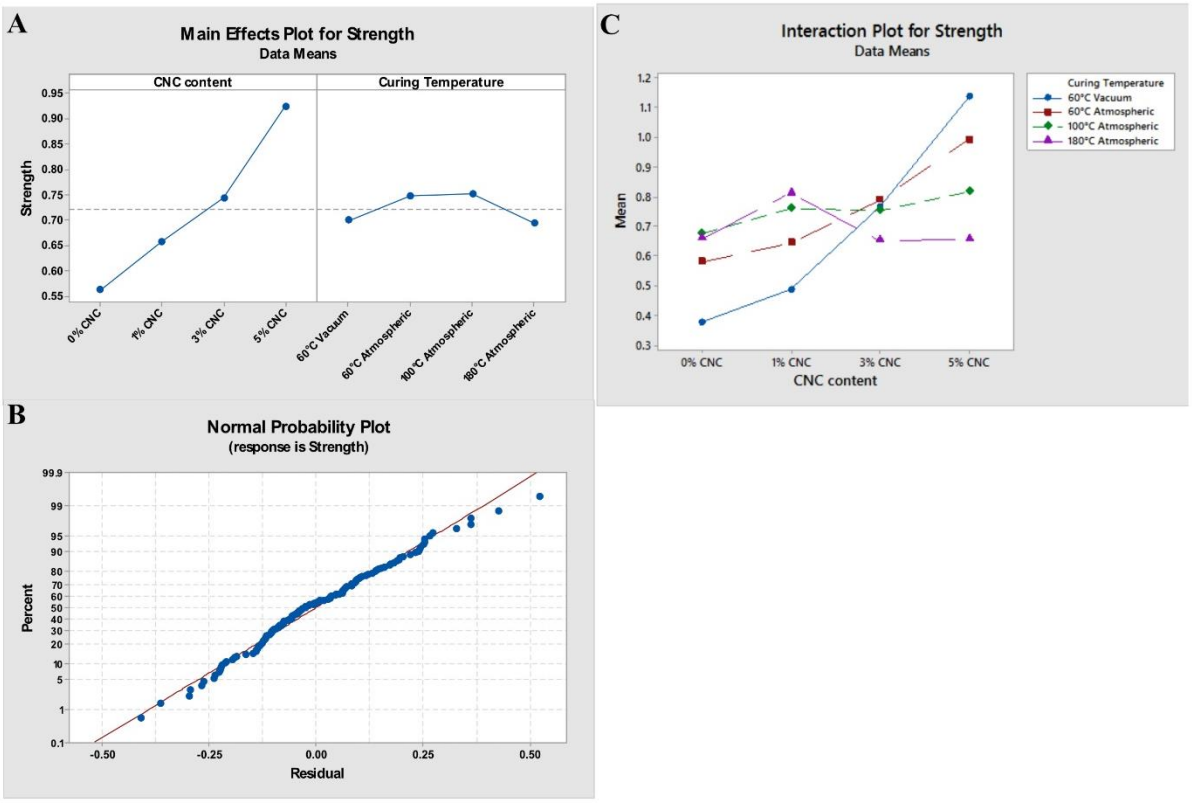

Figure 3-9. Statistical analysis of single-lap shear strength of the zein/CNC nanocomposite adhesives. (A) Main effects plot, (B) normal probability plot, and (C) interaction plot.

Table 3-4 shows the results of ANOVA analysis for the shear strength of the zein/CNC adhesives. The CNC content and adhesive curing temperature are the two analyzed factors. As shown in the table, the P-values of the curing temperature and the CNC content are less than 0.05, which indicates that both have significant effects on the shear strength. The coefficient of

determination R^2, an indicator of how close the experimental data to the fitted regression line, equals 74.37% (adjusted R^2 = 70.94%).

Table 3-4. ANOVA analysis results for the shear strength of zein/CNC nanocomposite adhesives.

Source	DF	Adj SS	Adj MS	F-Values	P-Value
Curing Temp	3	0.110	0.036	2.73	0.047
CNC Content	3	1.744	0.581	43.00	0.000
Error	112	1.514	0.013		
Total	127	5.910			

DF: Degree of freedom, Adj SS: Adjusted sum of squares, Adj MS: Adjusted mean squares.

The modulus of the zein/CNC adhesives was similarly analyzed. The effects of the CNC content and curing temperature on the modulus resemble that on the shear strength (Figure 3-10). The normal probability plot also shows that the distribution of the modulus data is normal. The interaction plot for the modulus shows that there exists an interaction between the CNC content and the curing conditions.

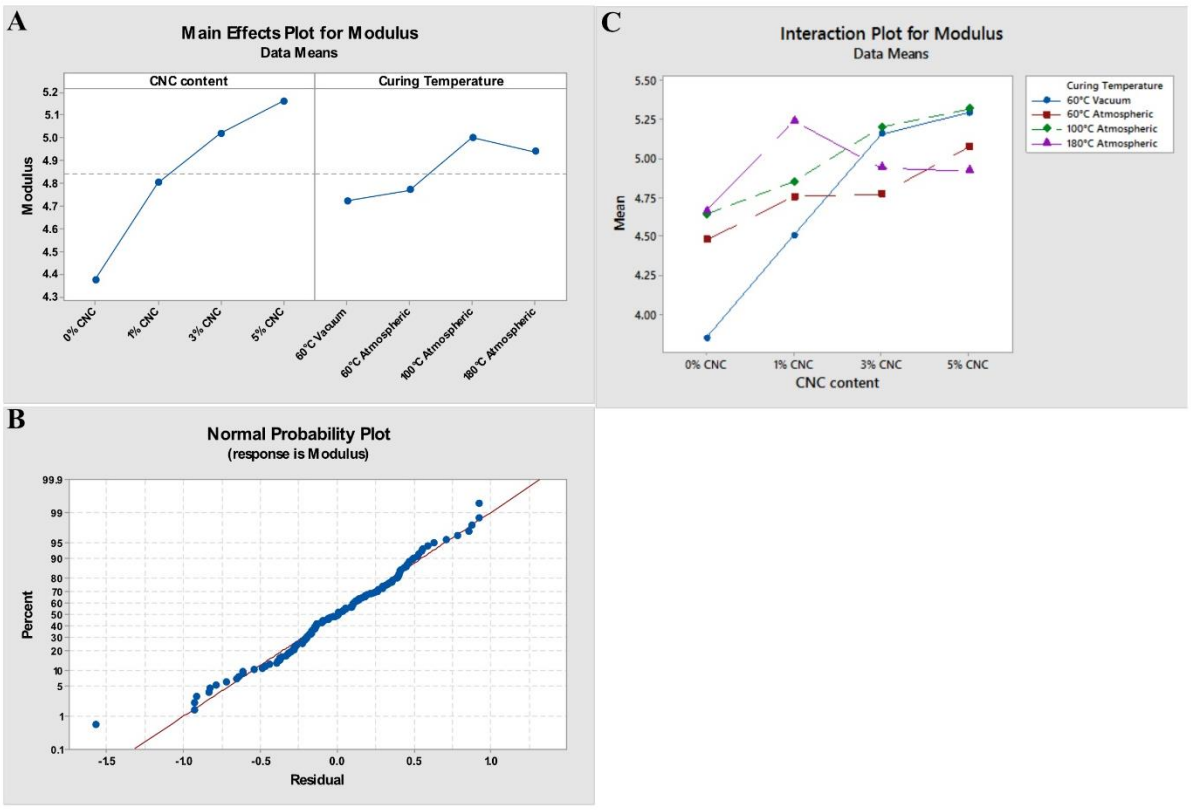

Figure 3-10. Statistical analysis of modulus of the zein/CNC nanocomposite adhesives. (A) Main effects plot, (B) normal probability plot, and (C) interaction plot.

The ANOVA analysis results for the modulus of the zein/CNC adhesives are summarized in Table 3-5. The P-values for both curing temperature and CNC content are less than 0.05, indicating that they are significant factors for the modulus. R^2 equals 52.02% (adjusted $R^2 = 45.59\%$) in this analysis.

Table 3-5. ANOVA analysis results for the modulus of zein/CNC nanocomposite adhesives.

Source	DF	Adj SS	Adj MS	F-Values	P-Value
Curing Temp	3	1.919	0.6397	4.15	0.008
CNC Content	3	9.678	3.2261	20.92	0.000
Error	112	17.268	0.1542		
Total	127	35.988			

DF: Degree of freedom, Adj SS: Adjusted sum of squares, Adj MS: Adjusted mean squares.

The single-lap shear strength and modulus of the zein/CNF nanocomposite adhesives were also statistically analyzed. Figure 3-11A confirms that the shear strength constantly increases with increasing CNF content and an optimal curing temperature, i.e., 100°C, exists for the strength. Figure 3-11B shows that the strength data set have a largely normal distribution. The interaction plot for the shear strength shows that there exists an interaction between the CNF content and the curing conditions.

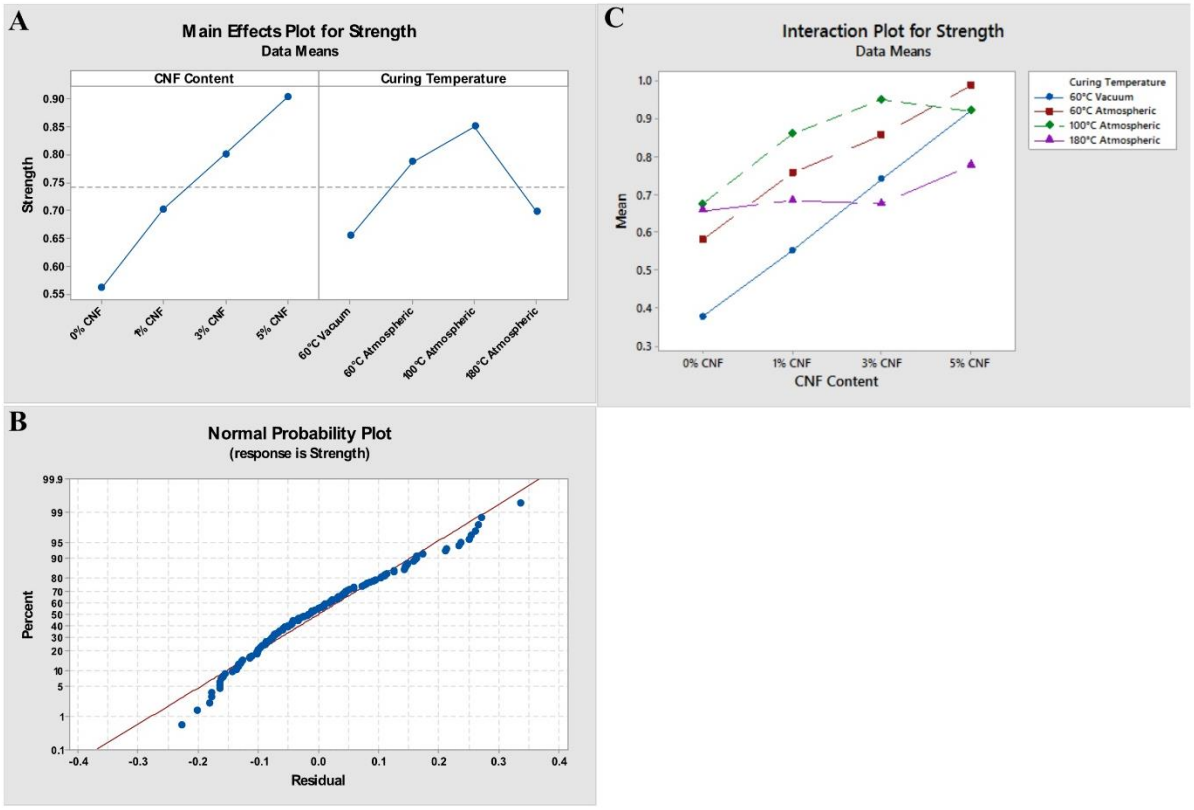

Figure 3-11. Statistical analysis of single-lap shear strength of the zein/CNF nanocomposite adhesives. (A) Main effects plot, (B) normal probability plot, and (C) interaction plot.

Table 3-6 shows the ANOVA results for the shear strength of the zein/CNF adhesives. The two factors, i.e., curing temperature and CNF content, show zero P-values, suggesting their strong influences on the strength property. The model accuracy is R^2=73.64% or adjusted R^2=70.11%.

Table 3-6. ANOVA analysis results for the shear strength of zein/CNF nanocomposite adhesives.

Source	DF	Adj SS	Adj MS	F-Values	P-Value
Curing Temp	3	0.8295	0.2765	25.57	0.000
CNF Content	3	1.7977	0.5992	55.41	0.000
Error	112	1.2111	0.0108		
Total	127	4.5949			

DF: Degree of freedom, Adj SS: Adjusted sum of squares, Adj MS: Adjusted mean squares.

The main effects plot in Figure 3-12A shows that the modulus of the zein/CNF adhesives is also significantly affected by the CNF content and the curing temperature. The modulus constantly increases with the CNF content while the temperature shows an optimal value of 100°C. The normal probability plot in Figure 3-12B shows that the modulus has a largely normal distribution. The interaction plot for the modulus shows the existence of interactions between the CNF content and the curing conditions.

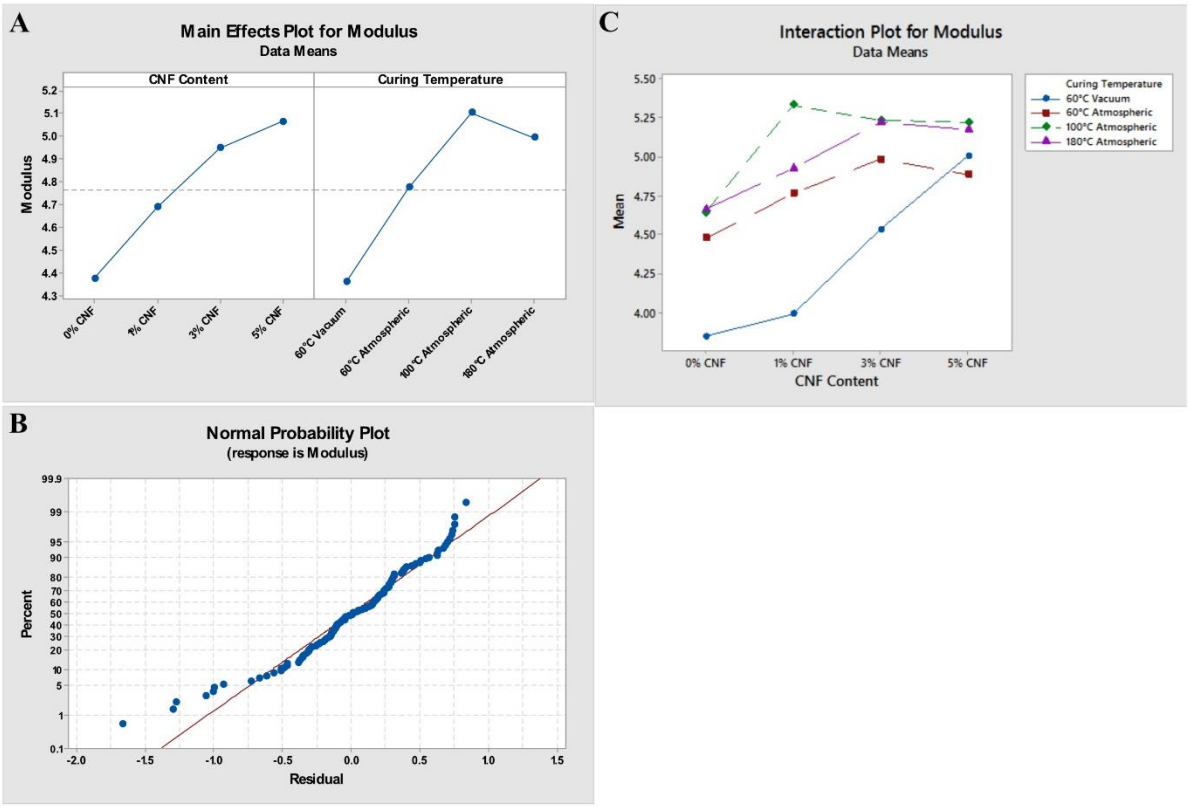

Figure 3-12. Statistical analysis of the modulus of the zein/CNF nanocomposite adhesives. (A) Main effects plot, (B) normal probability plot, and (C) interaction plot.

Table 3-7 lists the ANOVA analysis results of the modulus data. The P-values of both curing temperature and CNF content are zero, thus both are significant. The model accuracy is R^2=52.36% or adjusted R^2=45.97%.

Table 3-7. ANOVA analysis results for the modulus of zein/CNF nanocomposite adhesives.

Source	DF	Adj SS	Adj MS	F-Values	P-Value
Curing Temp	3	11.516	3.8385	19.83	0.000
CNF Content	3	8.148	2.7161	14.03	0.000
Error	112	21.680	0.1936		
Total	127	45.503			

DF: Degree of freedom, Adj SS: Adjusted sum of squares, Adj MS: Adjusted mean squares.

3.3.2. Gluten-based Nanocomposite Adhesives

The single-lap shear strength and modulus of the gluten/CNF adhesives were also statistically analyzed using the same software tools. The main effects and normal probability plots for the shear strength is shown in Figure 3-13. CNF content and GTA content are the two main effects. Figure 3-13A confirms the observation in Section 3.1.2 that 2% CNFs or GTA causes a large strength increase. At higher concentrations, neither of them shows strong effect on the property. The normal probability plot in Figure 3-13B proves the data distribution is normal. The interaction plot indicates an interaction between the CNF content and the GTA content.

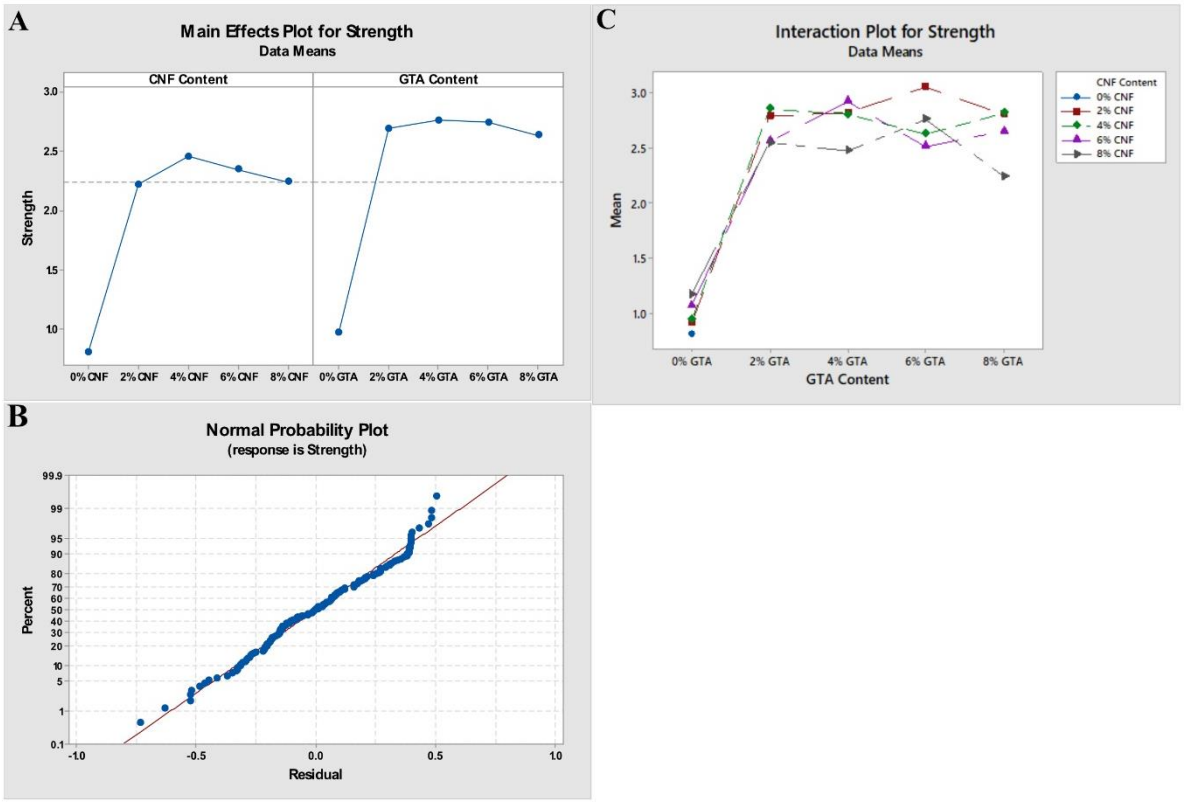

Figure 3-13. Statistical analysis of the shear strength of the gluten/CNF nanocomposite adhesives. (A) Main effects plot, (B) normal probability plot, and (C) interaction plot.

The results from ANOVA analysis about the strength data are summarized in Table 3-8. The P-values for the CNF content and the GTA content are less than 0.05; thus, both factors are significant. The accuracy of the model is R^2=90.02% or adjusted R^2=89.47%.

Table 3-8. ANOVA analysis results for the shear strength of the gluten/CNF adhesives.

Source	DF	Adj SS	Adj MS	F-Values	P-Value
CNF Content	4	1.111	0.2777	3.94	0.005
GTA Content	4	75.437	18.8592	267.35	0.000
Error	144	10.158	0.0705		
Total	152	101.820			

DF: Degree of freedom, Adj SS: Adjusted sum of squares, Adj MS: Adjusted mean squares.

The modulus of the gluten/CNF adhesives were similarly analyzed. Figure 3-14A shows that both CNF content and GTA content are strong factors affecting the modulus. Both lead to large property increase at low contents and the property levels off at higher contents. The normal probability plot demonstrates that the first few and last few points depart from the reference fitted line, but many other data points still fit the normal distribution model.

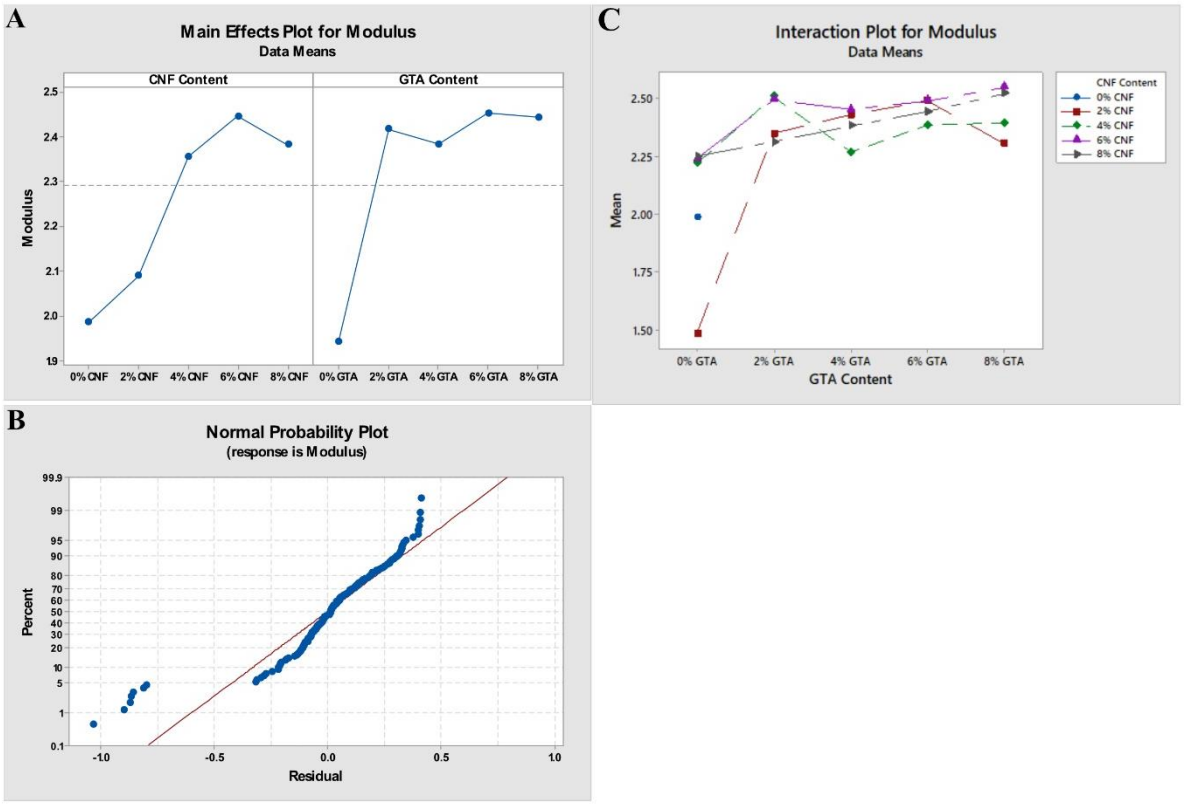

Figure 3-14. Statistical analysis of the modulus of the gluten/CNF nanocomposite adhesives. (A) Main effects plot, (B) normal probability plot, and (C) interaction plot.

The modulus data were also analyzed using ANOVA and the results are summarized in Table 3-9. The P-values for both factors, CNF and GTA content, is less than 0.05; thus, they are both significant. The accuracy of model is given by R^2=47.44% and adjusted R^2=44.54%.

Table 3-9. ANOVA analysis results for the modulus of gluten/CNF nanocomposite adhesives.

Source	DF	Adj SS	Adj MS	F-Values	P-Value
CNF Content	4	1.916	0.47908	6.95	0.000
GTA Content	4	5.409	1.35237	19.61	0.000
Error	145	10.001	0.06898		
Total	153	19.029			

DF: Degree of freedom, Adj SS: Adjusted sum of squares, Adj MS: Adjusted mean squares.

3.4. Mechanism of Bond Failure

3.4.1. Visual Observation

To understand wood bonding and bond failure mechanisms, many factors need to be considered including characteristics of wood, wood surface morphology and chemistry, adhesive characteristics, and the interaction between adhesive and wood [134]. Bonding is a complex process and the dominant mechanism of adhesion varies depending on the abovementioned factors [135]. The six sources of bonding strength are mechanical interlocking, adsorption or wetting, electrostatic forces, diffusion, chemical bonding, and interphases and weak boundary layers [136], [137]. The mechanical interlocking theory, which was first proposed by Mc Bain and Hopking [138], can be applied on porous or rough substrates such as wood, paper, fabrics, and some anodized aluminum substrates [139]. The mechanical interlocking mechanism could be attributed to the adhesive penetrating into the irregularities or pores of the substrate and interlocking before the adhesive solidification. Besides the mechanical interlocking theory, many studies have been conducted on adsorption and wetting mechanisms on wood substrate [140]; the diffusion theory also gained attention for wood bonding with thermoplastic adhesives in wood plastic composites [141], and another type of diffusion theory, which is a concept about penetrating monomer on a molecular level for thermosetting resins, have also been studied [142].

Microscopic studies of bond fracture surfaces are very useful in determining bond failure mechanism. Figure 3-15 shows the digital photos of the zein adhesive bonds after the single-lap shear test. Although the bonding strength is increased by the addition of CNCs or CNFs, the bond surfaces show negligible macroscale morphological difference. All the surfaces are relatively smooth without any sign of wood damage (i.e., adhesive failure). Figure 3-16 compares the gluten adhesive bonds after the single-lap shear test. The two bonds containing no GTA (A and B) show similar relatively smooth surfaces. The two bonds containing GTA (C and D) exhibit coarser surfaces because some wood material was removed from the surface during debonding (i.e., cohesive failure). The transition from adhesive failure to cohesive failure is due to significantly increased bond strength after the addtion of GTA and CNFs. This surface morphology change is in agreement with the bond strength trend determined by the single-lap shear test. The cohesive failure of the gluten-based adhesives indicates that the strength of the bond exceeds that of wood itself, so it shoud be safe to use them to bond wood fieces to make engineered wood products.

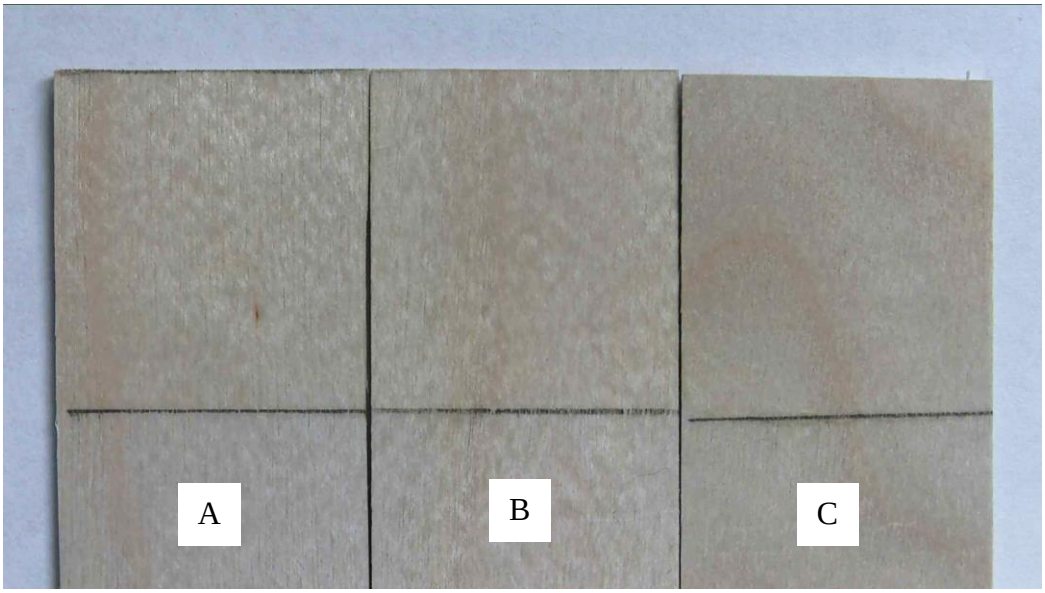

Figure 3-15. Photo of fracture bond surfaces: (A) pure zein; (B) zein with 5% CNCs; (C) zein with 5% CNFs.

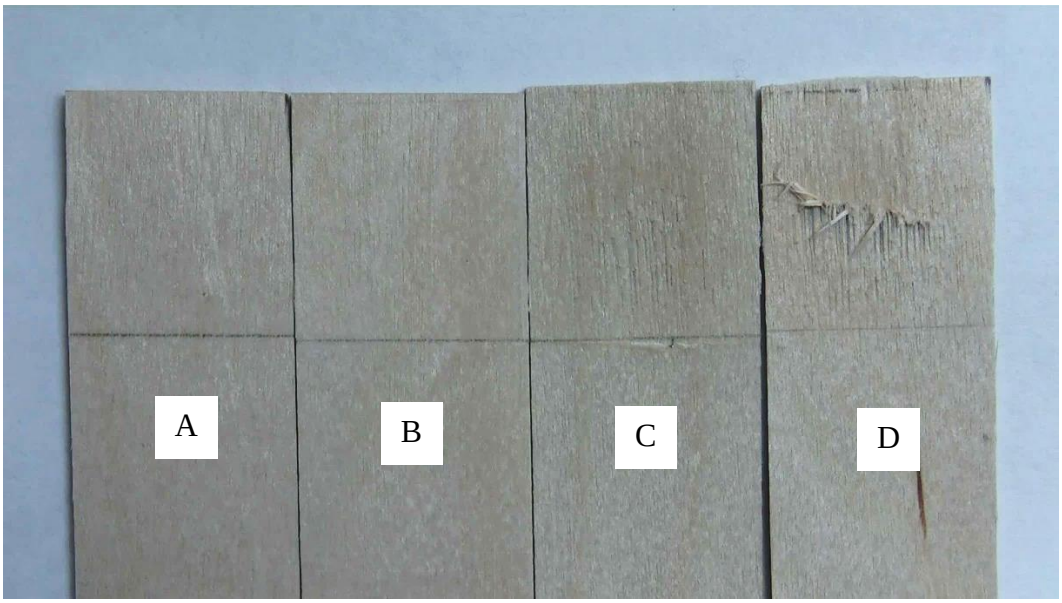

Figure 3-16. Photo of fracture bond surfaces: (A) pure gluten; (B) gluten with 2% CNFs; (C) gluten with 6% GTA; (D) gluten with 2% CNFs and 8% GTA.

3.4.2. SEM Study

The morphology of the fracture surfaces was also studied using SEM to understand the microscale surface deformation. In the single-lap shear test results, the bond strength of the zein adhesives is shown to increase after the addition of CNFs. Figure 3-17 compares the fracture surfaces of the pure zein and the zein/CNFs nanocomposite adhesives. The latter clearly shows fibril-like structure being pulled out from the fracture surface. These fibrils are postulated to be CNF bundles and/or CNFs coated with a zein surface layer. These high strength cellulose nanofibers act as nano-reinforcement to share the load from the zein matrix and increase the strength and modulus of the bond.

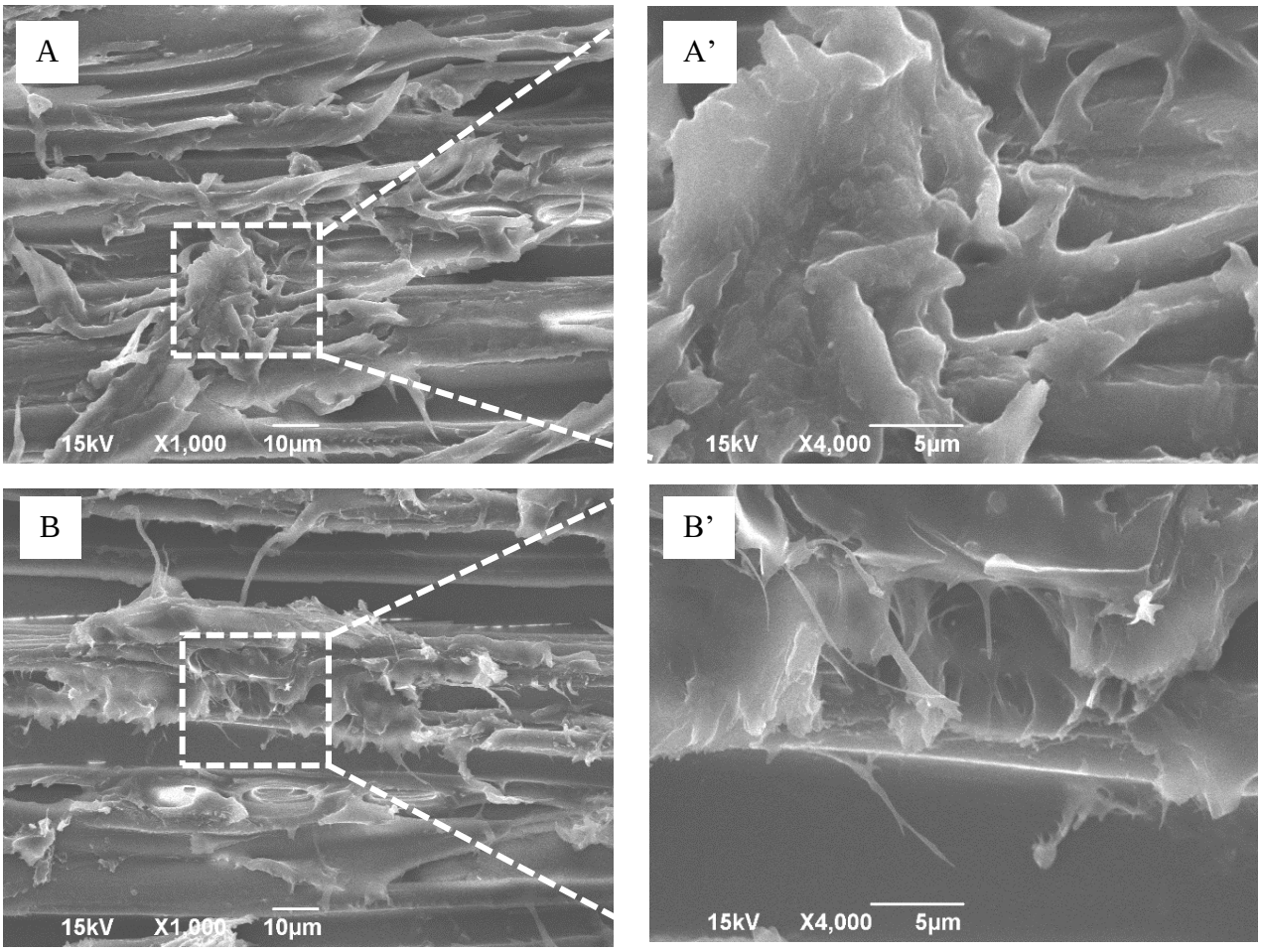

Figure 3-17. SEM images of the fracture bond surfaces after the single-lap shear tests: (A and A') pure zein; (B and B') zein containing 3% CNFs.

For the gluten-based adhesives, Figure 3-18 compares the SEM images of a clean wood surface and the fracture surfaces with pure gluten, gluten with 2% GTA, and gluten with 8% GTA. A general trend is that the surfaces become increasingly rough, as also demonstrated in the digital photos. The increase in surface roughness is due to the presence of the fractured gluten adhesive and peeled wood material, which becomes more obvious on the SEM images taken under a higher magnification (Figure 3-19). In figure A the clean wood surface, wood cells can be clearly seen being cut open and horizontal, cylindrical lumens are exposed, which produces a porous grooved surface. The surface gets rougher with pure gluten as sheet-like gluten adhesive can be seen being

pulled/peeled from the surface when the adhesive bond fails (Figure 3-19B). The sheet-like structure becomes increasingly extensive with the addition of 2% and 8% GTA, as shown in figures C and D. The pulled/peeled sheets appear to stand on the surface and the height of the sheets increases with the increasing GTA content. This observation agrees with the shear strength trend of the adhesive, which also increases with the crosslinker content. GTA reacts with and crosslinks gluten and therefore the adhesive's strength and modulus are increased. During the lap shear test, this reinforced adhesive can bear a higher load without fracture, and this higher load can lead to longer adhesive layer and surface wood material being pulled off the surface.

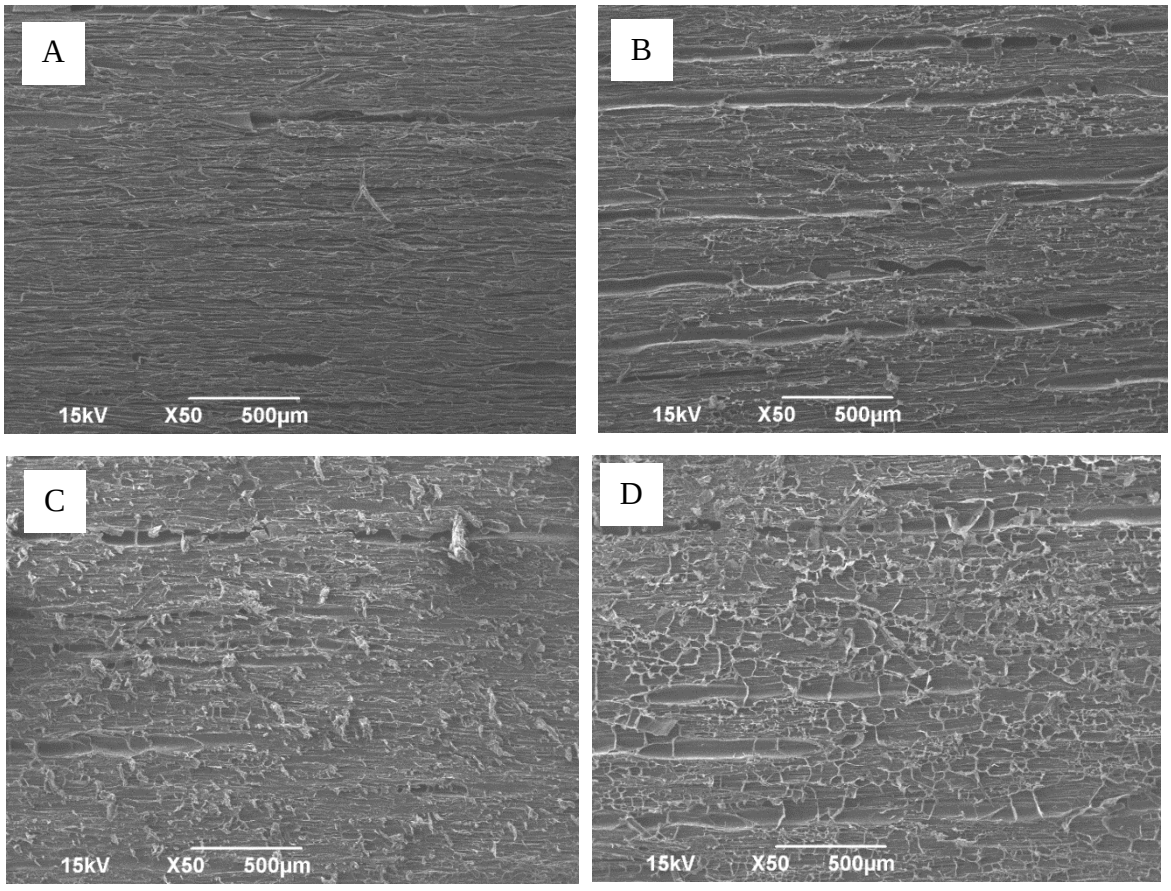

Figure 3-18. SEM images of the fracture bond surfaces after the single-lap shear test. (A) clean wood surface; (B) gluten; (C) gluten with 2% GTA; (D) gluten with 8% GTA.

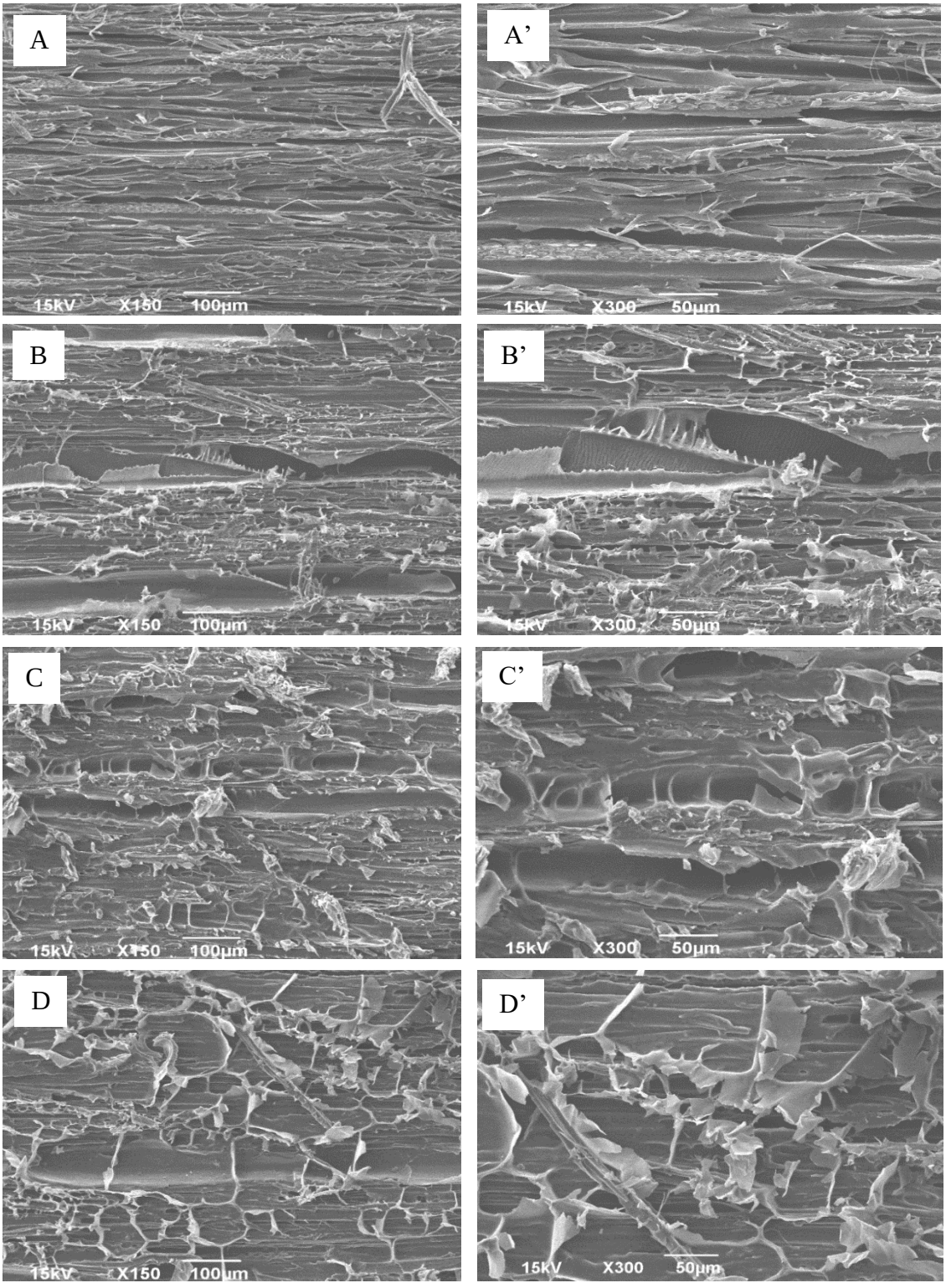

Figure 3-19. SEM images of the fracture bond surfaces after the single-lap shear tests. (A and A') clean wood surface; (B and B') gluten; (C and C') gluten with 2% GTA; (D and D') gluten with 8% GTA.

SEM images at high magnification are also compared between the pure gluten and the gluten containing 3% CNFs (Figure 3-20). On the fracture surface of the gluten/CNFs adhesive, some fibril-like features can be seen being pulled out from the surface, suggesting the presence of CNFs. By contrast, the fracture surface of the pure gluten appears to be smooth without any similar features. The CNFs in the gluten function as nano-reinforcement that increases the strength of the adhesive. Similar reinforcement effects have been found in many other polymer matrixs including polyethylene oxide (PEO) [6], alginate [49], poly(acrylamide) [50], and polyvinyl acetate (PVA) [106].

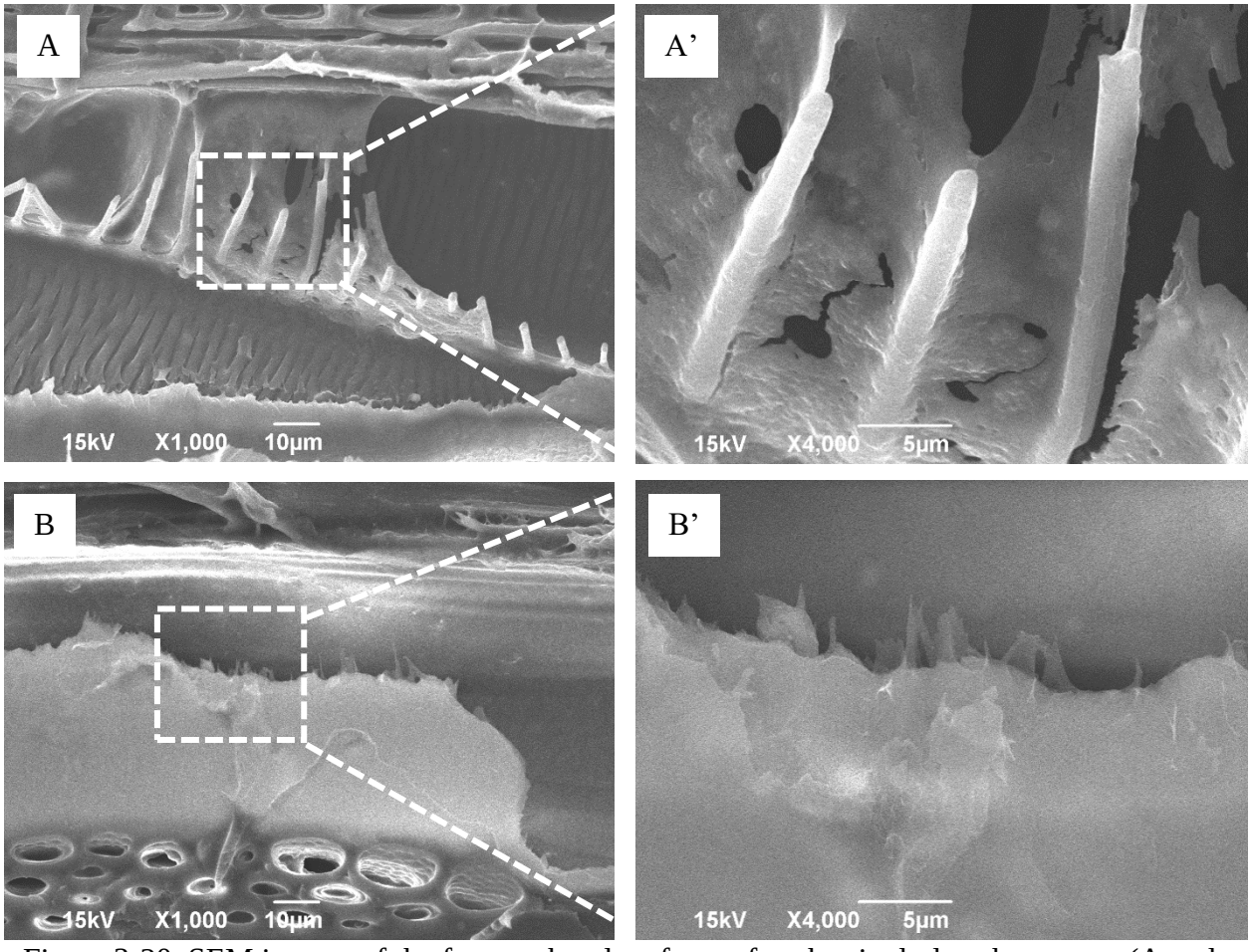

Figure 3-20. SEM images of the fracture bond surfaces after the single-lap shear tests: (A and A') pure gluten; (B and B') gluten containing 3% CNFs.

3.5. Thermal Stability Analysis

3.5.1. Zein Adhesives

Thermal stability of the nanocomposite adhesives was evaluated using thermogravimetric analysis (TGA). The TGA and derivative thermogravimetric (DTG) curves of as-received zein powder, neat zein adhesive, and two CNF-containing zein adhesives are shown in Figure 3-21. The TGA curves show the sample weight loss as a function of temperature while the DTG curves present the rate of the weight loss. The thermal degradation behaviors of the neat zein adhesive and the two CNF-containing zein adhesives are very similar: a single stage degradation with only one DTG peak at 312ºC, which indicates that CNFs have negligible effect on the thermal stability of the adhesives. The as-received zein powder exhibits a different degradation profile: a two-stage degradation with two DTG peaks at 297ºC and 541ºC. In a TGA test, multiple-stage degradation normally indicates the presence of different ingredients that have different degradation temperatures in a sample. The first peak represents the degradation of zein and the second peak, which has a much higher temperature than the first one, can be due to an impurity included in the product. All the zein-based adhesives only show one degradation peak, which can be attributed to the zein solution process used in adhesive preparation. The impurity is not soluble in aqueous ethanol and therefore is not present in the adhesive.

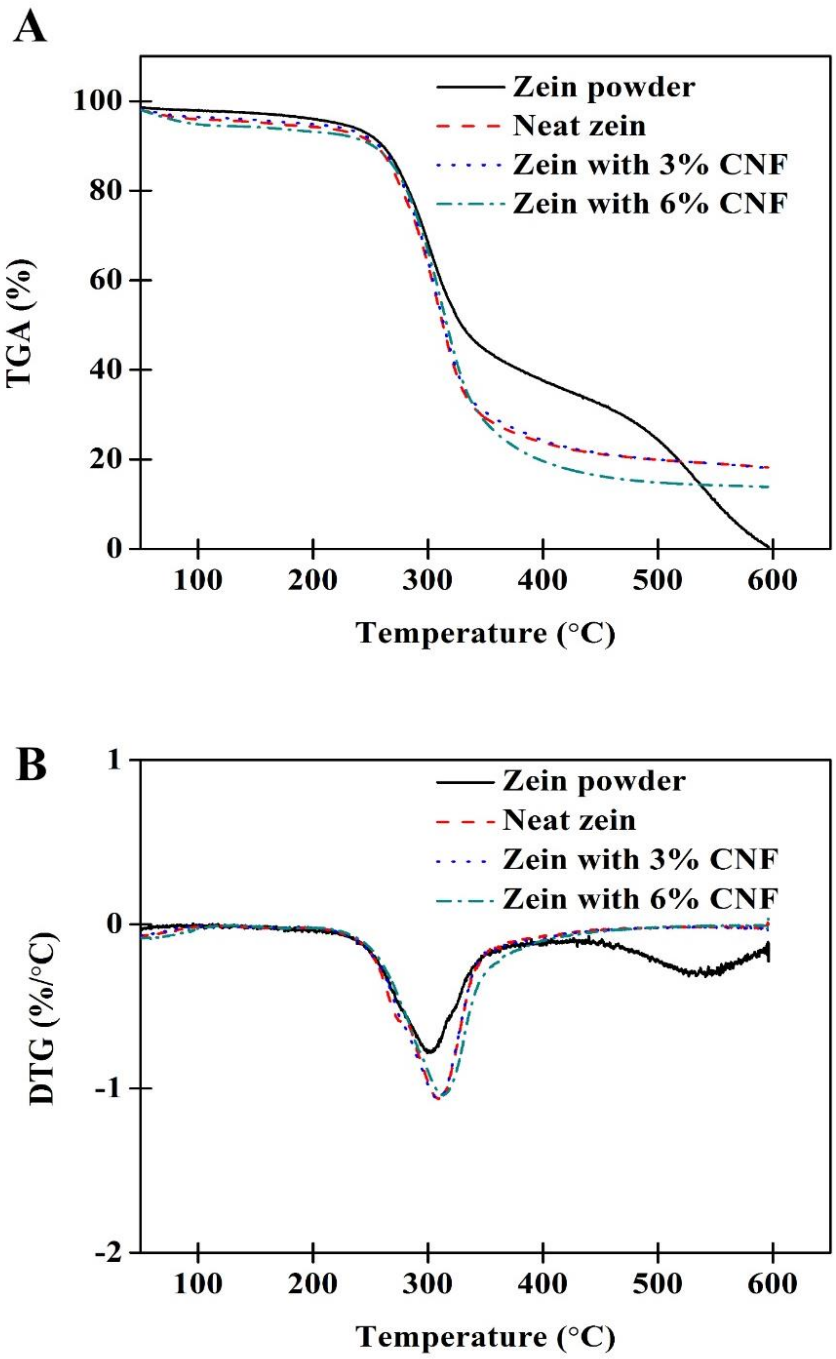

Figure 3-21. Thermal degradation of the as received zein powder, neat zein, zein adhesive containing 3% CNFs and zein adhesive containing 6% CNFs: (A) TGA curves and (B) DTG curves.

3.5.2. Gluten Adhesives

The TGA and DTG curves of as-received gluten powder, neat gluten adhesive, and CNF-containing gluten adhesives are presented in Figure 3-22. All samples show a two-stage degradation behavior with the as-received gluten powder possessing a much higher thermal stability than the adhesives. The as-received powder displays two degradation peaks at 290ºC and 534ºC, one representing the degradation of gluten and the other one representing possibly an impurity. The adhesives, by contrast, show peaks at 172 -191ºC and around 290ºC. The lower peak should be ascribed to the degradation of denatured gluten. Urea and reducing agent sodium sulfite were used in gluten solubilization. Urea can break hydrogen bonds and sodium sulfite can sever S-S bonds in the protein, leading to disrupted protein structure and reduced molecular weight. Therefore, the degradation temperature of gluten in the adhesives was significantly lower than the as-received gluten. A small portion of unaffected gluten was still present in the adhesives and it showed unchanged degradation temperature at 290ºC. Comparing the first degradation peaks of the neat gluten adhesive and the CNF-containing adhesives, the addition of CNFs is shown to lower the degradation temperature. Similar phenomenon has also been reported in PHBV/cellulose nanocrystal composites and a possible reason can be due to increased thermal conductivity of the nanocomposites after adding the cellulose [143].

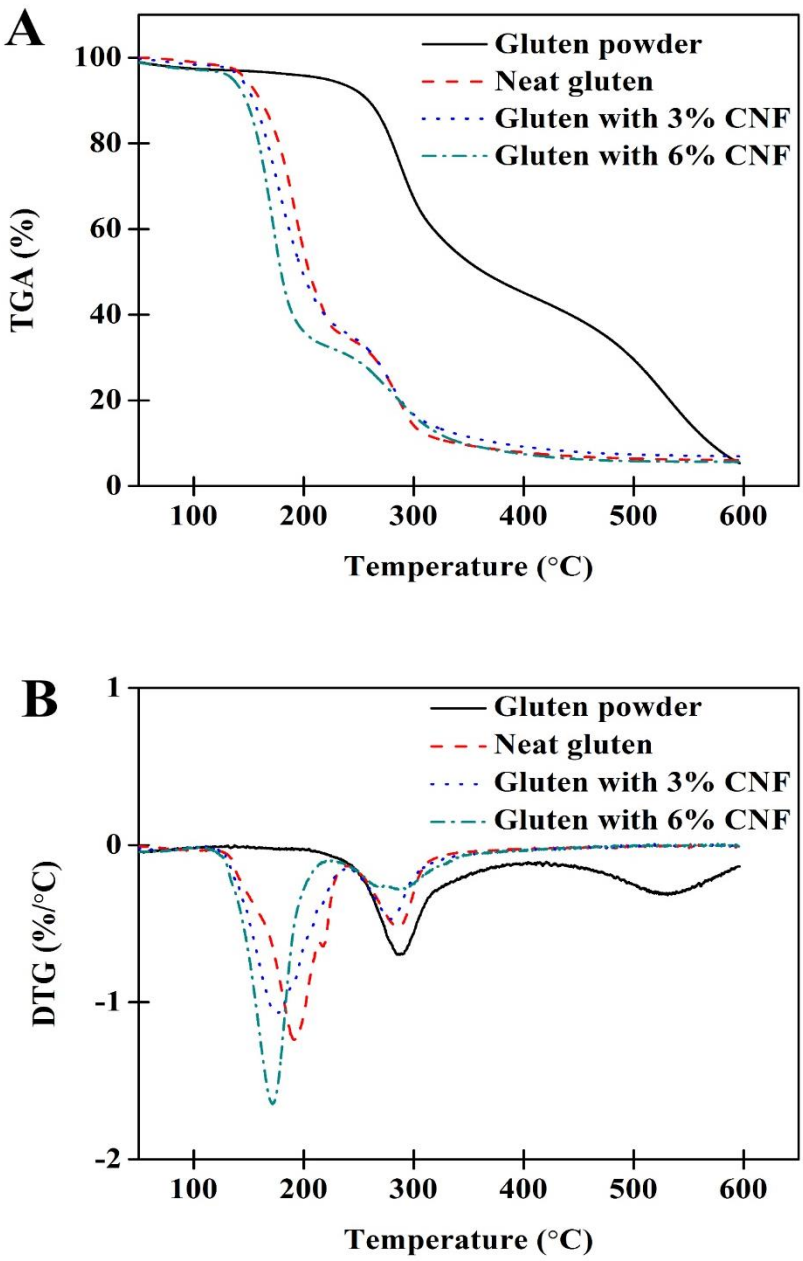

Figure 3-22. Thermal degradation of the as-received gluten powder, neat gluten adhesive, and the gluten adhesives containing CNFs: (A) TGA curves and (B) DTG curves.

In the case of the gluten adhesives containing GTA crosslinker, they show a degradation behavior similar to that of the CNF-containing gluten. One difference, though, is that GTA

crosslinking slightly increase the degradation temperature of the adhesive from 191ºC to 197ºC, indicating improved thermal stability by crosslinking.

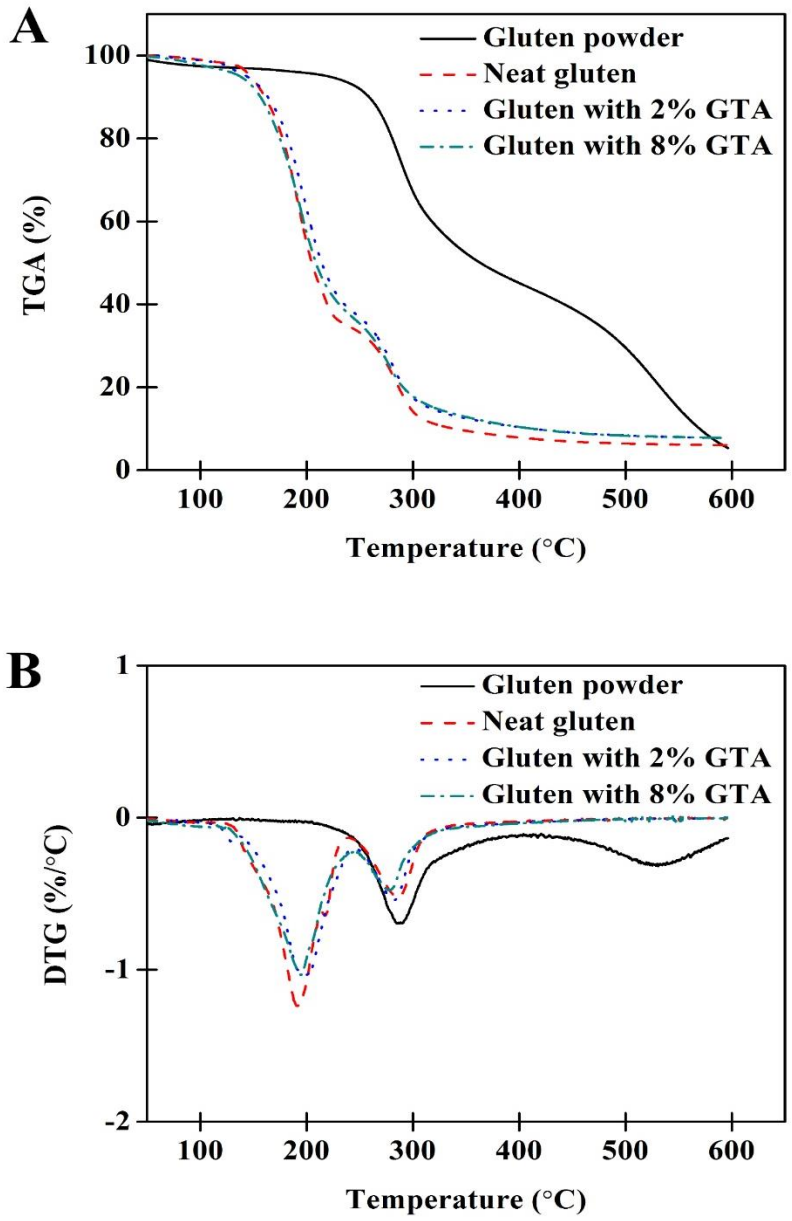

Figure 3-23. Thermal degradation of the as-received gluten powder, neat gluten adhesive, and the gluten adhesives containing GTA: (A) TGA curves and (B) DTG curves.

3.5. Fourier Transform Infrared Spectroscopy

Figure 3-24 shows the FTIR spectra of the neat zein and CNF-constaining zein adhesives. All three samples display amide I (1643 cm^{-1}), amide II (1538 cm^{-1}) and amide A (3280 cm^{-1}) peaks that belong to zein protein. There is an additional peak for zein/6% CNF adhesive at 1054 cm^{-1}, which can be attributed to C-O-C pyranose ring of cellulose [144]. This peak is not obvious for the zein/3% CNF adhesive and it is probably due to the low cellulose concentration. There are no other new peaks due to the addition of CNFs, suggesting that the zein-CNFs interactions are negligible.

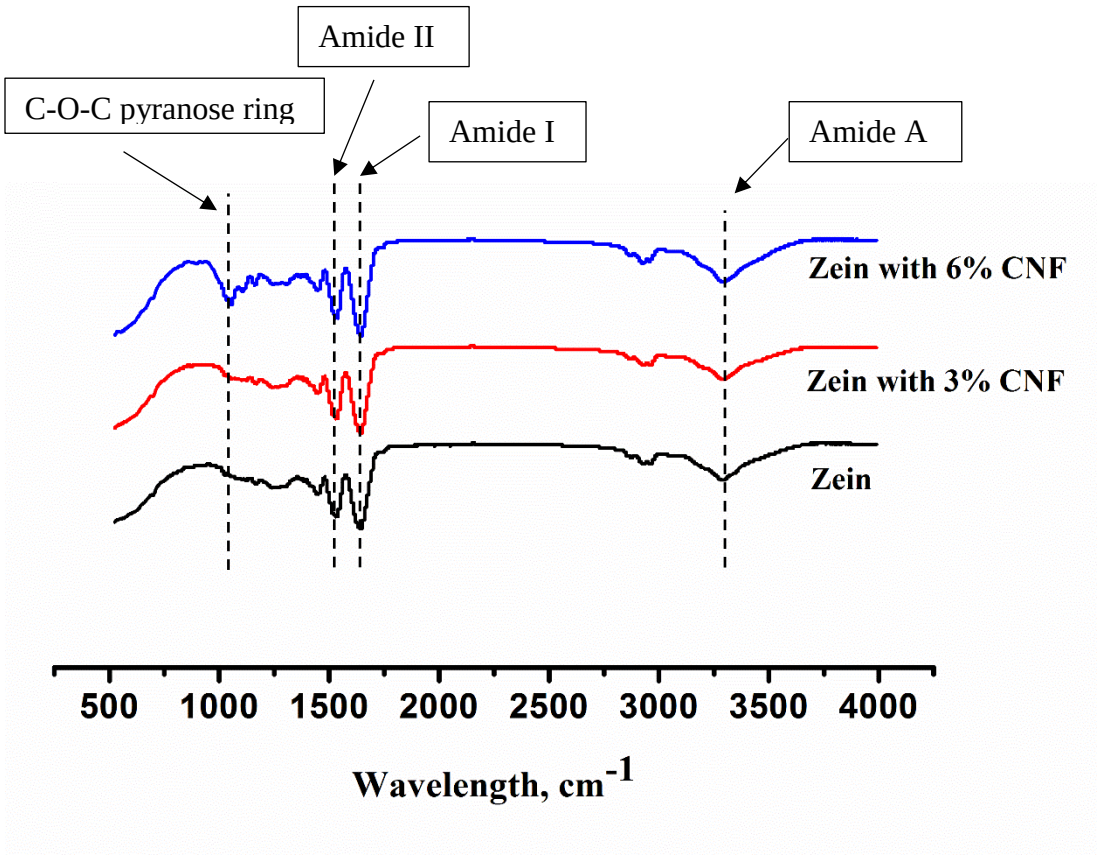

Figure 3-24. FTIR spectra of the neat zein and CNF-containing zein adhesives.

FTIR spectra of the neat gluten and the gluten containing GTA or CNFs are shown in Figure 3-25. The characteristic peaks for protein, i.e., 1643 cm^{-1} for C-O stretching (amide I), 1538 cm^{-1} for N-H deformation (amide II), and 1459 cm^{-1} for C-N stretching and N-H vibration (amide III) are present for all the samples [145], [146]. Another main two peaks at 3428 cm^{-1} and 3331 cm^{-1} are attributed to hydroxyl and amino groups in gluten [147]–[149]. Imines linkages are produced when gluten protein reacts with GTA. However, in this study the imine peak (1640 – 1690 cm^{-1}) cannot be easily identified on the spectra of the crosslinked gluten. The imine bond, which is produced through the Maillard reaction between the amine group in the protein and the aldehyde group in GTA, is hard to detect because its peak can overlap with the strong amide I peak. The color change of the gluten adhesive after adding GTA can indicate the occurrence of the Maillard reaction [150]. As shown in Figure 3-26, the adhesives containing GTA become darker/browner than the neat one, proving the occurrence of the crosslinking reaction.

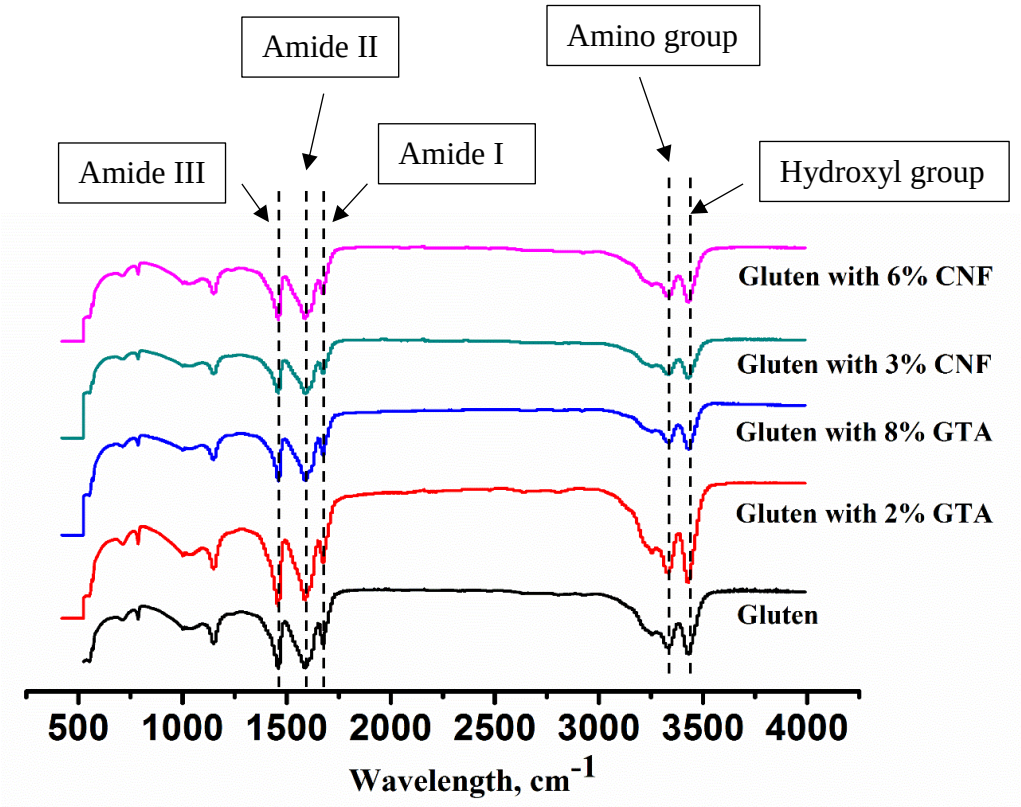

Figure 3-25. FTIR spectra of the neat gluten adhesive and the adhesives containing GTA or CNFs.

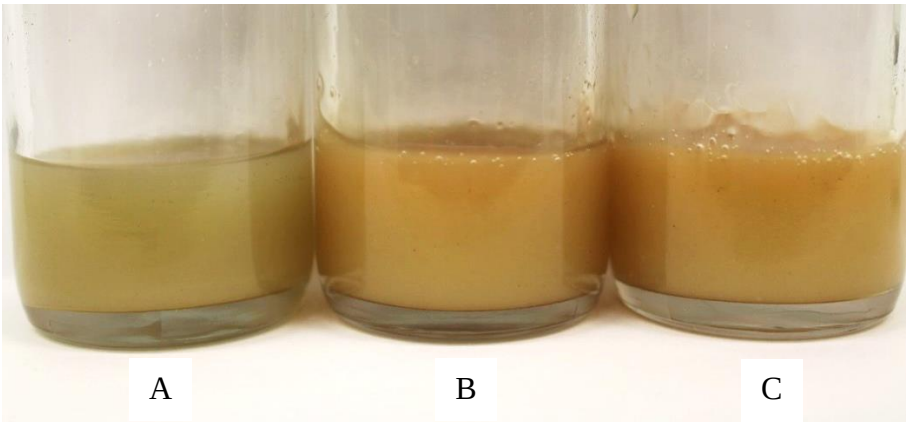

Figure 3-26. Color comparison between the neat gluten adhesive and the GTA-crosslinked gluten adhesive: (A) pure gluten, (B) gluten with 2% GTA, (C) gluten with 8% GTA.

CHAPTER 4. PROPERTY STUDIES OF PLYWOOD

4.1. Introduction

In this chapter, the best formulations of the zein- and gluten-based adhesives determined by the single-lap shear test are used to produce three-layer plywood. A commercial wood adhesive MDI resin, together with neat zein and neat gluten, are also used as control samples. Flexural and internal bonding tests are performed on the plywood to study their mechanical properties. Water resistance of the adhesives is evaluated through a water immersion test.

4.2. Flexural Test

Figure 4-1 compares the results of MOR and MOE of the plywood made using pure zein, zein/5% CNFs, pure gluten, gluten/2% CNFs/2% GTA, and MDI as the adhesives. The gluten/2% CNFs/2% GTA adhesive produces the strongest plywood with a MOR of 105 MPa, followed by the commercial MDI with a MOR of 73 MPa. The MOE of the gluten adhesive is 9762 MPa while the value for MDI is 5886 MPa. The zein/5% CNFs adhesive shows almost the same MOR as MDI but a much higher MOE (9295 MPa). These results indicate that the gluten/2% CNFs/2% GTA and zein/5% CNFs formulations are possible MDI replacements. It is also worth noting that pure zein possesses higher MOR and MOE than pure gluten, which contradicts the results from the single-lap shear test. This can be due to the different sample preparation conditions, i.e., higher pressure and temperature in plywood production than in lap shear sample production: 2 MPa vs. 0.05 MPa; 140ºC vs. 100ºC. It is postulated that zein forms stronger bond than gluten under these conditions.

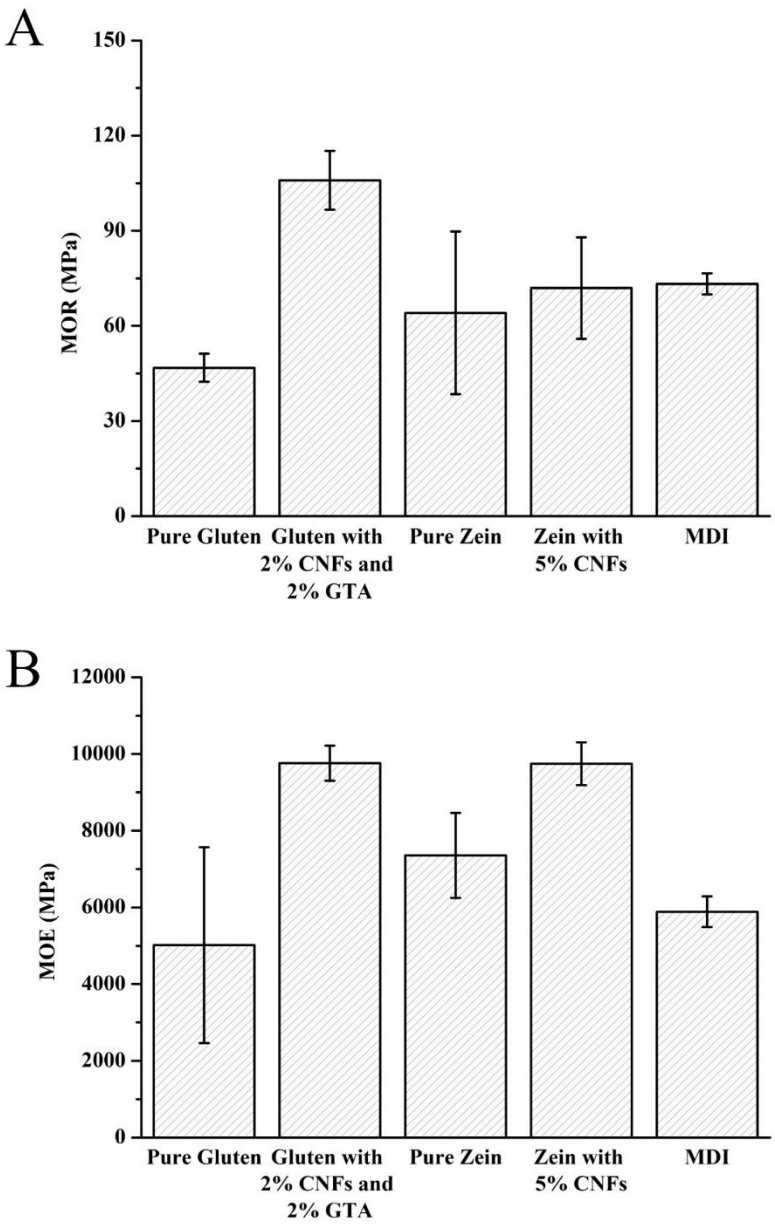

Figure 4-1. Three-point bending test results of plywood made using different adhesives: (A) MOR; (B) MOE.

It is important to study the mode of failure of the plywood. Delamination occurs on the samples bonded by pure gluten, pure zein, and zein/5% CNFs. Figure 4-2A shows a delaminated plywood sample (bonded by pure gluten) by the bending test. Delamination causes premature sample failure while the individual sheets of the plywood remain intact. The plywood bonded by

gluten/2% CNFs/2% GTA and MDI failed by tensile fracture on the bottom surface of the plywood (Figure 4-2B and B'), which is the normal failure mode of a beam. Delamination is caused by the shear flow along the sheet interfaces when the plywood is under bending. Two bonded layers separate if the interfacial shear flow exceeds the shear strength of the adhesive. The results show that gluten/2% CNFs/2% GTA and MDI have adequate shear strength to prevent delamination.

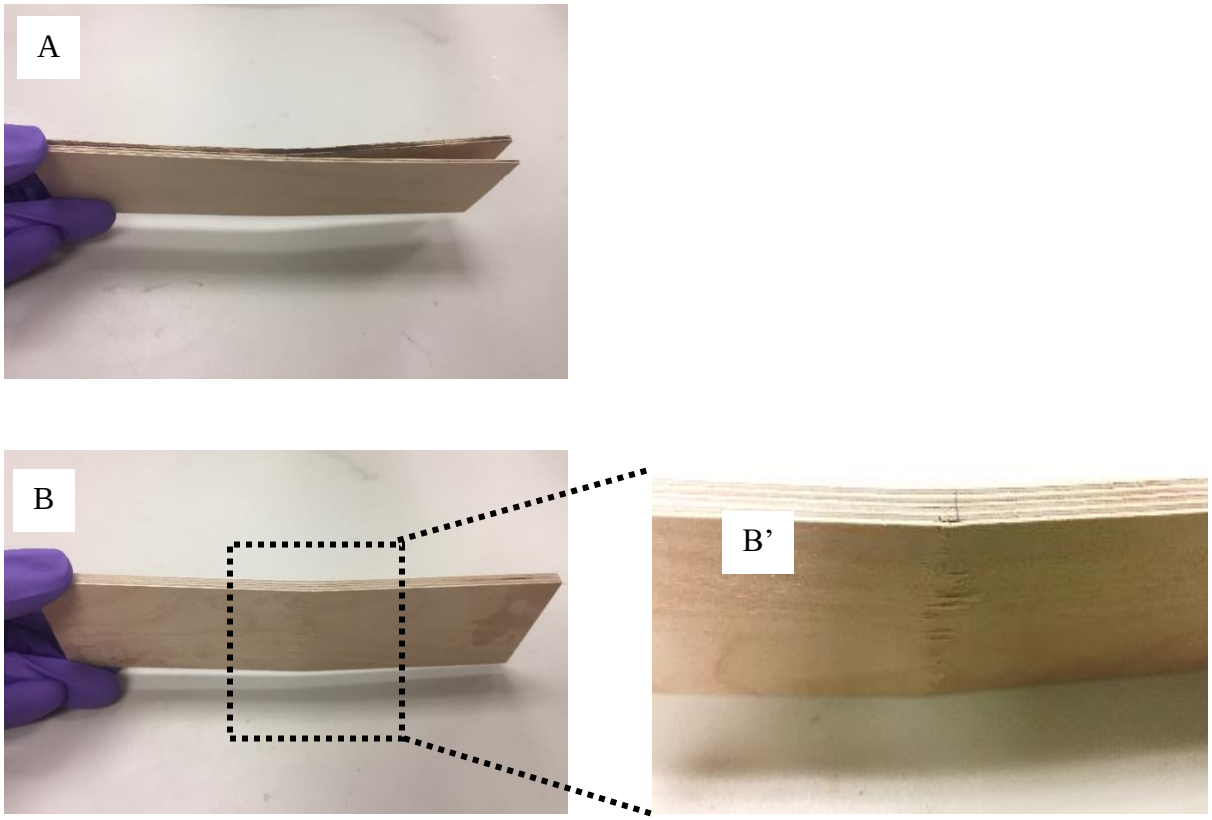

Figure 4-2. Photos showing fracture conditions of plywood in the flexural test: (A) pure gluten, (B and B') gluten containing 2% CNF and 2% GTA.

When delamination occurs, the applied load would drop during the bending process. These sudden load drops can be easily identified from the bending load-extension curves shown in Figure 4-3. In figures A and D, some curves show load recoveries from the load drops because the

delamination is local and the sample can continue to bear load until large scale/global delamination occurs. The curves in figure C show no load recovery because the initial delamination is large/global in this sample (pure zein). For the gluten/2% CNFs/2% GTA and MDI samples (figures B and E, respectively), no delamination occurs during the entire bending process and curves are continuous without any interruptions.

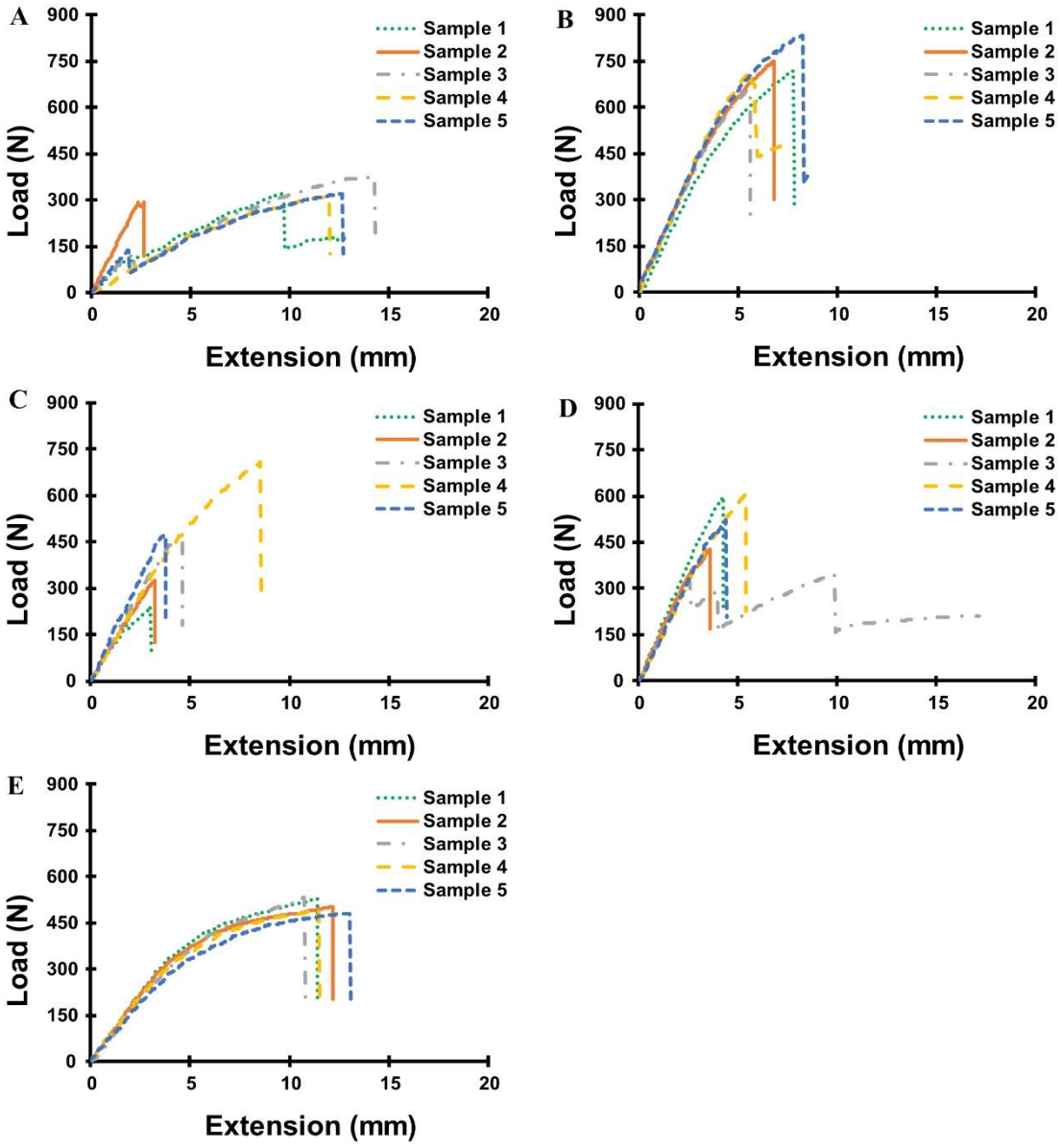

Figure 4-3. Load vs. extension curves from the three-point bending test for the plywood bonded by: (A) pure gluten, (B) gluten with 2% CNFs and 2%GTA, (C) pure zein, (D) zein with 5% CNFs, (E) MDI

4.3. Internal Bond Test

4.3.1. Dry State

The internal bond test is another way to test the strength of plywood. The plywood made using the same adhesives as in the flexural test were used for the new test. As shown in Figure 4-4, internal bond strength of gluten was increased by about 68% by adding 2% CNFs and 2% GTA, while the internal bond strength of zein was increased by about 30% by adding 5% CNFs. It should be made clear that the plywood bonded by MDI failed by debonding between the plywood and the aluminum loading block, which indicates that the MDI bond is stronger than the thermoplastic glue used to bond the sample to the loading block. Therefore, the actual bond strength of MDI is higher than the value reported in Figure 4-4, which represents the bond strength of the thermoplastic glue.

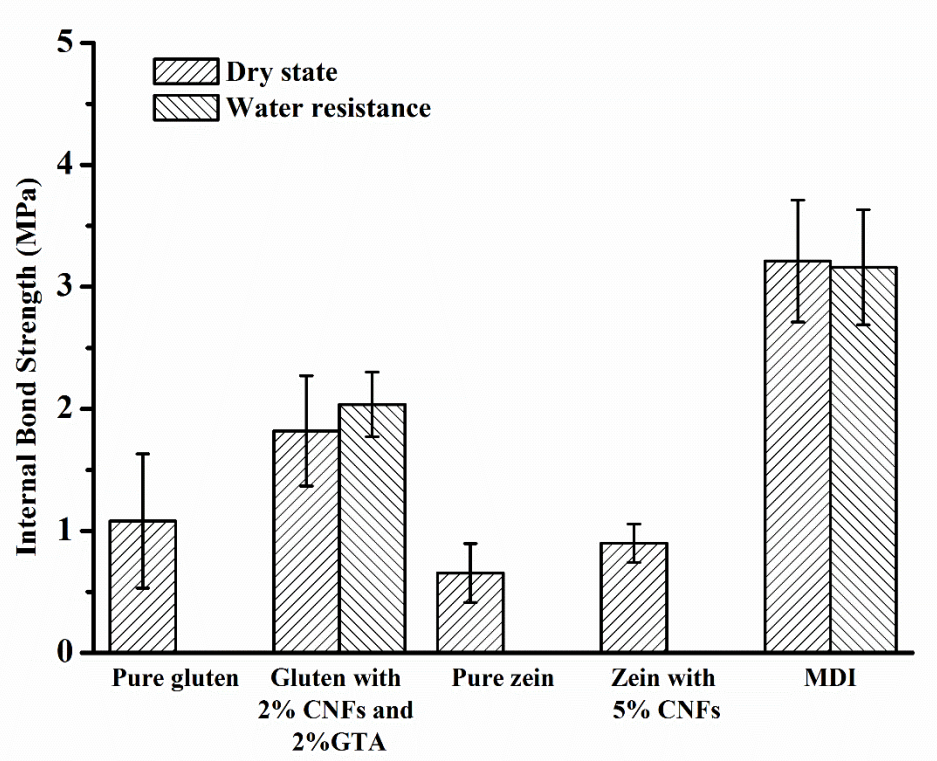

Figure 4-4. Internal bond test results of plywood made using different adhesives.

The representative load-extension curves of the different plywood are shown in Figure 4-5. The load increases continuously with increasing extension for all the samples. Table 4-1 summarizes the average bond strength and its standard distribution for each sample.

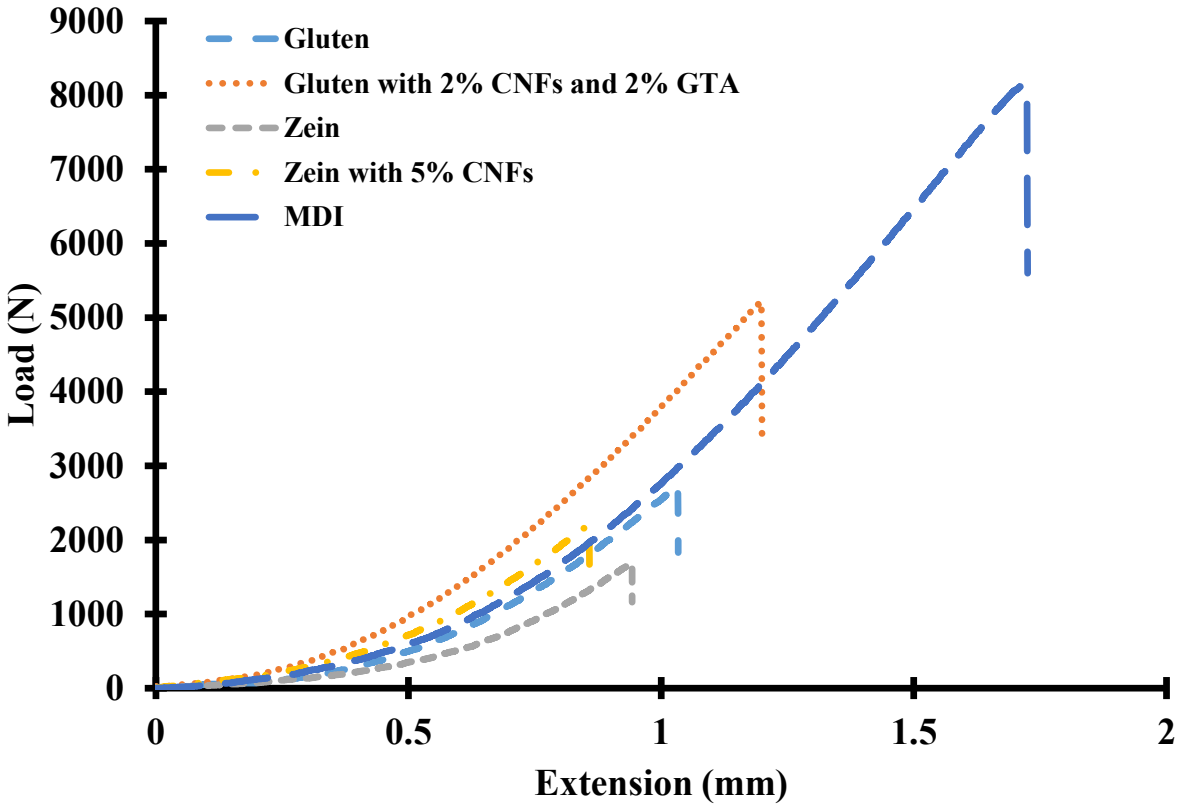

Figure 4-5. Representative load vs. extension curves of the plywood made using different adhesives.

Table 4-1. Average internal bond strength for the plywood made using different adhesives.

	Mean (MPa)	SD
Pure gluten	1.081	0.549
Gluten/2% CNFs/2% GTA	1.819	0.451
Pure zein	0.655	0.242
Zein with CNFs	0.899	0.158
MDI	3.211	0.500

SD: standard deviation.

4.3.2 Internal Bond Strength after Water Immersion

Water resistance of the adhesives was examined by testing internal bond strength of the plywood that had been through water immersion. The plywood made using pure zein, zein/5% CNFs, and pure gluten delaminated during the 24-hour water immersion process. Therefore, only the plywood made using gluten/2% CNFs/2% GTA and MDI were tested. Figure 4-6 shows the representative load-extension curves for the two samples and the internal bond strength is measured at 2.03MPa and 3.16MPa (Table 4-2), respectively. Compared with the dry samples, water immersion appears to have no detrimental effects on the sample made using gluten/2% CNFs/2% GTA. The plywood made using MDI again failed at the loading block/wood interface, and therefore the true strength is not reflected here.

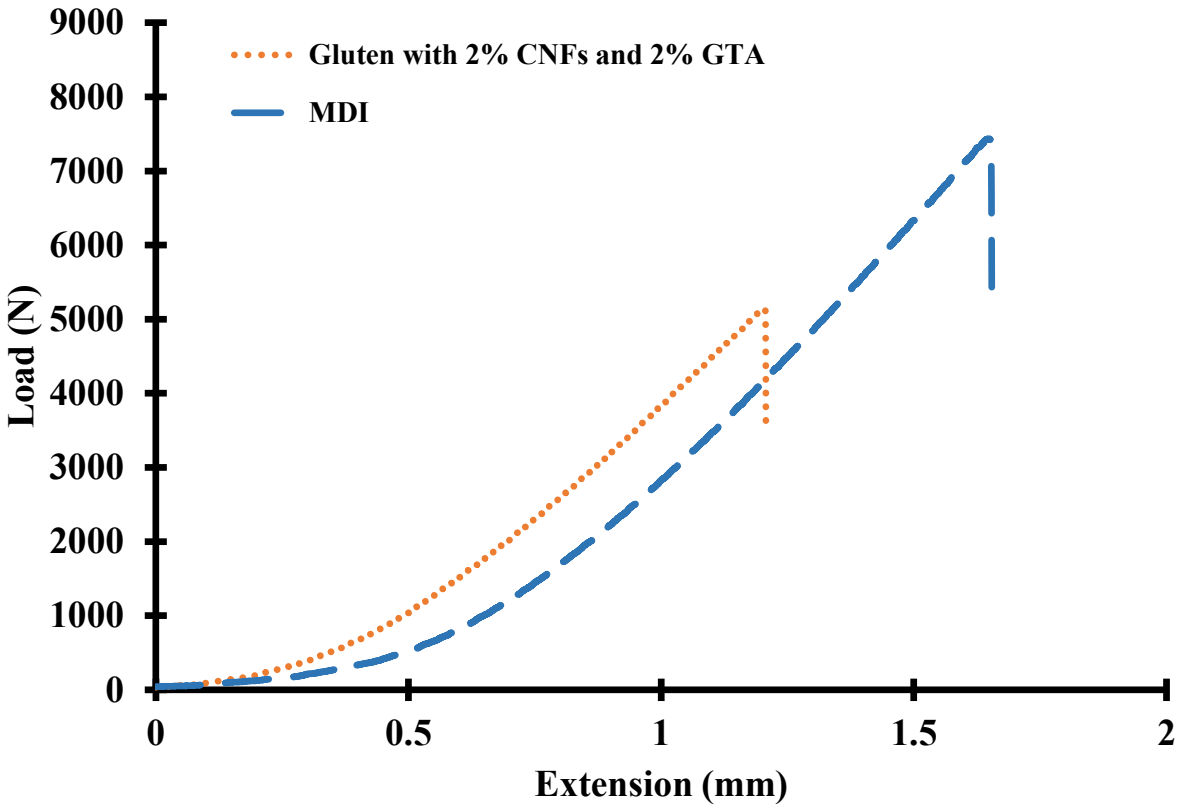

Figure 4-6. Representative load vs. extension curves of the plywood after water immersion.

Table 4-2. Average internal bond strength for the plywood after water immersion.

	Mean (MPa)	SD
Gluten/2% CNFs/2% GTA	2.036	0.266
MDI	3.161	0.471

SD: standard deviation.

CHAPTER 5. CONCLUSION AND FUTURE WORK

5.1. Conclusion

Biobased nanocomposite wood adhesives derived from zein and gluten were developed in this study. The effects of cellulose nanofibers, curing conditions, and GTA crosslinker on the adhesive bond strength were studied using single-lap shear test. For the zein adhesives, high shear strength was achieved at high cellulose nanofiber content, relatively high curing temperature, or curing under atmospheric pressure. Too high a curing temperature could lead to adhesive degradation and therefore decrease the strength. GTA showed negligible effect on the shear strength. For the gluten adhesives, GTA showed the strongest effect on the shear strength, with a higher GTA content leading to a higher strength.

Visual observation and SEM study with fracture surface were carried out to understand wood bond mechanism. For the cellulose nanofibers added both zein- and gluten-adhesives, the differences of fracture surface were negligible with visual observation, but presumed cellulose nanofibers or protein covered cellulose nanofibers were detected on the nanocellulose blended samples in the SEM study. Clear differences were shown on the fracture surfaces of GTA crosslinked gluten adhesives with both visual observation and SEM study. Coarse and damaged wood surfaces can be seen on the fracture surfaces of GTA crosslinked gluten adhesive through the visual observation. With the SEM study, the fracture surfaces become rougher by collapsed sheet-like gluten as crosslinker content increases. These observations are an agreement with the trends of bond strength increase with the nanocellulose and GTA content increases.

Thermal stability of zein and gluten adhesives were analyzed to determine the relationship of cellulose nanofibers and crosslinker content. From the results of zein adhesives, CNFs does not have distinct effect on the thermal stability. However, the addition of CNFs lower the initial

degradation temperature on the gluten adhesives. For the GTA crosslinked gluten adhesives, thermal stability slightly increases as GTA content increases. From the FTIR results, pure zein adhesive and 3% CNF/zein adhesive show very similar results, but one distinct peak, C-O-C pyranose ring, was shown on 6% CNF/zein adhesive, which is because of the CNF content increase. Pure gluten, CNFs blended glutens, and GTA crosslinked glutens were also investigated through FTIR, but no clear differences detected. This is probably because of the imine group, which is produced by crosslinking reaction between protein and aldehyde, was overlapped with strong amide I peak, so that, color change of protein crosslinking reaction (Maillard reaction) was conducted in this study.

Three-layer plywood was produced to determine MOE, MOR, and internal bond strength with the best formulations, zein/5% CNFs and gluten/2% CNFs/2% GTA, from single-lap shear test. Pure zein, pure gluten, and MDI resin were also chosen as control formulations. The results of MOE and MOR of gluten/2% CNFs/2% GTA adhesive and zein/5% CNFs adhesives were similar or higher than MDI resin, so they could be used as possible replacement for MDI resin. For the internal bonding test with dry state, gluten/2% CNFs/2% GTA was the highest strength among the bio-based adhesives, but the measurement of MDI was not possible due to the strength of thermoplastic glue, which is bonded between sample and loading blocks, was weaker than the MDI. For the internal bonding test after water immersion, two samples, only gluten/2% CNFs/2% GTA were possible to measure the internal bond strength because of other protein-based adhesives were delaminated in water immersion process. As same with the dry state, it was not possible to measure accurate internal bond strength of MDI because of the early break on commercial thermoplastic glue.

5.2. Future Work

In the thesis, we mainly focused on three different factors, i.e., curing temperature, nanocellulose reinforcement, and GTA crosslinking agent, to improve mechanical properties of bio-based wood adhesives. Further studies using other factors such as compression pressure and time are recommended. This study also showed that GTA was not an effective crosslinking agent for zein. More studies to identify a suitable crosslinking agent are also recommended. Finally, a comparative study following EN 204 and 205 and ASTM 2339 can be performed to determine if the adhesives meet standard requirements.

REFERENCES

[1] Q. Q. Wang, J. Y. Zhu, R. Gleisner, T. a. Kuster, U. Baxa, and S. E. McNeil, "Morphological development of cellulose fibrils of a bleached eucalyptus pulp by mechanical fibrillation," *Cellulose*, vol. 19, pp. 1631–1643, 2012.

[2] M. Henriksson, L. A. Berglund, P. Isaksson, and T. Lindstro, "Cellulose Nanopaper Structures of High Toughness," *Biomacromolecules*, vol. 9, pp. 1579–1585, 2008.

[3] H. Fukuzumi, T. Saito, T. Iwata, Y. Kumamoto, and A. Isogai, "Transparent and high gas barrier films of cellulose nanofibers prepared by TEMPO-mediated oxidation," *Biomacromolecules*, vol. 10, no. 1, pp. 162–165, 2009.

[4] N. Lavoine, I. Desloges, A. Dufresne, and J. Bras, "Microfibrillated cellulose – Its barrier properties and applications in cellulosic materials: A review," *Carbohydr. Polym.*, vol. 90, no. 2, pp. 735–764, 2012.

[5] I. a. Sacui, R. C. Nieuwendaal, D. J. Burnett, S. J. Stranick, M. Jorfi, C. Weder, E. J. Foster, R. T. Olsson, and J. W. Gilman, "Comparison of the properties of cellulose nanocrystals and cellulose nanofibrils isolated from bacteria, tunicate, and wood processed using acid, enzymatic, mechanical, and oxidative methods," *ACS Appl. Mater. Interfaces*, vol. 6, no. 9, pp. 6127–6138, 2014.

[6] X. Xu, F. Liu, L. Jiang, J. Y. Zhu, D. Haagenson, and D. P. Wiesenborn, "Cellulose Nanocrystals vs. Cellulose Nano fi brils: A Comparative Study on Their Microstructures and E ff ects as Polymer Reinforcing Agents," *ACS Appl. Mater. Interfaces*, vol. 5, pp. 2999–3009, 2013.

[7] I. M. Brown, R. M., Jr., and Saxena, *Cellulose: molecular and structural biology: selected articles on the synthesis, structure, and applications of cellulose*. Springer, 2007.

[8] Z. Cai and J. Kim, "Preparation and Characterization of Novel Bacterial Cellulose/Gelatin Scaffold for Tissue Regeneration Using Bacterial Cellulose Hydrogel," *J. Nanotechnol. Eng. Med.*, vol. 1, no. 2, p. 21002, 2010.

[9] B. M. Cherian, A. L. Leão, S. F. De Souza, L. M. M. Costa, G. M. De Olyveira, M. Kottaisamy, E. R. Nagarajan, and S. Thomas, "Cellulose nanocomposites with nanofibres isolated from pineapple leaf fibers for medical applications," *Carbohydr. Polym.*, vol. 86, no. 4, pp. 1790–1798, 2011.

[10] A. Alemdar and M. Sain, "Isolation and characterization of nanofibers from agricultural residues – Wheat straw and soy hulls," *Bioresour. Technol.*, vol. 99, no. 6, pp. 1664–1671, 2008.

[11] R. Zuluaga, J. L. Putaux, A. Restrepo, I. Mondragon, and P. Gañán, "Cellulose microfibrils from banana farming residues: Isolation and characterization," *Cellulose*, vol. 14, pp. 585–592, 2007.

[12] A. Dufresne and M. R. Vignon, "Improvement of Starch Film Performances Using Cellulose Microfibrils," *Macromolecules*, vol. 31, no. 8, pp. 2693–2696, 1998.

[13] B. S. L. Brito, F. V Pereira, and J. P. B. Jean, "Preparation , morphology and structure of cellulose nanocrystals from bamboo fibers," *Cellulose*, pp. 1527–1536, 2012.

[14] W. Chen, H. Yu, and Y. Liu, "Preparation of millimeter-long cellulose i nanofibers with diameters of 30-80 nm from bamboo fibers," *Carbohydr. Polym.*, vol. 86, no. 2, pp. 453–461, 2011.

[15] M. F. Rosa, E. S. Medeiros, J. A. Malmonge, K. S. Gregorski, D. F. Wood, L. H. C. Mattoso, G. Glenn, W. J. Orts, and S. H. Imam, "Cellulose nanowhiskers from coconut husk fibers: Effect of preparation conditions on their thermal and morphological behavior," *Carbohydr. Polym.*, vol. 81, no. 1, pp. 83–92, 2010.

[16] R. M. dos Santos, W. P. Flauzino Neto, H. A. Silvério, D. F. Martins, N. O. Dantas, and D. Pasquini, "Cellulose nanocrystals from pineapple leaf, a new approach for the reuse of this agro-waste," *Ind. Crops Prod.*, vol. 50, pp. 707–714, Oct. 2013.

[17] H. Yu, Z. Qin, B. Liang, N. Liu, Z. Zhou, and L. Chen, "Facile extraction of thermally stable cellulose nanocrystals with a high yield of 93% through hydrochloric acid hydrolysis under hydrothermal conditions," *J. Mater. Chem. A*, vol. 1, no. 12, p. 3938, Feb. 2013.

[18] S. Camarero Espinosa, T. Kuhnt, E. J. Foster, and C. Weder, "Isolation of thermally stable cellulose nanocrystals by phosphoric acid hydrolysis.," *Biomacromolecules*, vol. 14, no. 4, pp. 1223–30, Apr. 2013.

[19] H. Sadeghifar, I. Filpponen, S. P. Clarke, D. F. Brougham, and D. S. Argyropoulos, "Production of cellulose nanocrystals using hydrobromic acid and click reactions on their surface," *J. Mater. Sci.*, vol. 46, no. 22, pp. 7344–7355, Jun. 2011.

[20] F. Rafieian, M. Shahedi, J. Keramat, and J. Simonsen, "Mechanical, thermal and barrier properties of nano-biocomposite based on gluten and carboxylated cellulose nanocrystals," *Ind. Crops Prod.*, vol. 53, pp. 282–288, 2014.

[21] F. Jiang, S. Han, and Y.-L. Hsieh, "Controlled defibrillation of rice straw cellulose and self-assembly of cellulose nanofibrils into highly crystalline fibrous materials," *RSC Adv.*, vol. 3, no. 30, p. 12366, 2013.

[22] Y. Qing, R. Sabo, J. Y. Zhu, U. Agarwal, Z. Cai, and Y. Wu, “A comparative study of cellulose nanofibrils disintegrated via multiple processing approaches.,” *Carbohydr. Polym.*, vol. 97, no. 1, pp. 226–34, Aug. 2013.

[23] R. R. Lahiji, X. Xu, R. Reifenberger, A. Raman, A. Rudie, and R. J. Moon, “Atomic Force Microscopy Characterization of Cellulose Nanocrystals,” *Langmuir*, vol. 26, no. 6, pp. 4480–4488, 2010.

[24] G. Guhados, W. Wan, and J. L. Hutter, “Measurement of the elastic modulus of single bacterial cellulose fibers using atomic force microscopy.,” *Langmuir*, vol. 21, no. 18, pp. 6642–6646, 2005.

[25] S. J. Eichhorn, A. Dufresne, M. Aranguren, N. E. Marcovich, J. R. Capadona, S. J. Rowan, C. Weder, W. Thielemans, M. Roman, S. Renneckar, W. Gindl, S. Veigel, J. Keckes, H. Yano, K. Abe, M. Nogi, A. N. Nakagaito, A. Mangalam, J. Simonsen, A. S. Benight, A. Bismarck, L. A. Berglund, and T. Peijs, “Review: current international research into cellulose nanofibres and nanocomposites,” *J. Mater. Sci.*, vol. 45, no. 1, pp. 1–33, Sep. 2009.

[26] M. F. Ashby and D. R. H. Jones, *Engineering Materials 1: an introduction to their properties and application.* Pergamon Press, Oxford, 1989.

[27] I. Sakurada, Y. Nukushina, and T. Ito, “Experimental determination of the elastic modulus of crystalline regions in oriented polymers,” *J. Polym. Sci.*, vol. 57, no. 165, pp. 651–660, Mar. 1962.

[28] A. Dufresne, “Processing of polymer nanocomposites reinforced with polysaccharide nanocrystals.,” *Molecules*, vol. 15, no. 6, pp. 4111–28, Jun. 2010.

[29] B. L. Peng, N. Dhar, H. L. Liu, and K. C. Tam, “Chemistry and applications of nanocrystalline cellulose and its derivatives: A nanotechnology perspective,” *Can. J. Chem. Eng.*, vol. 89, no. 5, pp. 1191–1206, Oct. 2011.

[30] A. Dufresne, “Nanocellulose: a new ageless bionanomaterial,” *Mater. Today*, vol. 16, no. 6, pp. 220–227, Jun. 2013.

[31] B. Braun and J. R. Dorgan, “Single-step method for the isolation and surface functionalization of cellulosic nanowhiskers,” *Biomacromolecules*, vol. 10, no. 2, pp. 334–341, 2009.

[32] M. J. Sobkowicz, B. Braun, and J. R. Dorgan, “Decorating in green: surface esterification of carbon and cellulosic nanoparticles,” *Green Chem.*, vol. 11, no. 5, p. 680, May 2009.

[33] F. W. Herrick, R. L. Casebier, J. K. Hamilton, and K. R. Sandberg, “Microfibrillated cellulose: morphology and accessibility,” *J. Appl. Polym. Sci. Appl. Polym. Symp.; (United States)*, vol. 37, Jan. 1983.

[34] P. Huang, M. Wu, S. Kuga, D. Wang, D. Wu, and Y. Huang, “One-step dispersion of cellulose nanofibers by mechanochemical esterification in an organic solvent.,” *ChemSusChem*, vol. 5, no. 12, pp. 2319–22, Dec. 2012.

[35] C. Eyholzer, A. B. de Couraça, F. Duc, P. E. Bourban, P. Tingaut, T. Zimmermann, J. A. E. Månson, and K. Oksman, “Biocomposite hydrogels with carboxymethylated, nanofibrillated cellulose powder for replacement of the nucleus pulposus.,” *Biomacromolecules*, vol. 12, no. 5, pp. 1419–27, May 2011.

[36] N. T. Cervin, C. Aulin, P. T. Larsson, and L. Wågberg, “Ultra porous nanocellulose aerogels as separation medium for mixtures of oil/water liquids,” *Cellulose*, vol. 19, no. 2, pp. 401–410, Dec. 2011.

[37] C. Eyholzer, P. Tingaut, T. Zimmermann, and K. Oksman, “Dispersion and Reinforcing Potential of Carboxymethylated Nanofibrillated Cellulose Powders Modified with 1-Hexanol in Extruded Poly(Lactic Acid) (PLA) Composites,” *J. Polym. Environ.*, vol. 20, no. 4, pp. 1052–1062, Jul. 2012.

[38] L. Wågberg, G. Decher, M. Norgren, T. Lindström, M. Ankerfors, and K. Axnäs, “The build-up of polyelectrolyte multilayers of microfibrillated cellulose and cationic polyelectrolytes.,” *Langmuir*, vol. 24, no. 3, pp. 784–95, Feb. 2008.

[39] N. Ljungberg, C. Bonini, F. Bortolussi, C. Boisson, L. Heux, and J. Y. Cavaillé, “New nanocomposite materials reinforced with cellulose whiskers in atactic polypropylene: effect of surface and dispersion characteristics.,” *Biomacromolecules*, vol. 6, no. 5, pp. 2732–9, Jan. 2005.

[40] J. Araki, M. Wada, and S. Kuga, “Steric Stabilization of a Cellulose Microcrystal Suspension by Poly(ethylene glycol) Grafting,” *Langmuir*, vol. 17, no. 1, pp. 21–27, Jan. 2001.

[41] Y. Habibi, A.-L. Goffin, N. Schiltz, E. Duquesne, P. Dubois, and A. Dufresne, “Bionanocomposites based on poly(ε-caprolactone)-grafted cellulose nanocrystals by ring-opening polymerization,” *J. Mater. Chem.*, vol. 18, no. 41, p. 5002, Oct. 2008.

[42] J. Yi, Q. Xu, X. Zhang, and H. Zhang, “Temperature-induced chiral nematic phase changes of suspensions of poly(N,N-dimethylaminoethyl methacrylate)-grafted cellulose nanocrystals,” *Cellulose*, vol. 16, no. 6, pp. 989–997, Aug. 2009.

[43] J. Yi, Q. Xu, X. Zhang, and H. Zhang, “Chiral-nematic self-ordering of rodlike cellulose nanocrystals grafted with poly(styrene) in both thermotropic and lyotropic states,” *Polymer (Guildf).*, vol. 49, no. 20, pp. 4406–4412, Sep. 2008.

[44] Q. Xu, J. Yi, X. Zhang, and H. Zhang, “A novel amphotropic polymer based on cellulose nanocrystals grafted with azo polymers,” *Eur. Polym. J.*, vol. 44, no. 9, pp. 2830–2837, Sep. 2008.

[45] J. Araki, M. Wada, and S. Kuga, “Steric Stabilization of a Cellulose Microcrystal Suspension by Poly(ethylene glycol) Grafting,” *Langmuir*, vol. 17, no. 1, pp. 21–27, Jan. 2001.

[46] Y. Okita, S. Fujisawa, T. Saito, and A. Isogai, “TEMPO-Oxidized Cellulose Nanofibrils Dispersed in Organic Solvents,” *Biomacromolecules*, vol. 12, pp. 518–522, 2011.

[47] X. Xu, H. Wang, L. Jiang, X. Wang, S. A. Payne, J. Y. Zhu, and R. Li, “Comparison between Cellulose Nanocrystal and Cellulose Nano fi bril Reinforced Poly (ethylene oxide) Nano fi bers and Their Novel Shish- Kebab-Like Crystalline Structures,” *Macromoleculse*, vol. 47, pp. 3409–3416, 2014.

[48] A. J. Svagan, M. a. S. A. Samir, and L. a. Berglund, “Biomimetic Foams of High Mechanical Performance Based on Nanostructured Cell Walls Reinforced by Native Cellulose Nanofibrils,” *Adv. Mater.*, vol. 20, no. 7, pp. 1263–1269, Apr. 2008.

[49] T. Huq, S. Salmieri, A. Khan, R. A. Khan, C. Le Tien, B. Riedl, C. Fraschini, J. Bouchard, J. Uribe-Calderon, M. R. Kamal, and M. Lacroix, “Nanocrystalline cellulose (NCC) reinforced alginate based biodegradable nanocomposite film,” *Carbohydr. Polym.*, vol. 90, no. 4, pp. 1757–1763, 2012.

[50] J. Yang, C. R. Han, X. M. Zhang, F. Xu, and R. C. Sun, “Cellulose nanocrystals mechanical reinforcement in composite hydrogels with multiple cross-links: Correlations between dissipation properties and deformation mechanisms,” *Macromolecules*, vol. 47, no. 12, pp. 4077–4086, 2014.

[51] P. Z. and G. Y. Lina Fu, Yue Zhang, Chao Li, Zhihong Wu, Qi Zhuo, Xia Huang, Guixing Qiu, “Skin tissue repair materials from bacterial cellulose by a multilayer fermentation method,” *J. Mater. Chem.*, vol. 22, pp. 12349–12357, 2012.

[52] R. Shukla and M. Cheryan, “Zein: the industrial protein from corn,” *Ind. Crops Prod.*, vol. 13, no. 3, pp. 171–192, 2001.

[53] S. Bräuer, F. Meister, R. P. Gottlöber, and A. Nechwatal, “Preparation and thermoplastic processing of modified plant proteins,” *Macromol. Mater. Eng.*, vol. 292, no. 2, pp. 176–183, 2007.

[54] J. Gorham, “Analysis of Indian corn,” *QJ Sci. Lit. Arts*, pp. 206–208, 1821.

[55] I. Paraman and B. P. Lamsal, “Recovery and characterization of α-zein from corn fermentation coproducts.,” *J. Agric. Food Chem.*, vol. 59, no. 7, pp. 3071–7, Apr. 2011.

[56] A. Esen, “Separation of alcohol-soluble proteins (zeins) from maize into three fractions by differential solubility,” *Plant Physiol.*, 1986.

[57] J. Turner, J. Boundy, and R. Dimler, “Zein: A heterogeneous protein containing disulfide-linked aggregates,” *Cereal Chem*, 1965.

[58] D. Sessa, F. Eller, D. Palmquist, and J. Lawton, “Improved methods for decolorizing corn zein,” *Ind. Crops Prod.*, vol. 18, no. 1, pp. 55–65, 2003.

[59] C. Panchapakesan, N. Sozer, H. Dogan, Q. Huang, and J. L. Kokini, “Effect of different fractions of zein on the mechanical and phase properties of zein films at nano-scale,” *J. Cereal Sci.*, vol. 55, no. 2, pp. 174–182, Mar. 2012.

[60] A. Kriz and B. Larkins, *Molecular genetic approaches to maize improvement*. Berlin Heidelberg: Springer, 2009.

[61] N. Matsushima and G. Danno, “Three-dimensional structure of maize α-zein proteins studied by small-angle X-ray scattering,” *Biochim. Biophys. Acta*, pp. 14–22, 1997.

[62] E. Corradini, “Desenvolvimento de blendas de zeína e amido de milho,” Universidade de São Paulo, 2004.

[63] P. Nonthanum, Y. Lee, and G. W. Padua, “Effect of pH and ethanol content of solvent on rheology of zein solutions,” *J. Cereal Sci.*, vol. 58, no. 1, pp. 76–81, Jul. 2013.

[64] G. W. Selling, J. Lawton, S. Bean, C. Dunlap, D. J. Sessa, J. L. Willett, and J. Byars, “Rheological studies utilizing various lots of zein in N,N-dimethylformamide solutions.,” *J. Agric. Food Chem.*, vol. 53, no. 23, pp. 9050–5, Nov. 2005.

[65] S. Kim and J. Xu, “Aggregate formation of zein and its structural inversion in aqueous ethanol,” *J. Cereal Sci.*, vol. 47, no. 1, pp. 1–5, 2008.

[66] Y. Chen, R. Ye, and J. Liu, “Understanding of dispersion and aggregation of suspensions of zein nanoparticles in aqueous alcohol solutions after thermal treatment,” *Ind. Crops Prod.*, vol. 50, pp. 764–770, 2013.

[67] Y. Guo, Z. Liu, H. An, M. Li, and J. Hu, “Nano-structure and properties of maize zein studied by atomic force microscopy,” *J. Cereal Sci.*, vol. 41, no. 3, pp. 277–281, May 2005.

[68] K. Yamada, A. Noguchi, and H. Takahashi, “Effects of the Solvents on Properties of Zein,” *Nippon SHOKUHIN KAGAKU KOGAKU KAISHI*, vol. 43, no. 3, pp. 306–312, 1996.

[69] K. Yamada, H. Takahashi, and A. Noguchi, “Improved water resistance in edible zein films and composites for biodegradable food packaging,” *Int. J. Food Sci. Technol.*, vol. 30, no. 5, pp. 599–608, Jul. 2007.

[70] Y. Li, Q. Xia, K. Shi, and Q. Huang, “Scaling behaviors of α-zein in acetic acid solutions.,” *J. Phys. Chem. B*, vol. 115, no. 32, pp. 9695–702, 2011.

[71] K. Shi, J. L. Kokini, and Q. Huang, “Engineering zein films with controlled surface morphology and hydrophilicity,” *J. Agric. Food Chem.*, vol. 57, no. 6, pp. 2186–2192, 2009.

[72] W. V. K. Wheelwright, A. J. Easteal, S. Ray, and M. K. Nieuwoudt, “A one-step approach for esterification of zein with methanol,” *J. Appl. Polym. Sci.*, vol. 127, no. 5, pp. 3500–3505, Mar. 2013.

[73] P. Moore, S. Puvvada, and D. Blankschtein, “Role of the Surfactant Polar Head Structure in Protein-Surfactant Complexation: Zein Protein Solubilization by SDS and by SDS/C12En Surfactant Solutions,” *Langmuir*, vol. 19, no. 4, pp. 1009–1016, 2003.

[74] O. Ozcalik and F. Tihminlioglu, “Barrier properties of corn zein nanocomposite coated polypropylene films for food packaging applications,” *J. Food Eng.*, vol. 114, no. 4, pp. 505–513, 2013.

[75] M. J. Fabra, A. López-Rubio, and J. M. Lagaron, “Use of the electrohydrodynamic process to develop active/bioactive bilayer films for food packaging applications,” *Food Hydrocoll.*, vol. 55, pp. 11–18, 2016.

[76] V. a. Gaona-Sánchez, G. Calderón-Domínguez, E. Morales-Sánchez, J. J. Chanona-Pérez, G. Velázquez-de la Cruz, J. V. Méndez-Méndez, E. Terrés-Rojas, and R. R. Farrera-Rebollo, “Preparation and characterisation of zein films obtained by electrospraying,” *Food Hydrocoll.*, vol. 49, pp. 1–10, 2015.

[77] S.-Y. Cheng, B.-J. Wang, and Y.-M. Weng, “Antioxidant and antimicrobial edible zein/chitosan composite films fabricated by incorporation of phenolic compounds and dicarboxylic acids,” *LWT - Food Sci. Technol.*, vol. 63, no. 1, pp. 115–121, 2015.

[78] P. Oymaci and S. A. Altinkaya, “Improvement of barrier and mechanical properties of whey protein isolate based food packaging films by incorporation of zein nanoparticles as a novel bionanocomposite,” *Food Hydrocoll.*, vol. 54, pp. 1–9, 2016.

[79] Q. Wang and G. Padua, “AGFD 124-Controlled self-organization of zein nanostructures for encapsulation of active food ingredients,” *Abstr. Pap. Am. Chem. Soc.*, vol. 233, pp. 46–46, 2007.

[80] H. Guo and Y. Shi, “A novel zein-based dry coating tablet design for zero-order release,” *Int. J. Pharm.*, pp. 81–86, 2009.

[81] P. Hurtado-López and S. Murdan, “Zein microspheres as drug/antigen carriers: A study of their degradation and erosion, in the presence and absence of enzymes,” *J. Microencapsul.*, no. 23, pp. 303–314, 2006.

[82] D. Geraghty and M. Peifer, “The primary structure of a plant storage protein: zein,” *Nucleic Acids Res.*, vol. 9, pp. 5163–5174, 1981.

[83] X. Liu, Q. Sun, H. Wang, L. Zhang, and J. Y. Wang, “Microspheres of corn protein, zein, for an ivermectin drug delivery system,” *Biomaterials*, vol. 26, no. 1, pp. 109–115, 2005.

[84] V. Müller, J. F. Piai, A. R. Fajardo, S. L. Fávaro, A. F. Rubira, and E. C. Muniz, “Preparation and characterization of zein and zein-chitosan microspheres with great prospective of application in controlled drug release,” *J. Nanomater.*, vol. 2011, 2011.

[85] Y. Luo, B. Zhang, M. Whent, L. (Lucy) Yu, and Q. Wang, “Preparation and characterization of zein/chitosan complex for encapsulation of α-tocopherol, and its in vitro controlled release study,” *Colloids Surfaces B Biointerfaces*, vol. 85, no. 2, pp. 145–152, 2011.

[86] X. Chen, D. Li, G. Li, L. Luo, N. Ullah, Q. Wei, and F. Huang, “Facile fabrication of gold nanoparticle on zein ultrafine fibers and their application for catechol biosensor,” *Appl. Surf. Sci.*, vol. 328, pp. 444–452, 2015.

[87] B. Dhandayuthapani, A. C. Poulose, Y. Nagaoka, T. Hasumura, Y. Yoshida, T. Maekawa, and D. S. Kumar, “Biomimetic smart nanocomposite: in vitro biological evaluation of zein electrospun fluorescent nanofiber encapsulated CdS quantum dots.,” *Biofabrication*, vol. 4, no. 2, p. 25008, 2012.

[88] J. A. Bietz and J. A. Rothfus, “Comparison of peptides from wheat gliadin and glutenin,” *Cereal Chem.*, 1970.

[89] L. Day, M. A. Augustin, I. L. Batey, and C. W. Wrigley, “Wheat-gluten uses and industry needs,” *Trends Food Sci. Technol.*, vol. 17, no. 2, pp. 82–90, 2006.

[90] L. Liao, X. Han, L. Chen, L. Ni, Z. Liu, W. Zhang, and Q. Chen, “Comparative characterization of the deamidation of carboxylic acid deamidated wheat gluten by altering the processing conditions,” *Food Chem.*, vol. 210, pp. 520–529, Nov. 2016.

[91] P. Kanerva, O. Brinck, T. Sontag-Strohm, H. Salovaara, and J. Loponen, “Deamidation of gluten proteins and peptides decreases the antibody affinity in gluten analysis assays,” *J. Cereal Sci.*, vol. 53, no. 3, pp. 335–339, 2011.

[92] I. L. Batey and P. W. Gras, “Preparation of salt-free protein products from acid or alkali-treated proteins,” *Food Chem.*, vol. 12, no. 4, pp. 265–273, 1983.

[93] M. . Majzoobi and E. Adebi, “Effects of pH changes on functional properties of native and acetylated wheat gluten,” *Int. Food Res. J.*, vol. 21, no. 3, pp. 1219–1224, 2014.

[94] F. Cabrera-Ch??vez and A. M. Calder??n de la Barca, “Trends in wheat technology and modification of gluten proteins for dietary treatment of coeliac disease patients,” *J. Cereal Sci.*, vol. 52, no. 3, pp. 337–341, 2010.

[95] S. Khosravi, F. Khabbaz, P. Nordqvist, and M. Johansson, “Protein-based adhesives for particleboards,” *Ind. Crops Prod.*, vol. 32, no. 3, pp. 275–283, 2010.

[96] P. Nordqvist, D. Thedjil, S. Khosravi, M. Lawther, E. Malmstrom, and F. Khabbaz, “Wheat Gluten Fractions as Wood Adhesives-Glutenins Versus Gliadins,” *J. Appl. Polym. Sci.*, vol. 123, pp. 1530–1538, 2012.

[97] H. Lei, A. Pizzi, P. Navarrete, S. Rigolet, A. Redl, and A. Wagner, “Gluten Protein Adhesives for Wood Panels,” *J. Adhes. Sci. Technol.*, vol. 24, no. October, pp. 1583–1596, 2010.

[98] P. Nordqvist, M. Lawther, E. Malmström, and F. Khabbaz, “Adhesive properties of wheat gluten after enzymatic hydrolysis or heat treatment - A comparative study,” *Ind. Crops Prod.*, vol. 38, no. 1, pp. 139–145, 2012.

[99] P. Nordqvist, F. Khabbaz, and E. Malmström, “Comparing bond strength and water resistance of alkali-modified soy protein isolate and wheat gluten adhesives,” *Int. J. Adhes. Adhes.*, vol. 30, no. 2, pp. 72–79, 2010.

[100] N. A. El-Wakil, R. E. Abou-Zeid, Y. Fahmy, and A. Y. Mohamed, “Modified Wheat Gluten as a Binder in Particleboard Made from Reed,” *J. Appl. Polym. Sci.*, vol. 106, pp. 3592–3599, 2007.

[101] N. Reddy, Y. Tan, Y. Li, and Y. Yang, “Effect of glutaraldehyde crosslinking conditions on the strength and water stability of wheat gluten fibers,” *Macromol. Mater. Eng.*, vol. 293, no. 7, pp. 614–620, 2008.

[102] B. Sen Chiou, H. Jafri, T. Cao, G. H. Robertson, K. S. Gregorski, S. H. Imam, G. M. Glenn, and W. J. Orts, “Modification of wheat gluten with citric acid to produce superabsorbent materials,” *J. Appl. Polym. Sci.*, vol. 129, no. 6, pp. 3192–3197, 2013.

[103] C. Frihart, *Handbook of wood chemistry and wood composites*. CRC press, 2012.

[104] R. Kumar, V. Choudhary, and S. Mishra, “Adhesives and plastics based on soy protein products,” *Ind. Crops Prod.*, vol. 16, pp. 155–172, 2002.

[105] I. Santoni and B. Pizzo, “Evaluation of alternative vegetable proteins as wood adhesives,” *Ind. Crops Prod.*, vol. 45, pp. 148–154, 2013.

[106] A. Kaboorani, B. Riedl, P. Blanchet, M. Fellin, O. Hosseinaei, and S. Wang, “Nanocrystalline cellulose (NCC): A renewable nano-material for polyvinyl acetate (PVA) adhesive,” *Eur. Polym. J.*, vol. 48, no. 11, pp. 1829–1837, 2012.

[107] X. Kong, G. Liu, and J. M. Curtis, “Characterization of canola oil based polyurethane wood adhesives,” *Int. J. Adhes. Adhes.*, vol. 31, no. 6, pp. 559–564, 2011.

[108] N. Chen, Q. Lin, J. Rao, and Q. Zeng, “Water resistances and bonding strengths of soy-based adhesives containing different carbohydrates,” *Ind. Crops Prod.*, vol. 50, pp. 44–49, 2013.

[109] G. Habenecht, *Kleben-Grundlagen, Technolgier, Anwendung, Springer, Beriln*. Berlin/Heidelberg: Springer-Verlag, 2002.

[110] S. Veigel, U. Müller, J. Keckes, M. Obersriebnig, and W. Gindl-Altmutter, “Cellulose nanofibrils as filler for adhesives: Effect on specific fracture energy of solid wood-adhesive bonds,” *Cellulose*, vol. 18, pp. 1227–1237, 2011.

[111] S. Veigel, J. Rathke, M. Weigl, and W. Gindl-Altmutter, “Particle Board and Oriented Strand Board Prepared with Nanocellulose-Reinforced Adhesive,” *J. Nanomater.*, 2012.

[112] J. H. Kwon, S.-H. Lee, N. Ayrilmis, and T. H. Han, “Tensile shear strength of wood bonded with urea–formaldehyde with different amounts of microfibrillated cellulose,” *Int. J. Adhes. Adhes.*, vol. 60, pp. 88–91, 2015.

[113] E. Mahrdt, S. Pinkl, C. Schmidberger, H. W. G. van Herwijnen, S. Veigel, and W. Gindl-Altmutter, “Effect of addition of microfibrillated cellulose to urea-formaldehyde on selected adhesive characteristics and distribution in particle board,” *Cellulose*, 2015.

[114] F. López-Suevos, C. Eyholzer, N. Bordeanu, and K. Richter, “DMA analysis and wood bonding of PVAc latex reinforced with cellulose nanofibrils,” *Cellulose*, vol. 17, no. 2, pp. 387–398, 2010.

[115] D. Aydemir, “The Lap Joint Shear Strength of Wood Materials Bonded by Cellulose Fiber-Reinforced Polyvinyl Acetate,” *BioResources*, vol. 9, no. 1, pp. 1179–1188, 2014.

[116] Y. Sharma, “Engineered Wood Market by Product Type (Plywood, Laminated Veneer Lumber (LVL), Glulam, I-Beams, Oriented Strand Board (OSB), Cross-Laminated Timber (CLT)) and Application Type (Residential Construction and Non-residential Construction) - Global Opportuni,” 2016.

[117] W. D. Kerns, K. L. Pavkov, D. J. Donofrio, E. J. Gralla, and J. a Swenberg, “Carcinogenicity of Formaldehyde in Rats and Mice after Long-Term Inhalation Exposure,” *Cancer Res.*, vol. 43, no. September, pp. 4382–4392, 1983.

[118] R. B. Conolly, J. S. Kimbell, D. Janszen, P. M. Schlosser, D. Kalisak, J. Preston, and F. J. Miller, “Human respiratory tract cancer risks of inhaled formaldehyde: Dose-response predictions derived from biologically-motivated computational modeling of a combined rodent and human dataset,” *Toxicol. Sci.*, vol. 82, no. 1, pp. 279–296, 2004.

[119] T. Malaka and A. M. Kodama, “Respiratory health of plywood workers occupationally exposed to formaldehyde,” *Arch. Environ. Heal. An Int. J.*, vol. 45, no. 5, pp. 288–294, 1990.

[120] H. Guo, F. Murray, and S. Wilkinson, “Evaluation of total volatile organic compound emissions from adhesives based on chamber tests.,” *J. Air Waste Manage. Assoc.*, vol. 50, no. 2, pp. 199–206, 2000.

[121] R. D. Mitchell, “Raw materials for hot melt adhesives in the 21st century,” *Adhes. age*, vol. 42, no. 1, pp. 24–27, 1999.

[122] F. I. Khan and A. K. Ghoshal, “Removal of Volatile Organic Compounds from polluted air,” *J. Loss Prev. Process Ind.*, vol. 13, no. 6, pp. 527–545, 2000.

[123] J. Luo, J. Luo, C. Yuan, W. Zhang, J. Li, Q. Gao, and H. Chen, “An eco-friendly wood adhesive from soy protein and lignin: performance properties,” *R. Soc. Chem.*, pp. 100849–100855, 2015.

[124] H. Lei, G. Du, Z. Wu, X. Xi, and Z. Dong, “Cross-linked soy-based wood adhesives for plywood,” *Int. J. Adhes. Adhes.*, vol. 50, pp. 199–203, 2014.

[125] A. Moubarik, B. Charrier, A. Allal, F. Charrier, and A. Pizzia, “Development and optimization of a new formaldehyde-free cornstarch and tanninwood adhesive,” *Eur. J. Wood Wood Prod.*, vol. 68, no. 2, pp. 167–177, 2010.

[126] Y. Zhang, L. Ding, J. Gu, H. Tan, and L. Zhu, “Preparation and properties of a starch-based wood adhesive with high bonding strength and water resistance,” *Carbohydr. Polym.*, vol. 115, pp. 32–57, 2015.

[127] Z. Li, J. Wang, C. Li, Z. Gu, L. Cheng, and Y. Hong, “Effects of montmorillonite addition on the performance of starch-based wood adhesive,” *Carbohydr. Polym.*, vol. 115, pp. 394–400, 2015.

[128] Z. Wang, Z. Li, Z. Gu, Y. Hong, and L. Cheng, “Preparation, characterization and properties of starch-based wood adhesive,” *Carbohydr. Polym.*, vol. 88, no. 2, pp. 699–706, 2012.

[129] E. Norström, L. Fogelström, P. Nordqvist, F. Khabbaz, and E. Malmström, “Gum dispersions as environmentally friendly wood adhesives,” *Ind. Crops Prod.*, vol. 52, pp. 736–744, 2014.

[130] S. D’Amico, M. Hrabalova, U. Müller, and E. Berghofer, “Bonding of spruce wood with wheat flour glue-Effect of press temperature on the adhesive bond strength,” *Ind. Crops Prod.*, vol. 31, no. 2, pp. 255–260, 2010.

[131] A. J. Stamm, *Wood and Cellulose Science*. Wood and cellulose science, 1964.

[132] J. D. MacLean, *Preservative Treatment of Wood by Pressure Method*. US Government Printing Office, 1952.

[133] N. Reddy, Y. Tan, Y. Li, and Y. Yang, “Effect of glutaraldehyde crosslinking conditions on the strength and water stability of wheat gluten fibers,” *Macromol. Mater. Eng.*, vol. 293, no. 7, pp. 614–620, 2008.

[134] D. J. Gardner, “Adhesion Mechanisms of Durable Wood Adhesive Bonds,” in *Characterization of the Cellulosic Cell Wall*, 2008, pp. 254–265.

[135] J. Cognard, *Science et technologie du collage*. PPUR presses polytechniques, 2004.

[136] A. Pocius, *Adhesion and Adhesive Technology 2E: An Introduction*. Carl Hanser Verlag GmbH & Co, 2002.

[137] A. Pizzi and K. L. Mittal, "Theories and Mechanism of Adhesion," in *Handbook of Adhesive Technology*, MATERIALS ENGINEERING-NEW YORK- 14, 1994, pp. 19–33.

[138] J. W. McBain and D. G. Hopkins, "On Adhesives and Adhesive Action," *J. Phys. Chem.*, vol. 29, no. 2, pp. 188–204, 1925.

[139] G. Fourche, "An overview of the basic aspects of polymer adhesion. Part I: Fundamentals," *Polym. Eng. Sci.*, vol. 35, no. 12, pp. 957–967, Jun. 1995.

[140] S. Q. Shi and D. J. Gardner, "Dynamic Adhesive Wettability of Wood," *Wood Fiber Sci.*, vol. 33, no. 1, pp. 58–68, 2001.

[141] D. J. Gardner, F. P. Liu, M. . Wolcott, and T. G. Rials, ". Improving interfacial adhesion be- tween wood fibers and thermoplastics: A case study examining chemically modified wood and polystyrene.," in *Proc. Second Pacific Rim Biobased Composites Symposium*, 1994, pp. 55–63.

[142] J. J. Marcinko, C. Phanopoulos, and Teachey, "Why does chewing gum stick to hair and what does this have to do with lignocellulosic structural composite adhesion? InWood Adhesives 2000," in *Forest Products Society*, 2001, pp. 111–121.

[143] E. Ten, J. Turtle, D. Bahr, L. Jiang, and M. Wolcott, "Thermal and mechanical properties of poly(3-hydroxybutyrate-co-3-hydroxyvalerate)/cellulose nanowhiskers composites," *Polymer (Guildf).*, vol. 51, no. 12, pp. 2652–2660, 2010.

[144] P. Zhang, S.-J. Dong, H.-H. Ma, B.-X. Zhang, Y.-F. Wang, and X.-M. Hu, “Fractionation of corn stover into cellulose, hemicellulose and lignin using a series of ionic liquids,” *Ind. Crop. Prod.*, vol. 76, pp. 688–696, 2015.

[145] W. Li, B. J. Dobraszczyk, A. Dias, and A. M. Gil, “Polymer Conformation Structure of Wheat Proteins and Gluten Subfractions Revealed by ATR-FTIR,” *Cereal Chem.*, vol. 83, no. 4, pp. 407–410, 2006.

[146] J. M. Purcell, D. D. Kasarda, and C.-S. C. Wu, “Secondary structures of wheat α- and ω-gliadin proteins: Fourier transform infrared spectroscopy,” *J. Cereal Sci.*, vol. 7, no. 1, pp. 21–32, 1988.

[147] N. Zhong and Q. Yuan, “Preparation and properties of molded blends of wheat gluten and cationic water-borne polyurethanes,” *J. Appl. Polym. Sci.*, vol. 128, no. 1, pp. 460–469, 2013.

[148] A. Mohamed, V. L. Finkenstadt, S. H. Gordon, G. Biresaw, P. D. E., and P. Rayas-Duarte, “Thermal Properties of PCL/Gluten Bioblends Characterized by TGA, DSC, SEM, and Infrared-PAS,” *J. Appl. Polym. Sci.*, pp. 3256–3266, 2008.

[149] B. Dhandayuthapani, R. Mallampati, D. Sriramulu, R. F. Dsouza, and S. Valiyaveettil, “PVA/gluten hybrid nanofibers for removal of nanoparticles from water,” *ACS Sustain. Chem. Eng.*, vol. 2, no. 4, pp. 1014–1021, 2014.

[150] T. Ghosh Dastidar and A. N. Netravali, “A soy flour based thermoset resin without the use of any external crosslinker,” *Green Chem.*, vol. 15, no. 11, pp. 3243–3251, 2013.